MASTERARBEIT | MASTER‘S THESIS

Titel | Title

Genetic engineering of *Methanothermobacter marburgensis* for bioplastic production

verfasst von | submitted by

Ing. Alex-Ionuţ Totolici, M.

angestrebter akademischer Grad | in partial fulfilment of the requirements for the degree of

Master of Science (MSc)

Wien | Vienna, 2026

Studienkennzahl lt. Studienblatt | Degree programme code as it appears on the student record sheet:	UA 066 830
Studienrichtung lt. Studienblatt | Degree programme as it appears on the student record sheet:	Masterstudium Molecular Microbiology, Microbial Ecology and Immunobiology
Betreut von | Supervisor:	Mag. Mag. Dr.techn. Simon Karl-Maria Rasso Rittmann Privatdoz. Bakk.

Table of Contents

Acknowledgments

I would like to begin by thanking my supervisor, doc. Mag. Mag. Dr. techn. Simon K.-M. R. Rittmann, Privatdoz. Bakk., for the opportunity to be part of his team. I am very grateful for his guidance and all the support he provided to help me complete this thesis. I remember that his presentation on research topics made me realize I would like to work under his supervision. Also, the day before, I'd left my water bottle in the classroom, and during the presentation, he used it as a prop to describe a closed batch bioreactor. Through him, I was also able to secure financial support for this thesis.

This thesis was conducted within the COMET Centre CHASE, funded within the COMET − Competence Centers for Excellent Technologies programme by the BMIMI, the BMWET and the Federal Provinces of Upper Austria and Vienna. The COMET programme is managed by the Austrian Research Promotion Agency (FFG). In addition to the institutional support, I want to thank my manager, Dr. Karin Wieland. for her support and our highly productive communication throughout this project.

Likewise, I would like to thank my co-supervisor, Ing. Walter Hofmann, MSc, for all his guidance and advice on the experiments. He was very involved in this project, and without his contribution, I would not have been able to obtain the necessary resources to complete it. I would also like to thank Hayk Palabikyan, MSc, for all his help with cultivation and microscopy; his guidance and the assistance he provided in the lab were a great help to me.

Throughout this project, I was fortunate to have many people by my side who provided scientific guidance and helped me grow. I would like to thank Dr. Christian Fink for his patience and assistance in deciphering the induced genetic modifications. I would also like to thank Mag. Nika Pende, PhD, MSc, for all her advice on presentations and image analysis. And I would like to extend my gratitude to Mag. Isabelle Anna Zink, PhD, for providing to me the SnapGene license and for her support in the laboratory. I would like to thank Selina Madlmayr, BSc, for guiding me through the early days of the project and sharing her practical knowledge with me. I would also like to mention my fellow students, whose work was of immense help to me: Wenlong Liu, BSc, Nicolás Salas Wallach, MSc, Lena Winter, BSc, Sharanya Sridhara, MSc. And I especially haven't forgotten the technical support provided by Ulf Naumann and all his advice in the lab. I'd also like to thank all the department's administrative staff who keep everything in order and help ensure we have a suitable working environment.

Special thanks go to my sister (Giulia-Amalia Totolici) and cousins in Romania (Ing. Darius-Razvan Radu, Paul-Ionuț Petridian, BSc, and many other cousins), and also to my friends in Vienna (Diana-Andreea Codrean, BA, Nikolaus Haunschmied, BSc, Raymond Blaskievics, BA, and the whole band) for all the memories we share. I always enjoy spending time with them, and they are very dear to me.

My entire story in Vienna would never have come to be if I hadn't met Diana-Raluca Frîncean, BA, my beloved partner, who has transformed my life and my perceptions. There are no words to describe the joy I feel living my daily life with her. And without her, any writing of mine would be far worse.

To conclude this section, I would like to say that I am deeply grateful to all the people who have helped me grow and achieve this milestone. And I would like to extend my final thanks, in Romanian, to the people who have supported me throughout my life.

Dragii mei părinți, Vasile și Silvia Totolici, prin această lucrae doresc să vă mulțumesc pentru că mi-ați ofeit libertatea necesară pentru a devein ceea ce sunt, și pentru toata iubirea voastră. Vă respect în totalitate, iar tot ce îmi doresc este ca în final să vă fac mândri și să vă răplătesc cât aș putea. De asemenea, doresc să o menționez pe bunica mea, Maria Sămărtean, care sper că este mândră de mine din ceruri și pe care o port mereu în gând.

Mulțumesc!

Abstract

This thesis establishes a thermophilic, CO_2-to-PHB conversion platform by engineering *Methanothermobacter marburgensis* to express a thermostable PhaABC pathway and benchmarking three acetoacetyl-CoA reductases (PhaB): a NADPH-dependent PhaB from *Caldimonas thermodepolymerans* (Ther), a chimeric variant designed into preferring NADH (Chim), and a candidate from *Caldichromatium japonicum* hypothesized to be NADH dependent (Jap). The final goal is the creation of a viable biotechnologically alternative for sustainable and efficient biodegradable plastic production. Enzyme assays corroborated the cofactor preferences: $PhaB_{(Ther)}$ was highly active with NADPH (54.75 U mg^{-1}) but nearly inactive with NADH (0.09 U mg^{-1}), $PhaB_{(Jap)}$ showed strong NADH activity (21.96 U mg^{-1}; 8.07 U mg^{-1} with NADPH), and $PhaB_{(Chim)}$ showed low-activity despite NADH preference (0.67 U mg^{-1}). Genome integration of *PhaABC* and mutants isolation were confirmed by PCR strategies targeting *Δhpt* signature signal loss and pathway gene presence, ensuring stable strains for phenotyping. Under H_2/CO_2 (4:1) at 3 bar and 55 ºC, BODIPY imaging indicated robust intracellular PHB accumulation in the *M. marburgensis* Jap strain, moderate and cell-heterogeneous signals in *M. m.* Ther, and only faint signals in *M. m.* Chim. These results prove that aligning PhaB cofactor usage with the host's redox metabolism (NADH) enables effective thermophilic PHB biosynthesis, with *M. m.* Jap emerging as the detected most promissing strain for PHA production. While PHB quantitation and chemical confirmation by LC–MS still need to be confirmed, these findings position *M. marburgensis* as a genetically tractable, thermostable solution for sustainable gas-to-plastic bioprocesses which motivate for: (i) modelling and optimization of the metabolic pathways in methanogens; (ii) development of new genetic tools for methanogens; (iii) scale-up and downstream bioprocess developments.

Zusammenfassung

In dieser Arbeit wird eine thermophile Plattform zur Umwandlung von CO_2 in PHB etabliert, indem *Methanothermobacter marburgensis* genetisch so modifiziert wird, dass es einen thermostabilen PhaABC-Stoffwechselweg exprimiert, und drei Acetoacetyl-CoA-Reduktasen (PhaB) verglichen werden: Eine NADPH-abhängige PhaB aus *Caldimonas thermodepolymerans* (Ther), eine chimäre Variante, die so konstruiert wurde, dass sie NADH bevorzugt (Chim), und einen Kandidaten aus *Caldichromatium japonicum*, von dem angenommen wird, dass er NADH-abhängig ist (Jap). Das Ziel ist die Schaffung einer tragfähigen biotechnologischen Alternative für die nachhaltige und effiziente Produktion biologisch abbaubarer Kunststoffe. Enzymtests bestätigten die Cofaktorpräferenzen: $PhaB_{(Ther)}$ war mit NADPH hochaktiv (54,75 U mg^{-1}), mit NADH jedoch nahezu inaktiv (0,09 U mg^{-1}), $PhaB_{(Jap)}$ zeigte eine starke NADH-Aktivität (21,96 U mg^{-1}; 8,07 U mg^{-1} mit NADPH), und $PhaB_{(Chim)}$ blieb trotz NADH-Präferenz inaktiv (0,67 U mg^{-1}). Die Genomintegration von *PhaABC* und die Isolierung der Mutanten wurden durch Amplifikation mittels Polymerasekettenreaktion bestätigt, die auf den Verlust des *Δhpt*-Signatursignals und das Vorhandensein von Stoffwechselweg-Genen abzielten, wodurch stabile Stämme für die Phänotypisierung sichergestellt wurden. Unter H_2/CO_2 (4:1) bei 3 bar und 55 ºC zeigte die BODIPY-Färbung und Bildgebung durch Mikroskopie eine robuste intrazelluläre PHB-Akkumulation im *M. m.* Jap-Stamm, moderate und zellheterogene Signale in *M. m.* Ther sowie nur schwache Signale in *M. m.* Chim. Diese Ergebnisse zeigen, dass die Abstimmung der PhaB-Cofaktorverwertung auf den Redoxstoffwechsel des Wirts (NADH) eine effektive thermophile PHB-Biosynthese ermöglicht, wobei sich *M. m.* Jap als vielversprechender Stamm für die thermophile PHA Produktion herauskristallisiert. Zwar müssen die PHB-Quantifizierung und die chemische Bestätigung mittels LC–MS noch bestätigt werden, doch positionieren diese Ergebnisse *M. marburgensis* als genetisch manipulierbare, thermostabile Lösung für nachhaltige Gas-zu-Kunststoff-Bioprozesse, was Anreize bietet für: (i) die Modellierung und Optimierung der Stoffwechselwege in Methanogenen; (ii) die Entwicklung neuer genetischer Werkzeuge für Methanogene; (iii) die Skalierung und die Entwicklung entprechender Bioprozesse.

1. Introduction

1.1. Global importance of Bioplastics

Plastic is a material that is extensively used due to its physical properties (higher durability with an excellent strength to weight ratios) and the capacity to be produced cheaply and in high amounts (Mitrano & Wohlleben, 2020; MacLeod et al., 2021). The global-scale use of plastic makes it crucial for the modern world, but the impact on the environment is also more visible and harder to ignore (Mitrano & Wohlleben, 2020; MacLeod et al., 2021). The toxic chemicals, plastic debris, and microplastics, that result from the large-scale production of traditional petrochemical, plastics harm the environment and impact human health, showing that new regulations and sustainable strategies need to be applied (MacLeod et al., 2021; Stoett et al., 2024). Biodegradable polymers, such as polylactic acid (PLA), poly(butylene adipate-co-terephthalate) (PBAT) and polyhydroxyalkanoates (PHA), are a desirable substitution for conventional plastics which are already produced and used for shopping bags and packaging (Markl et al., 2018; Narancic et al., 2020). However, biobased plastics production is still small compared to petrochemical plastics production, representing only 1.1% of the European plastics production in 2024 (Plastics Europe, 2026).

Among the biobased plastics, PHA has attracted substantial research interest. PHAs represent a group of biopolymers which various microorganisms accumulate as granules in the cell when subjected to carbon source excess, but other essential growth nutrients are missing as well (Sharma et al., 2021). There are many types of PHAs with diverse structures and properties depending on the monomeric composition (Yao et al., 2025). In the PHA class of biopolymers poly(3-hydroxybutyrate) (PHB) is included, whose natural production is highly investigated in bacteria (*Azohydromonas lata, Caldimonas thermodepolymerans, Cupriavidus necator, Nostoc muscorum*), but also in some halophilic archaea (*Haloferax mediterranei*), to serve in biobased bioplastic applications (Haase et al., 2012; Mozumder et al., 2015; Atarés et al., 2024; P. Fink et al., 2025; Jang et al., 2025). PHB has similar physical characteristics with other traditionally used plastics such as polypropylene (PP) or polyethylene (PE), that make this biopolymer a desirable material to be used as packaging material, as coating material or for medical and pharmaceutical products (Markl et al., 2018; Vlaeminck et al., 2022; Atarés et al., 2024). Even so, because of the PHB's high production costs, it is not economically feasible over conventional plastics based on fossil fuels. Progress was made in reducing production costs, according to reports to around 3 € kg^{-1} PHB^{-1}, but it

is significantly higher compared with the price of about 1 € kg^{-1} for conventional petrochemical plastics such as PP (Vlaeminck et al., 2022; Yao et al., 2025). The cost of production is reflected in the amount of produced PHA, representing only 4.7% of the global biobased plastics produced, and only 0.6% of the bioplastics produced in Europe in 2025 (European Bioplastics, 2026).

To overcome the economic feasibility barriers, different alternatives are being researched, including improvements to productive strains, the exploration of alternative carbon sources, and the optimisation of medium composition and downstream purification processes (Mozumder et al., 2015; Akkoyunlu et al., 2024; J. Wang et al., 2024; Thiele & Riedel, 2025). The carbon source represents the major production cost, contributing to approximately 50% of the final cost of PHB (Vlaeminck et al., 2022). One strategy to reduce these costs is the use of cheap or waste-derived carbon sources, such as corn stover, discarded vegetable oils, animal fats, or C1/C2 substrates (Ventura & Ventura, 2024; Yao et al., 2025). Another key approach is the use of metabolic and genetic engineering to enhance PHB accumulation and growth rates in naturally producing organisms (Subramanian et al., 2024; Z. Zhang et al. 2024). Beyond strain optimisation, genetic engineering also enables the transfer of PHB biosynthetic pathways into non-natural producers (Y. Wang et al. 2026). Microorganisms that do not natively synthesise PHB may offer significant biotechnological advantages, such as faster growth rates, higher biomass yields, tolerance to industrial conditions, or the ability to efficiently utilise low-cost or waste-derived substrates (Y. Wang et al. 2026). This strategy is well-established in industrial biotechnology and represents a promising route to expand the range of production hosts and reduce the overall costs associated with PHB manufacturing (Y. Wang et al. 2026). Among the microorganisms being explored for industrial biotechnological applications, Archaea remain considerably less studied than bacteria as biotechnological hosts. Recent advances in our understanding of their physiology and the development of archaeal genetic tools are slowly unveiling new opportunities for their exploitation in industrial biotechnology, including potential applications for the PHB production.

1.2. Archaea Biotechnology

Archaea are a large and diverse group of prokaryotic microorganisms that inhabit almost every environment on Earth and are more closely related to Eukarya than to Bacteria in terms of their biochemical and cellular machinery (Nagrale & Gawande, 2018; De Lise et

al., 2023). Although many archaeal species are found in common environments such as soils, oceans, and the human body, this domain is perhaps best known for encompassing organisms capable of thriving in the most extreme conditions in which life is possible (Nagrale & Gawande, 2018). These so-called extremophiles have evolved remarkable adaptations in their cellular structure and metabolism that not only allow them to withstand, but actively exploit, harsh environmental conditions (Aparici-Carratalá et al., 2023). Understanding the molecular basis of these adaptations opens exciting possibilities for biotechnology, offering nature-inspired solutions for the development of sustainable industrial processes.

One of the earliest and most impactful applications of Archaea in biotechnology was the isolation of the DNA polymerase from *Pyrococcus furiosus*, a thermostable enzyme with exceptional proofreading activity that became foundational to molecular biology techniques such as PCR (Takagi et al., 1997; Nagrale & Gawande, 2018; Aparici-Carratalá et al., 2023; De Lise et al., 2023). This discovery highlighted the potential of thermophilic archaea as a reliable source of industrially valuable enzymes, capable of functioning under high temperatures and extreme pH levels where conventional bacterial enzymes would fail (Aparici-Carratalá et al., 2023; De Lise et al., 2023). Beyond enzyme discovery, *P. furiosus* and other members of the Thermococcaceae familiy have also been explored as a microbial cell factories, representing a prime target for the development of bioprocesses aimed at producing green molecular hydrogen (H_2) as a sustainable energy carrier (Ergal et al., 2018; Pfeifer et al., 2021). Furthermore, the extensive development of genetic tools for Thermococcaceae have enabled its metabolic engineering for the laboratory-scale production of a range of valuable compounds, including ethanol, butanol, isobutane, and lactate (Pfeifer et al., 2021).

Another group of extremophilic archaea with significant biotechnological potential are the halophiles. These organisms have already proven reliable as production hosts for high-value compounds such as carotenoids, bacteriorhodopsins, and exocellular polymeric substances (EPS), and certain species, such as *H. mediterranei*, are also natural PHB accumulators that have been investigated as platforms for biopolymer production (Pfeifer et al., 2021). A key advantage of using halophiles in industrial bioprocesses is their inherent resistance to contamination, as their requirement for high salt concentrations helps create a selectively hostile environment for most other microorganisms, reducing the need for costly sterilisation procedures (Haque et al., 2020). In the context of PHB production specifically, halophiles present an additional economic benefit through their ability to utilise saline or

hypersaline wastewater streams as carbon sources, reducing the cost of substrate pre-treatment and contributing to a more sustainable and cost-effective process (Koller et al., 2016; Wang & Zhang, 2020). However, PHB yields in halophilic systems remain relatively low, with reported values of approximately 0.54 g g^{-1} (Wang & Zhang, 2020) and 0.78 g g^{-1} (Pais et al., 2016), and further optimisation is still required before these organisms can be considered competitive production hosts. To address this, Atarés et al., 2024 proposed integrative biorefinery approaches, in which the simultaneous production of multiple concomitant bioproducts from *H. mediterranei*, (PHB alongside carotenoids, bacteriorhodopsins, and EPS) could maximise the value extracted from a single fermentation process, improving the overall economic feasibility.

The Archaea domain also encompasses the methanogens, which are a group of strictly anaerobic microorganisms widely distributed across molecular oxygen-depleted environments such as marine sediments, wetlands, the gastrointestinal tracts of ruminants, and anaerobic digesters (Nagrale & Gawande, 2018; Pfeifer et al., 2021). This group takes its name from their unique energy-conserving metabolism, in which the terminal product is methane (CH_4), until now being the only known biological agents of methanogenesis (Enzmann et al., 2018). Within the methanogenic class, a variety of methanolic pathways exist, and the most common classification is based on the substrate utilised: hydrogenotrophic methanogens use H_2 and CO_2; aceticlastic methanogens use acetate; and methylotrophic methanogens use methylated compounds such as methanol or methylamines (Fu et al., 2021; Chegini, 2025).

Among these, hydrogenotrophic methanogens have attracted the greatest biotechnological interest, particularly in the context of biological methanation, which has been intensively researched as a strategy for renewable energy and carbon capture storage (CCS) (Rittmann, 2015; Rittmann et al., 2018; Mauerhofer et al., 2018). This process is especially relevant in the framework of Power-to-Gas technologies, where excess renewable electricity is used to generate H_2 via water electrolysis, which is subsequently fed to hydrogenotrophic methanogens for biological CH_4 production (Chegini, 2025). Several approaches have been developed to improve the efficiency and scalability of this process. Electromethanation directly couples microbial methanation with electrochemical systems, where methanogens receive electrons directly from a cathode to reduce CO_2 to CH_4, bypassing the need for exogenous H_2 supply (Enzmann et al., 2018; Fu et al., 2021). Co-feeding strategies, in which formate is supplied alongside H_2 and CO_2 as an additional electron donor, have also been explored to enhance methanation rates and provide metabolic flexibility to the culture (Sabel-

Becker et al., 2025). Furthermore, the use of flue gases (CO_2-rich exhaust streams derived from the combustion of methane or other fossil fuels) as a direct carbon feedstock for methanogenic cultures has been proposed as a particularly attractive approach, as it would simultaneously improve the industrial waste stream and produce a renewable fuel, contributing to a circular carbon economy (Sieborg et al., 2024). Collectively, these strategies have led to significant improvements in volumetric methane productivity and process stability, bringing biological methanation closer to industrial applicability and expend the biogas technology (Contreras et al., 2022; Chegini, 2025).

Despite this progress, a major limitation constraining the further development of methanogen biotechnology is the scarcity of available genetic and molecular tools, restricting the scope of metabolic engineering efforts across the broader methanogenic diversity (Myers & Dykstra, 2024). *Methanococcus maripaludis* and *Methanosarcina acetivorans*, that already have robust genetic systems, and CRISPR-based techniques are implemented to research how the metabolism can be tuned (Akinyemi et al., 2021; Du et al., 2024; Myers & Dykstra, 2024). However, improvised transformation protocols, promoter systems, and reliable selection markers also for other methanogens are needed to unlock their potential (Myers & Dykstra, 2024). The foundation of genetic system in *Methanothermobacter* genus was built by C. Fink et al. (2021) by creating the shuttle vector which allows for heterologous expression in *Methanothermobacter thermautotrophicus* ΔH. The conjugation protocol was further optimised for *M. thermautotrophicus* ΔH over the last 5 years and successfully used in metabolic engineering for acetoin production (C. Fink et al., 2022; Baur et al., 2025). Looking forward, these advances open the possibility of reprogramming the highly efficient CO_2-fixing metabolism of methanogens not only for optimised CH_4 production, but also for the biosynthesis of other valuable products (Contreras et al., 2022; Mühling et al., 2024).

1.3. Perspective on different organisms that produce PHB from CO_2

The recent initiatives on the sustainable production of value-added chemicals encourage the development of industrial fermentation processes with microbes that use C1 sources (CO_2, CO, CH_4, methanol and formate) and C2 substrates (mainly ethanol and acetate), that are not heavily reliant on expansive carbohydrate substrates like glucose and sucrose (C. Zhang et al., 2022). The use of C1 and C2 substrates as feedstocks is challenging because of the microbes low assimilating rate into biomass and bioproducts, but these aspects are gradually addressed and overcome (C. Zhang et al., 2022). By implementing bioprocess

that use C1 and C2 substrate, the effect for greenhouse gasses (CO_2, CO, CH_4) will be reduced, contributing also to the implementation of a circular economy (C. Zhang et al 2022; Y. Wang et al. 2026). Among the valuable products obtainable from C1 sources are biopolymers such as PHA and PLA (Y. Wang et al. 2026). From the C1 substates, CO_2 is the most abundant and is produced when microorganisms consume PHA, and by pollution of human activity (J. Lee et al 2021). In this condition, the cheap renewable CO_2 feedstock can be used to crate valuable added products in form of PHB to mitigate the greenhouse effects, and at the same time, it creates a circular, closed loop for the biodegradable plastic economy (J. Lee et al., 2021).

Cupriavidus necator is the model microorganism for producing PHB. It has a flexible metabolism and well-established tools for genetic modification, making it ideal for research aimed at improving production (L. Zhang et al, 2022). *C. necator* is a H_2-oxidizing bacterium that can grow in aerobic/anaerobic interfaces and can easily adapt between heterotrophic and autotrophic lifestyles (L. Zhang et al, 2022). When fed with high amounts of sugar they accumulate a high percentage of PHB during the nitrogen starvation stage. This organism has been also proved to be able to convert CO_2 into PHB through the Calvin–Benson–Bassham (CBB) cycle (L. Zhang et al., 2022). To perform the autotrophic growth of CO_2, *C. necator* also needs H_2 and O_2 in the gas composition to satisfy the energy needs, and different gas mixture compositions were tested and modelled to see the effect on PHB accumulation (Mozumder et al., 2015; Garcia-Gonzalez et al., 2015). Still, one of the biggest concerns on this strategy is the usage of gas mixture that contains H_2 and O_2 together, having a high risk of explosion. This issue is being addressed by finding a composition that has the H_2 concentration bellow the explosion risk threshold, but this also reduces growth capacities of the organises and PHB yield (Miyahara et al., 2020).

Photoautotrophic synthesis of PHB is another strategy that was investigated in cyanobacteria. Their simple condition for cultivations and use of renewable, eco-friendly energy (light) and carbon (CO_2) sources makes them desirable (Y. Wang et al. 2026). Despite the clear advantages, the low percent of PHB per cell dry weight (CDW^{-1}) and the need of the 2 stages fermentation are making it more complicated (P. Fink et al., 2025). Despite this, P. Fink et al. (2025) managed to overcome some of the limitations by genetically engineering *Nostoc* sp. PCC7120 into accumulation of PHB, avoiding the nitrogen starvation and showing that cell viability can be improved by expressing heterologous phasins together with the genes needed for the PHB synthesis pathway. All of this makes light fermentation interesting, but the light requirements are a limitation when it comes to the scalability and time efficiency of

the process compared to dark fermentation strategies, which is not affected by the night day cycle or the need of special bioreactors designs to facilitate light penetration (Hannon et al., 2020; Rueda et al., 2023).

The use of methanogens for PHB production has been considered a promising concept, yet experimental evidence demonstrating its feasibility has remained scarce. Thevasundaram et al. (2022) provided the first proof that methanogens can produce PHB, by introducing and expressing bacterial PHB biosynthetic enzymes in *Methanococcus maripaludis*. The study established that methanogenic cells could support the foreign biosynthetic machinery needed for PHB accumulation, proving the basic feasibility of using methanogens as PHB production hosts. However, this work also identified a critical bottleneck: the availability of the cofactors NADH and NADPH, which are essential for the biosynthesis of the PHB monomer. Unlike conventional bacterial producers, methanogens have a very different cofactor metabolism, which limits the amount of NADH and NADPH available for PHB biosynthesis, resulting in low yields. They (Thevasundaram et al., 2022) highlight the need for targeted cofactor engineering strategies to rewire the methanogenic metabolism and improve the supply of these essential cofactors. Despite these current limitations, they manage to produce up to 171 mg L^{-1} of PHB with the NADH improved *M. maripaludis* strain in closed batch cultivation mode. This study indicates that natural autotrophic metabolism of methanogens worth further investigation in the direction of PHB production.

1.4. *Methanothermobacter marburgensis* as a platform for CO_2 conversion

Among hyperthermophilic methanogens, *Methanothermobacter marburgensis* is one of the best study representatives and a prime candidate for biotechnological applications (Unger et al., 2025). This strictly hydrogenotrophic methanogen grows optimally at 65 °C, using H_2 and CO_2 as its sole energy and carbon sources, and exhibits a high specific growth rate of up to 0.69 h^{-1}, making it one of the fastest-growing methanogens described to date (Abdel Azim et al., 2017; Rittmann et al., 2018). The capacity to grow in high temperature is reducing the risk of contamination during cultivation and reduces the need of cooling systems in bioreactors (Mauerhofer et al., 2021). Furthermore, *M. marburgensis* has proved the ability to reach high cell densities in fed-batch cultivation and in continuous culture conditions and could successfully be scale-up (Abdel Azim et al., 2017; Rittmann et al., 2018; C. Fink et al., 2025). The organism harbours an archaeal peptidoglycan cell wall that confers remarkable

resistance to shear forces and high pressure, making it well suited for industrial gas fermentation processes (Mauerhofer et al., 2021; Mukhopadhyay, 2024; Orthofer et al., 2025). Collectively, these characteristics establish *M. marburgensis* as a robust and promising cell factory for CO_2-based bioprocesses, where its efficient autotrophic metabolism can be harnessed for the CO_2 conversion and sequestration into valuable products using the genetic tools that were recently developed.

1.4.1. Development of the genetic system

M. marburgensis is capable of natural transformation by taking up genetic material from its environment, but this not sufficient to develop precise genetic engineering (Worrell et al., 1988). Because of its similarity to *M. thermautotrophicus*, Klein et al. (2025) manged to adapt the genetic system available to be used for *M. marburgensis*. Furthermore, developing a technique for markerless mutagenesis using deletion and insertion of hypoxanthine phosphoribosyltransferase (*hpt*) gene for negative selection in order to recycle resistance (Klein et al., 2025). Using this method, they created the *M. marburgensis Δhpt* strain and de modular vector pArk, which allow for homologous recombination using the up and down regions of the *Δhpt* region facilitating the integration into genome of heterologous genes. This then opened up the possibility of creation of new metabolic pathways such as engineering a novel pathway in *M. marburgensis* for isoleucine biosynthesis from threonine (Klein et al., 2025).

1.4.2. Biotechnological applications

In the field of biotechnology, *M. marburgensis* first shines as a potent CH_4 producer, achieving up to 950 mmol L^{-1} h^{-1} MER, and performing good in high pressure systems that could be applied in biomethanation processes (Seifer et al., 2014; Orthofer et al., 2025). A new application was discovered when *M. marburgensis* was found to be capable to synthetase all the 20 essential amino acids (AA) and excrete them into the growth medium (Taubner et al 2023). This can be improved by supplementing them with molecular nitrogen (N_2) for AAs secretion (Reischl et al., 2025; Reischl et al., 2026). This led to the exploration of sustainable production of AAs from CO_2, and further fed-batch cultivation showed up different AA patterns based on the NH_4^+ concentration (Reischl et al., 2026). Together with the development of the genetic tools, metabolic engineering and process optimisation, the AA production was further improved, achieving 40 mg g(CDW)$^{-1}$ h $^{-1}$ of valine in fed-batch cultivation, and on pilot-plant scale 65 mg L $^{-1}$ h^{-1} of leucine volumetric productivity (C. Fink et al., 2025; Unger

et al., 2025). All this encompasses the capabilities and the feasibility of *M. marburgensis* as a cellular refinery for CO_2-based production of chemicals.

1.5. Establishing the PhaABC pathway into *M. marburgensis*

The pathway for production PHBs starts at the acetyl-CoA molecule, an important energy metabolite that is essential to metabolic pathways (Yao et al., 2025). To be converted into the monomer 3-hydroxybutyrate it needs to be processed by 2 enzymes. First, an acetyl-CoA acetyltransferase (3-ketothiolase) (PhaA) transforms 2 molecules of acetyl-CoA in 1 of acetoacetyl-CoA. The second reaction is a reduction of the acetoacetyl-CoA by a NADPH- or NADH- dependent acetoacetyl-CoA reductase (PhaB), resulting the 3-hydroxybutyrat monomer. The formation of the polymer is catalysed by poly(R)-hydroxyalkanoic acid synthase (PhaC), which belongs to Class I PhaC in the case of PHB synthesis. By having only these 3 enzymes, many microorganisms would in principle able to be engineered to produce PHB using the genes that code for the *PhaABC* operon from model organisms like *C. necator* (P. Fink et al., 2025). Introducing a PhaABC operon could add the PHB synthesis pathway to *M. marburgensis* and potentially couple it to CO_2 fixation; this approach aims to test whether the coupling can be achieved (*Figure 1*).

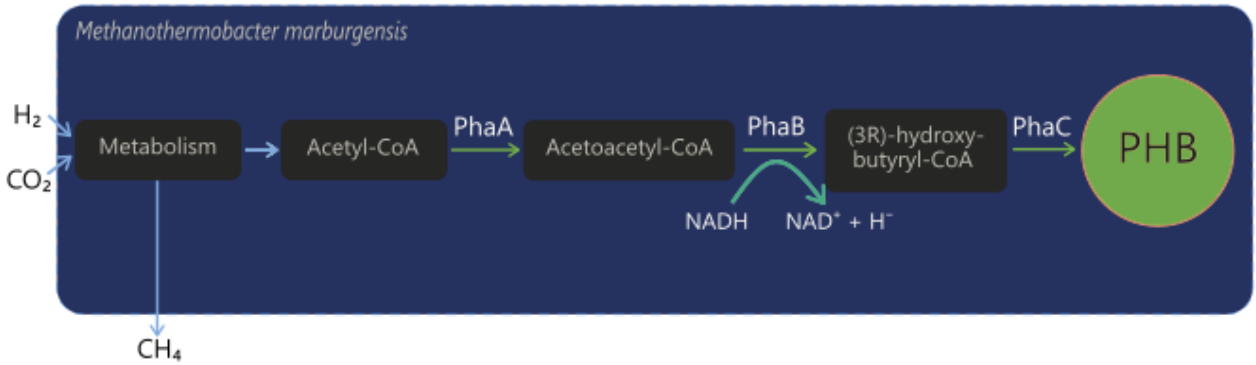

Figure 1. Proposed PHB biosynthetic pathway to be engineered into *M. marburgensis*.

To make *M. marburgensis* a PHA producer, which grows at temperatures between 45-70 ºC, and optimally at 65 °C, genes that encode thermostable PHA synthesis proteins would be necessary. Because of that, the use of genes from mesophilic organisms like *H. mediterranei* or *C. necator* (30 ºC) would not be indicated (Serna-García et al., 2024). One of the best described thermophilic PHB producer is *Caldimonas thermodepolymerans*, which grows and accumulates PHB even at 55 ºC (Jang et al., 2025). Considering a good fit for use in *M. marburgensis* the starting geneses for the transformation were the *PhaA*, *PhaB*, and *PhaC* from *C. thermodepolymerans*.

Another important consideration in designing the metabolic pathway in *M. marburgensis* is the cofactor requirements of the enzymes. In the case of *M. maripaludis* engineering for PHB production, the NADH/NADPH pool represents a bottleneck for the PhaB activity, activity which requires NADH or NADPH as cofactor (Thevasundaram et al., 2022). *M. marburgensis* was shown to possess a cytosolic NADH:quinone oxidoreductase that would help with the NADH regeneration, indicating that this organism might possess and increased pool of NADH (Ullmann et al., 2014). Unfortunately, the PhaB from *C. thermodepolymerans* is described in the literature as NADPH (Musilova et al., 2023). Therefore, some alternatives in the PhaB selection need to be explored, because the PHB accumulation in anaerobic fermentations, favours NADH reoxidation (Olavarría et al., 2022).

One possible adjustment would be trying to change the affinity of the cofactor binding site to preferre NADH. This was done in previews work by Liu (2026), in which he analysed and evaluated the change in the sequence coding region for the cofactor binding site, influencing the catalytic activity of the PhaB from *C. thermodepolymerans*. This was achieved this by creating 4 chimeric PhaB which have different modifications in the coding sequence for the cofactor binding site that were taken from *Halomonas bluephagenesis* (Chimera I-blue), *Allochromatium vinosum* (Chimera II-vin), *Azotobacter beijerinckii* (Chimera III-beij) and Candidatus *Accumulibacter phosphatis* (Chimera IV-phos) (Olavarría et al., 2022; Liu 2026). The sequences used for modifications are coding for the NADH binding sites of PhaB enzymes of PHB producing microorganisms (Olavarría et al., 2022). Hence obtaining chimeras PhaB that will keep the thermostability from *C. thermodepolymerans* and the NADH affinity from other PhaB. By testing chimera activity with NADH and NADPH, Liu (2026) reported a reduced preference for NADPH but no significant improvement in activity with NADH. In his study, the best chimera was considered ChimII-vin, with the NADH site from *A. vinosum*, which showed the greatest activity difference in favour of NADH cofactor (NADH: 0.013 U mg^{-1}; NADPH: 0.009 U mg^{-1}; ratio 1.486). Because the overall activity reported being low also for NADH, other thermophilic PhaB should be identify to that would have better activity with NADH as coenzyme.

Given that overall activity was low with NADH as well for ChimII-vin, additional thermophilic PhaB variants form thermophilic organisms should be identified with improved NADH-dependent activity. To identify thermophilic NADH-dependent acetoacetyl-CoA reductases, the PhaB sequence from *A. vinosum* was used as a query in BLAST analysis, yielding several thermophilic homologs (Liebergesell & Steinbüchel, 1992). The most

promising candidates were identified in *Caldichromatium japonicum* (81.7% sequence identity), *Inmirania thermothiophila* (61.1%), and *Hydrogenophilus thermoluteolus* (syn. *Pseudomonas hydrogenothermophila*; 60.7%). *C. japonicum* is a thermophilic phototrophic purple sulphur bacterium isolated from hot springs by Saini et al. (2020) and showed to grow within the 40-56 ºC range at a pH of 7.2. Their study indicated the presence of the genes for PHB synthesis and showed the granules from the cell, but the enzymes were not experimentally characterized (Saini et al., 2020). Because the PhaB from *C. japonicum* shows high sequence identity to the *A. vinosum* PhaB, which produced the best chimera, it is a strong candidate to evaluate for high NADH-dependent specific activity.

The scope of this thesis is to assess whether one of the three PhaB proteins, Ther (*C. thermodepolymerans* PhaB) Chim (Chimera II-vin PhaB) and Jap (*C. japonicum* PhaB) will enable PHA accumulation in *M. marburgensis*. We will also evaluate the activity of the PhaB with each cofactor from a crude protein lysate extracted from BL21(DE3) overexpressing enzyme of interest.

1.6. Research questions and hypotheses

RQ1: Is it the PhaB from *C. japonicum* a very active NADH-dependent enzyme when compared to the other 2 enzymes (Ther and Chim)? Assumptions: Because $PhaB_{(Jap)}$ shows 81.71% identity with the *A. vinosum* PhaB, this will have a strong affinity for NADH.

RQ2: Can *M. marburgensis* be efficiently transformed for PHB production? Hypothesis: The integration of a *PhaABC* operon into the genome of *M. marburgensis* leads to a PHB accumulation through expression of thermostable enzymes.

RQ3: Which of the three PhaB proteins is most suitable for PHB production by *M. maburgensis*? Hypothesis: The highest PHB accumulation in *M. marburgensis* will be observed in mutants engineered with the PhaB variant exhibiting the greatest activity when using NADH as coenzyme.

2. Materials and Methods

2.1. Microbial strains and medium

2.1.1. *Escherichia coli*

Escherichia coli Top10 (Thermo Fisher Scientific, Waltham, MA, USA) and DH5α (New England Biolabs, Ipswich, MA, USA) strains were used for cloning of the generated plasmids, BL21(DE3) (Thermo Fisher Scientific, Waltham, MA, USA) for expression of the proteins investigated in this study, and S17-1 (DSM 9097) for conjugal transfer of DNA. The genetic engineering was performed on *Methanothermobacter marburgensis* DSM 2133 *Δhpt*.

The stains used and the mutants that were generated during this study were preserved in a strain collection at -70 ºC. The *E. coli* cells were prepared for cryopreservation by mixing 800 µL of culture with 600 µL 50% (v/v) sterile glycerol solution in screw cap 2 mL micro tube (Sarstedt AG & Co. KG, Nümbrecht, Germany). The *M. marburgensis* culture were prepared by transferring 1 mL of culture in a sterile screw cap 2 mL micro tube inside of the anaerobic glove box (Coy Laboratory Products, Grass Lake, MI, USA). The tubes were flash frozen in liquid molecular nitrogen quickly after preparation and transferred to the -70 ºC TSX Universal Series Ultra-Low Temperature Freezers (Thermo Fisher Scientific, Waltham, MA, USA).

2.1.2 *Methanothermobacter marburgensis*

All the *E. coli* cultures were cultivated in premix Luria-Bertani (LB) broth (Carl Roth GmbH + Co. KG, Karlsruhe, Germany) that was supplemented when required with the appropriate antibiotic (100 µg mL^{-1} ampicillin, 50 µg mL^{-1} kanamycin, or 30 µg mL^{-1} chloramphenicol) for positive selection with the according plasmids. Solidify Agar-LB (Carl Roth GmbH + Co. KG, Karlsruhe, Germany) plates were prepped using a premix broth with the required antibiotic added after autoclaving (121 ºC, 15 min) in a vertical autoclave (HMC Europe GmbH, Tüssling, Germany). When cultivating *E. coli* S17-1, the medium was supplemented with 10 µg mL^{-1} trimethoprim in addition to the other required antibiotics for the stabilization of the *tra* gene cassette. Super Optimal broth with Catabolite repression (SOC) was used in the recovery step of transforming competent *E. coli* cells.

The *M. marburgensis Δhpt* strain was cultivated in sea salt (MS) medium prepared as described by Fink et al., 2021 with small modifications. The MS medium was prepared by mixing salts (0.45 g NaCl, 6 g $NaHCO_3$, 0.17 g K_2HPO_4, 0.19 g NH_4Cl, 0.08 g $MgCl_2$, 0.06 g

$CaCl_2 \cdot 2H_2O$, 0.23 g KH_2PO_4) in 800 mL MilliQ water. After dissolving the salts, the following solutions were added: 1 mL $(NH_4)_2Ni(SO_4)_2$ 0.2% (w/v), 1 mL $FeCl_2 \cdot 5H_2O$ 0.2% (w/v), 1 mL Resazurin 0.025% (w/v) and 1 mL trace elements (TE) 10x (Annex 1, *Table S1*). The pH was adjusted to 7.2 by adding 5 mol L^{-1} HCl and then the volume was fill to 1.000 mL with H_2O. The medium was sparged with molecular nitrogen/CO_2 (4:1) (20 Vol.-% CO_2 in molecular nitrogen) for 45 min and afterward the anaerobic medium was transferred to the anaerobic chamber (Coy Laboratory Products, Grass Lake, MI, USA). Inside the glove box, 0.5 g L-cysteine and 2 mL Na_2S $0.5 \cdot 9H_2O$ mol L^{-1} were added to the medium. The prepared medium was aliquoted by distributing 20 mL medium into 120 mL serum bottles. After sealing the serum bottles with butyl stoppers and aluminum crimps, the headspace was exchanged to H_2/CO_2 (4:1) (20 Vol.-% CO_2 in H_2) with three cycles of -0.8 bar and 1 bar overpressure with a final pressure of 1 bar H_2/CO_2 (4:1) gas mixture. The purity of all gases was 5.0 (99.999%). The ready-made medium bottles were autoclaved at 121 °C for 20 min and 1.2 bar above atmospheric pressure in a vertical autoclave. For the conjugation with *E. coli*, MS/LB medium was prepared by mixing 1:1 (v/v) MS medium with modified LB medium (10 g tryptone, 5 g yeast extract per L). The solidify MS and MS/LB medium was prepared by adding 1.5% (w/v) BD Bacto agar (Becton, Dickinson and Company, Franklin Lakes, NJ, USA) before autoclavation.

The physiological characterization and expression of the *PhaABC* of the mutants was performed using a growth medium (MM medium) for biomass accumulation (C. Fink et al., 2025). The medium was prepared by mixing 2.1 g NH_4Cl, 6.8 g KH_2PO_4 and 1 mL 1x Novasign TE (Annex 1, *Table S2*) in 800 mL MilliQ water. The pH was adjusted to 7.2 by adding 5 mol L^{-1} NaOH and then the volume was filled to 1000 mL with H_2O. The O_2 from the liquid was removed by sparging with N_2/CO_2 (4:1) for 45 min and afterward the anaerobic medium was transferred to the anaerobic chamber. Inside the glove box, 2 mL Na_2S $0.5 \cdot 9H_2O$ mol L^{-1} were added to the medium. The prepared medium was aliquoted by distributing 20 mL medium into 120 mL serum bottles. After sealing the serum bottles with butyl stoppers and aluminum crimps, the headspace was exchanged to H_2/CO_2 (4:1) with three cycles of -0.8 bar and 1 bar overpressure with a final pressure of 2 bar H_2/CO_2 (4:1) gas mixture. The medium was supplemented with 250 µg mL^{-1} neomycin when cultivating mutants. All the gaseous substrates were introduced manually through an offline gassing manifold.

2.1.3. Cultivation conditions

The cultivation of *E. coli* was performed by incubation in a shaking incubator (Labwit, Burwood East, VIC, Australia) at 37 ºC or 25 ºC set at 160 rpm for liquid cultures, and in static incubator (Binder GmbH, Tuttlingen, Germany) at 37 ºC for the solidified LB plates.

The cultivation of *M. marburgensis* in MS medium was performed in the prepared sterile medium bottles, and the headspace overpressure was set to 2 bars. The liquid cultures were cultivated at 62 °C in a GFL 1083 shaking water bath (Gesellschaft für Labortechnik GmbH, Burgwedel, Germany) filled with MilliQ water at 140 rpm. Cultures on solidified minimal medium were incubated in an anaerobic steel jar with 1-2 bar overpressure of H_2/CO_2 (4:1). Anaerobic jars were incubated in a static incubator at 62 °C, or 37 °C when conjugating with *E. coli* on LB/MS-Agar. After inoculating, the headspace pressure was set to ~3 bars. The cultivation on MM medium was performed in the prepared sterile medium bottles, and the headspace overpressure was set to 3 bars.

2.3. Primers, synthesized DNA fragments, plasmids and markers

All primers used in this study (Annex 1, *Table S3*) were purchased from Eurofins Genomics (Eurofins Genomics GmbH, Ebersberg, Germany). The synthetic genes (Annex 1, *Table S4*) have been codon optimised for *E. coli* or for *M. marburgensis* expression using SnapGene software (GSL Biotech, Chicago, IL, USA) and ordered over Twist Bioscience (Twist Bioscience, South San Francisco, CA, USA). The *PhaABC* monocistronic gene cluster was designed and codon optimised for *M. marburgensis* expression using SnapGene software, ordered from Eurofins Genomics and received in the form of pEX-A258-*PhaABC* plasmid (Annex 1, *Figure S1*). The plasmids from this study were generated using as vector pET15b (NovoPro Bioscience Inc., Shanghai, China) for the NADH/NADPH assays and pArk_*hptU_NeoRHPT_LysCGS_hptD* for the genetic modification of *M. marburgensis*.

The DNA sizes of the analysed samples in this study were determined using Invitroge™ 1 Kb Plus DNA Ladder or GeneRuler™ 1 kb Plus DNA Ladder (Thermo Fisher Scientific, Waltham, MA, USA) depending on the availability of these makers in the laboratory.

The marker to determinate the size of the protein used was a PageRuler™ Plus Prestained Protein Ladder, 10 to 250 kDa (Thermo Fisher Scientific, Waltham, MA, USA).

2.4. Molecular techniques for genetic modification of *E. coli*

2.4.1. Transformation of competent cells procedure

The 30 µL competent *E. coli* cell aliquots preserved at -70 ºC were taken out and slowly defreezed on ice for 10-20 min. In a new 1.5 mL tube the competent cells were mixed with 3 µL of the ligation mix or ~30 ng of purified plasmid DNA and was incubated 20 min on ice. After incubation, the cells were heatshocked at 42 ºC for 60 s and quickly transferred on ice for 5 min. The cells were removed by adding 200 µL SOC medium an incubating them for 1h at 37 ºC 350 rpm. The transformed culture was then plated on selective solid LB with the corresponding antibiotics by pipetting 120 µL of the recovered cells on the plate then spread with a Drigalski spatula, and the remaining culture was also plated on another plate.

2.4.2. Colony PCR

From the plates, 3-5 colonies were picked with the 10 µL tip of a pipette and transferred to 10 µL fresh LB (without antibiotic) in 0.5 mL PCR tubes and mixed by pipetting. This samples were incubated for 30 min at 37 ºC, and during the incubation period, the master mix was prepared by mixing GoTaq buffer (Promega, MA, USA), dNTPs and the primers. After incubation 2 µL of the picked colony sample was added into the PCR reaction, followed by adding the Taq G2 polymerase before staring the PCR reaction.

2.4.3. Gibbson assembly of the plasmids and cloning

The pET15b plasmids and the fragments were amplified using primers designed for the Gibbson assembly by PCR with Q5 high-fidelity polymerase (New England Biolabs, Ipswich (MA), USA) according to the manufacturer's protocol for a final volume of 50 µL in a Biometra Professional thermocycler (Analytik Jena GmbH + Co. KG, Jena, Germany). The PCR protocol used is described in the Annex 1, *Table S5*. The PCR products were confirmed on 1% agarose gel. The right fragments were purified by cutting the respective bands and cleaned up using a Monarch DNA Gel extraction Kit (New England Biolabs, Ipswich, MA, USA). The plasmids were constructed using NEBuilder HiFi DNA Assembly by calculating the DNA amount needed for backbone and fragmented using NEB calculator to a 1:5 ratio, mixed with the 2X Assembly Master Mix an incubated at 50 ºC for 30-60 min. After incubation, the Top10 *E. coli* competent cells were transformed using the assembled mix. To test for positive transformation, we performed a PCR colony using primers for the T7 promoter (Annex 1, *Table S6*). The PCR product was checked on 1% agarose gel, and the positive colonies were grown for plasmid purification using a Promega plasmid miniprep kit. The

plasmids were sequence by Plasmidsaurus (Cologne, Germany) and used for transformation of BL21(DE3) *E. coli* competent cells.

2.5. Protein investigation techniques

2.5.1. Enzymes expression

Overnight cultures of the transformed *E. coli* BL21(DE3) were used to inoculate 10 mL LB medium (100 µg mL^{-1} ampicillin) at a starting point optical density (OD) of 0.1. The cultures were grown to a ~ 0.4 OD and then induced by supplementing them with 1 or 0.1 mmol L^{-1} IPTG to induce the protein expression at 37 ºC for 3 h or at 24 ºC overnight. After induction, the cells were harvested by centrifugation (30 min, 3,620 × *g*, 4 ºC), and the pellet was resuspended in cold lysing buffer (50 mmol L^{-1} Sodium Phosphate, 150 mmol L^{-1} NaCl, 1 mmol L^{-1} DTT, 1:1,000 Benzonase, 1x Roche cOmplet, Mini, EDTA-free Protease-Inhibitor-Cocktail) and all the next steps were performed on ice to prevent protein degradation. The cell suspension was transferred into Bead Beating tubes (MP Biomedicals Inc, Irvine, CA, USA) and set to beating for 45 s, 6 m s^{-1}, 4 times with 1 min rest in between. Next, the tubes were centrifugated (10 min, 10,000 × *g*, 4 ºC) and 1 mL supernatant was transferred into 1.5 mL Eppendorf tubes. The protein concentration was checked using NanoPhotometer (Implen GmbH, München, Germany) and samples were taken for SDS-PAGE gel, and the rest of the protein suspensions were preserved by adding glycerol to a 20% per volume concentration, aliquoted 75 µL into PCR tubes, frozen with liquid molecular nitrogen and stored at -70 ºC.

2.5.2. SDS-PAGE

The lysate samples were prepared for SDS-PAGE by mixing 30 µL samples with 10 µL 4x Lithium Dodecyl Sulfate sample buffer (Invitrogen™ NuPAGE™ LDS) with 1 mmol L^{-1} dithiothreitol (DTT) and boiled at 96 ºC for 5 min with 1.050 rpm (Eppendorf™ Thermomixer™ R**)**. The proteins were migrated into 12.5% acrylamide gel in 3-(*N*-morpholino)propanesulfonic acid (MOPS) running buffer, at 60 V for 20 min and 100 V for 40 min, followed by a staining of the proteins using Instant Blue Coomassie Protein Stain (Abcam Limited, Cambridge, UK).

The samples for the SDS-PAGE of the *M. marburgensis* strains were done by resuspending the pellet of 2 mL culture in 500 µL lysing buffer and transferring into a screw cap micro tube (Thermo Fisher Scientific, Waltham, MA, USA) with 100 µL glass beads (0.2-0.5 mm) inside. The samples were bead beated for 30 s, 6 m s^{-1}, 4 times with 1 min rest in between. The supernatant was extracted and transferred into 1.5 mL tubes, and centrifuged for

10 min, at 10,000 × *g*, 4 ºC. the clean lysate supernatant was taken and transferred to another tube and kept cold. Next, 30 µL sample with 10 µL 4x LDS with 1 mmol L^{-1} DTT were boiled at 96 ºC for 5 min with 1050 rpm. The proteins were migrated into 8–16% acrylamide precast gel (Thermo Fisher Scientific, Waltham, MA, USA) with Tris-Glycine running buffer, at 60 V for 20 min and 100 V for 40 min, followed by a staining of the proteins using Instant Blue Coomassie Protein Stain (Abcam Limited, Cambridge, UK).

2.5.3. NADH/NADPH Assays

All the photometrical measurements were done with a SPECORD 200 Plus UV/Vis spectrophotometer (Analytik Jena GmbH + Co. KG, Jena, Germany), using UV micro cuvettes (Brand GmbH + Co. KG, Wertheim, Germany). The final volume for the samples in cuvettes was 400 µL and the measurements were taken at 360 nm wavelength with the temperature set at a constant temperature of 30 ºC. On the day of the assay, we prepared 1 mmol L^{-1} stock solutions of NADH and NADPH dissolved in phosphate buffer pH 7.2 (50 mmol L^{-1} Sodium Phosphate, 150 mmol L^{-1} NaCl). The standard curves for NADH and NADPH were created by measuring the absorptions for prepared samples with 0.05, 0.075, 0.1, 0.125, 0.15, 0.2, 0.25, and 0.3 mmol L^{-1} concentration of NADH/NADPH in triplicate and used to evaluate the consumption of NADH/NADPH by the crude enzymatic lysate solutions. The lysate solutions were taken from -70 ºC and thawed slowly on ice for 20 min. During the waiting time Zebra™ spin desalting columns were loaded with the phosphate buffer pH 7.2 by centrifugation for 4 times each 1 min at 1,000 × g with 150 µL of buffer. After defrizzing the 3-4 samples, proteins lysates were buffered exchanged by spinning 1 min at 1,000 × g in the column.

The protein concentrations of the lysate samples were determined by Bradford protein assay. The standard curve was created using known concentrations of serial dilution of Bovine Serum Albumin (BSA). From the standards and the samples 10 µL were pipetted in a 96-well-plate (Greiner-CELLSTAR), followed by the starting of the reaction with the addition of Bradford protein reagent (Thermo Fisher Scientific, Waltham, MA, USA). The plate was incubated for 5 min, and the absorbents of the standards and samples were measured in a Tecan Sunrise plate reader (Tecan Group Ltd., Männedorf, Switzerland).

The samples were prepared by adding into the reaction solution 0.25 mmol L^{-1} NADH or NADPH and a volume of lysate solution depending on the pretested activity of the enzymes and measured concentration, to a final volume of 400 µL. After that, the samples were placed into the spectrophotometer for a short incubation at 30 ºC, then the rection was started by

adding 0.5 mmol L^{-1} acetoacetyl-CoA (substrate) final concentration. The consumption of NADH/NADPH was monitored for 5 to 6 min and then the data was analysed to select the linear phase of the reaction. The data points were used to calculate the initial velocity of the enzymes and the specific activity in that time frame. The negative control measurements represent the normal reaction combination but without adding the substrate. The negative control indicating the normal background degradation of NADH or NADPH without the consumption caused by the PhaB activity. This data was used to calculate the decay rate and was subtracted from specific activity results.

2.6. Conjugation procedure for genetic modification of *M. marburgensis*

2.6.1. Construction of the pArk-*PhaABC*

The pEX-A258-*PhaABC* plasmid was cloned into Top10 *E. coli* competent cells and positive colonies were selected and grown for the purification of more plasmid product (Promega plasmid miniprep kit). The presence of the right genes was checked by sequencing by Plasmidsaurus. Additionally, Additionally, pArk*_hptU_NeoRHPT_LysCGS_hptD* was used as backbone in Top 10 *E. coli* (*Figure 2*). Both plasmids were cut with the KasI and XbaI restriction enzymes (New England Biolabs, Ipswich, MA, USA) by incubating them at 37 ºC for 1 h, then purified using a PCR clan-up kit (New England Biolabs, Ipswich (MA), USA). The DNA concentration was measured by nanodrop, and the fragment and backbone were added to the Quick Ligation (New England Biolabs, Ipswich, MA, USA) reaction in a 3:1 ratio. After 1h at room temperature, the Ligation mix was used for transformation of DH5α *E. coli* competent cells. Colonies were picked and grown and plasmid were extracted. The plasmids were tested using KpnI and XhoI restriction enzymes (New England Biolabs, Ipswich, MA, USA) by incubating them for 30 min at 37 ºC and checking the fragments generated on an 1% agarose gel. The positive results were sent to sequencing. After confirmation of the plasmid by sequencing, the pArk-*PhaABC* was transformed in *E. coli* S17-1 competent cells to be used for the *M. marburgensis Δhpt* conjugation. All the coding genes from the pArk-PhaABC were put under expression control of the constitutive promoter P_{hmtB}.

2.6.2. Exchange of the *PhaB*$_{(Ther)}$ from pArk-*PhaABC* with other PhaB's.

The pArk-*PhaABC* plasmid that contains the *PhaA*, *PhaB* and *PhaC* from *Caldimonas thermodepolymerans* was used as a base line, and the *PhaB* gene was exchanged with the Chim and Jap *PhaB* genes. The exchange was achieved by cutting pArk-*PhaABC* and the other synthetic *PhaB* genes with the PacI and MfeI restriction enzymes (New England

Biolabs, Ipswich, MA, USA), incubated at 37 ºC for 1h, then purified using a PCR clean-up kit (New England Biolabs, Ipswich, MA, USA). The DNA concentration was measured by nanodrop, and the fragment and backbone were added to the Quick Ligation (New England Biolabs, Ipswich, MA, USA) rection in a 3:1 ratio. After 1 h at RT, the ligation mix was used for transformation of DH5α *E. coli* competent cells. Positive colonies were picked, grown and plasmids were extracted and sent to sequencing for conformation. After confirming the presence of the replaced *PhaB* in the pArk-*PhaABC*, the plasmid was used for transformation of S17-1 *E. coli*.

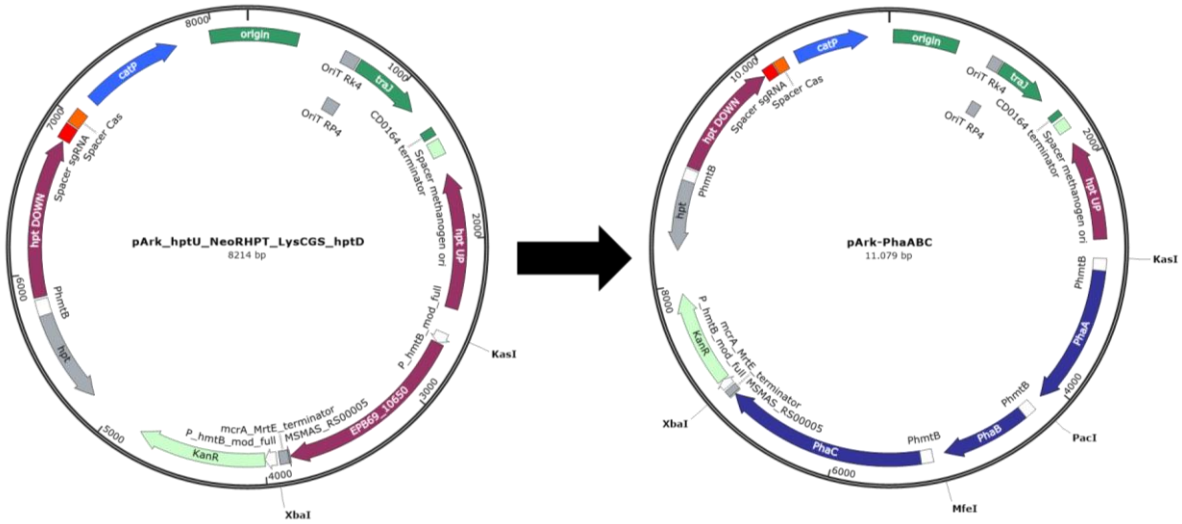

Figure 2. Plasmid maps of the pArk vectors illustrating replacement of the gene module from the previous application with the *PhaABC* operon module using the restriction enzymes KasI and XbaI; The introduced *PhaB*$_{(Ther)}$ gene was individually replaced with *PhaB*$_{(Chim)}$ or *PhaB*$_{(Jap)}$ using the MfeI and PacI restriction sites; The plasmids also include: *hpt* flanking regions (*hpt* UP and DOWN) to facilitate homologous recombination, the *hpt* gene for negative selection, the aminoglycoside phosphotransferase (*KanR*) gene for neomycin resistance and positive selection in *M. marburgensis*, the chloramphenicol acetyltransferase (*catP*) gene for selection in *E. coli*, and the *E. coli* replicon (origin of replication [ori] and *traJ*).

2.6.3. Interdomain conjugation

M. marburgensis Δhpt was grown over night util the culture reached around 0.3 OD. The grown culture was transferred into the anaerobic tend and 8 mL of the cells were centrifuged at 10,000 rpm for 3 min and resuspended in 200 µL cultured medium. The *E. coli* S17-1 cell that were carrying pArk-*PhaABC* were inoculated in 5 ml LB with the corresponding antibiotic and grown overnight. In the morning the culture was used to inoculate 10 mL LB (Cmp, Tmp) at a starting OD of 0.3 and left to grow until it reached 2.5 OD. After the *E. coli* culture was fully grown the cells were harvested aerobically at 3,500 × *g* for 10 min at RT. The supernatant was discarded, and the pellet was transferred to the anaerobic chamber. In anaerobic conditions, the *E. coli* pellet was resuspended using the 200 µL for concentrated *M. margugensis Δhpt* culture. To facilitate mating, 100 µL of the cell mixture were spotted on

MS/LB plates. After the spots were completely dry the plates were put into an anaerobic jar with 1 bar H_2/CO_2 atmosphere. The anaerobic jar was transferred into a 37 ºC static incubator for 16-20 h. After incubation, the anaerobic jar was opened in the anaerobic tent, and the spot was washed using 1 mL MS medium (from a 50-mL serum bottle containing 5 mL MS medium with an H_2/CO_2 gas phase) and transferred back into the remaining 4 mL in the 50 mL serum bottle. The recovery culture with nonselective medium was incubated at 62 ºC with shaking (120 rpm) for 4 h. Then 1 mL of the recovery was transferred into 20 mL selective MS medium (250 µg mL^{-1} neomycin) with the atmosphere set to 2 bars of H_2/CO_2 and incubated with shaking (120 rpm) at 62 ºC until growth was noticeable. When growth was visible and a considerable amount of the gas substrate was consumed (pressure drop in serum bottle to 1 bar or lower), the culture was used for inoculation of a new 20 mL selective MS medium. The second transfer was important to reduce the amount of DNA left from the *Δhpt* strain. If the PCR indicated the presence of the desired mutant, the culture was spread-plated on solid MS plates and incubated in an anaerobic jar for 48 h (65 ºC, 2 bar H_2/CO_2). For the purpose of this experiment 5 single colonies were picked and grown. The cultures from single colonies were analysed by PCR and checked for the right insertion. The positive mutants were selected and checked for the presence of the genes by sequencing the purified *PhaB* PCR amplified fragments and preparing them with a Mix2Seq kit (Eurofins Genomics GmbH, Ebersberg, Germany). The whole procedure is illustrated in *Figure 3* for a better representation of the seps.

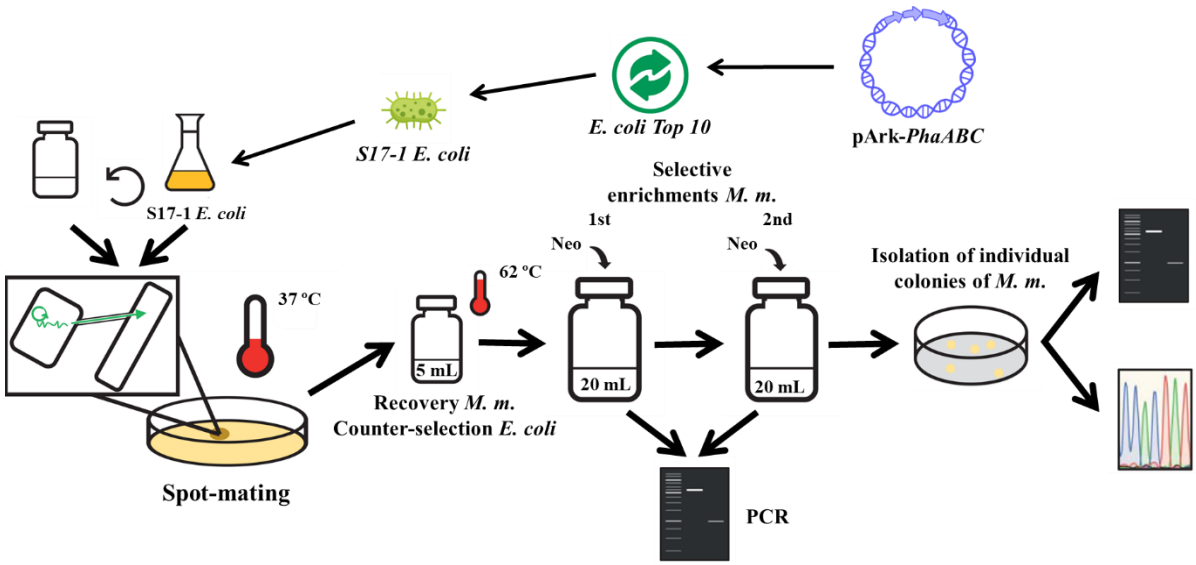

Figure 3. Schematic overview of the interdomain conjugation workflow used to integrate the *PhaABC* module from *E. coli* S17-1 into *M. marburgensis* (adapted from Fink et al., 2021).

2.6.4. PCR analysis of *M. marburgensis* mutants.

The PCR technique was used to distinguish between false positive result that can come up because of spontaneous resistance to neomycin of the *M. marburgensis Δhpt* strain. The DNA samples were prepared by taking 1 mL form the grown cultures in a 1.5 mL Eppendorf tube, centrifuge at 10,000 × *g* for 5 min, the pellet was kept and resuspended in another 200 µL of the same culture. The sample was heated at 99 ºC to facilitate the lysing of the cells for 10 min in a thermomixer (Eppendorf SE, Hamburg, Germany). From the sample 1 µL was used as template and in 4 reaction mix (1X GoTaq Geen Buffer, 10 mmol L^{-1} dNTP, 10 mmol L^{-1} forward primer, 10 mmol L^{-1} reversed primer) with different primer combination to distinguish between the *Δhpt* strain and the mutants. The reaction tubes have been kept on ice, and after adding 0.25 µL of the G2 Taq polymerase, the PCR program (Annex 1, *Table S*7) of the thermocycler was started. The PCR products were evaluated into a 1% agarose gel.

2.6.5. Genomic DNA extraction

The genomic DNA of *M. marburgenis* mutants was extracted for further sequencing and precise PCR reaction. From the overnight cultures, 2-3 mL were re-elevated and centrifuged at 16,000 × *g* for 2 min. The supernatant was discarded and the pellet was resuspended in 100 µL lysis buffer (prepared by mixing 1 mL SDS 10 %, 200 µL NaCl 5 mol L^{-1}, 100 µL TrisHCl 1 mol L^{-1} pH 8, 20 µL EDTA 0.5 mol L^{-1} filed to 10 mL with MilliQ water). The resuspension was transferred into a fastprep tube containing 100 µL glass beads (0.2-0.5 mm) and 100 µL of phenol/chloroform was added using a 1 mL graduated glass pipette. These samples were bead beated 4 times at 6 m s^{-1} for 30 s with a 60 s break between beating. Into the same tube 200 µL of 1X SSC was added and vortexed for 5 s then centrifuged at 16,000 × *g* for 3 min. The top layer resulted was transferred into a new 1.5 mL tube and mixed with 200 µL phenol/chloroform before centrifuging again at 16,000 × *g* for 3 min. The top layer was transferred again to a fresh 1.5 mL tube (around 180 µL) followed by the addition of 400 µL of 100% ethanol and a 10 min incubation on ice. After incubation, the samples were centrifuged at 16,000 × *g* for 1 min, the supernatant was discarded and the pellet was gently resuspended with 70% ethanol. The resuspended DNA was lastly centrifuged at 16,000 × *g* for 5 min at 4 ºC to facilitate the precipitation and then the supernatant was discarded. The pellet was dried by flipping the tube upside down and gently touching a paper towel. After that the tube was let open for 3-4 min to air dry and that the pellet was resuspended in 30 µL of DEPC water before incubating at 42 ºC for 10 min to remove the last traces of ethanol. The DNA concentration was measured at the NanoPhotometer and then sored at -20 ºC.

2.7. Evaluation of PHB accumulation

2.7.1. Experiment to evaluate the PHB production

From the precultures grown to ~0.3-0.4 OD was inoculated 0.8 mL in 50 mL MM medium and neomycin to 250 µg mL^{-1} final concentration was added before the inoculation for the mutants. The cultivation was done for the mutants and the negative control (*M. margugensis Δhpt*) at 55°C in a shaker incubator (GFL 1083 Water Bath) at 170 rpm and with a H_2/CO_2 (4:1) atmosphere with a pressure of 3 bar relative. Growth was observed by measuring the OD with a SPECORD 200 Plus spectrophotometer at 578 nm. Before every OD measurement, the pressure in the bottle was measured with a digital manometer (Keller LEO1 Pressure Gauges) and after taking the ample for the OD, the pressure was readjusted to 3 bar realtive pressure with H_2/CO_2 (4:1). After 10 days of incubation for PHB accumulation, the cultures were harvested by centrifugation at 10,000 × g for 20 min. The supernatant was removed, and the cell pellet was flash-frozen in liquid nitrogen for later LC-MS measurements.

2.7.2. Boron-dipyrromethene (BODIPY) staining for PHB granule identification

The slides were coated with poly-L-lysin 0.01% (v/v) and incubated at RT for 15 min. The slides were washed with MQ water and dried at 46°C in a static incubator. The samples for the cultures for which the OD was measured, were diluted in 1x Phosphate Buffered Saline (PBS) to a final OD of 0.05 with a 50 µL final volume. In a dark room, 1.6 µL of BODIPY stain solution was mixed with the samples and incubated for 5 min in the dark. After the incubation, the samples were pipetted on the slides and left to dry at 46 ºC. When the slides were sufficiently dry, 10 µL of Vectashield (Vector Labs) was added on the slides and covered with cover slides. The samples were viewed under Nikon Eclipse Ni microscope using a lens for the phase contrast imaging, and a Nikon Alexa 488 nm lens for the BODIPY staining with the light coming from a Nikon Intensilight C-HGFI. The pictures were taken using a ProgRes MF camera (Jenoptik, Jena, Germany) attached to the microscope. The images were analysed and processed in Fiji (ImageJ) Software.

2.8. Data analysis and statistics

The data measurements from the NADH/NADPH assays and growth experiments were collected and processed in Microsoft Excel 365 for the normalisation of the data and calculation of the activity reporting to the NADH/NADPH consumption To calculate the NADH/NAPHA concentration from the absorbance data we followed the Lambert Beer law and used following equation: $c = A/(\varepsilon \times l)$ in which c represent the concentration in mol L^{-}

[1], A is the absorption measured at 340 nm, ε is the molar absorption coefficient (which is 6,220 L mol^{-1} cm^{-1} for NADH/NADPH at 340 nm), and l is the cuvette path length (which is 1 cm). The results were further multiplied by 1,000 to express the concertation in mmol L^{-1}. The calculation of the specific activity for each enzyme is shown in Annex 2.

The graphs and statistical analysis were made with Jupyter notebook (python version 3.12). The script for NADH/NADPH specific activity comparison are shown in Annex 3 in which the data was pretested with Shapiro-Wilk test for normal distribution and with F-test for equal variance, before using a Welch-t-test to compare the two activities of the same enzyme. Annex 3 also includes the script for the OD measurements and pressure measurements data analysis, in which the data was pretested with Shapiro-Wilk test for normal distribution and with Levenne's test for equal variance, before using the Dunnett test to compere the mutants with the negative control strain, *M. marburgensis Δhpt*.

3. Results

3.1. Constriction of the pET28a-T7_*PhaB*$_{(Jap)}$

The pET28a linearized backbone (5676 bp) and the linearized *PhaB*$_{(Jap)}$ (770 bp) were successfully synthetised and showed the right size on the gel (*Figure 4*). After purifying the fragments form the gel, they were assembled using a 4 (insertion fragment) to 1 (backbone) ratio to prevent the recircularization of the vector. Correct insertion in colonies was verified by PCR using T7-region primers, yielding a 907 bp amplicon when the PhaB(Jap) insert was present. In the gel (*Figure 5a*) only 1 colony showed positive signal, and this was picked to be preserved and for the extraction of the plasmid. The plasmid was sequenced at Plasmidsaurus and the results confirmed the successful transformation BL21(DE3), which is also visible in a good transformation signal for all the colonies analysed by PCR colony with T7 primers (*Figure 5b*).

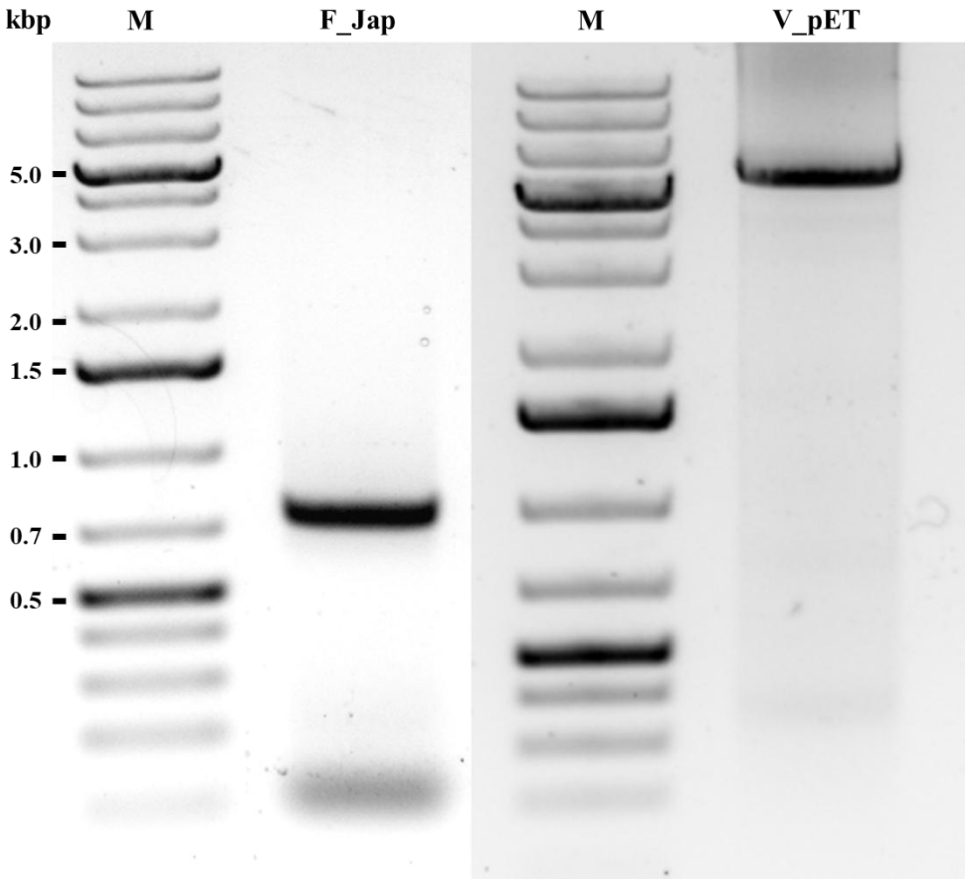

Figure 4. Agarose gel (1%) showing the sizes of the PCR-amplified *PhaB*$_{(Jap)}$ fragment (F_Jap) and the PCR-linearized pET28a backbone (V_pET) for Gibson assembly.

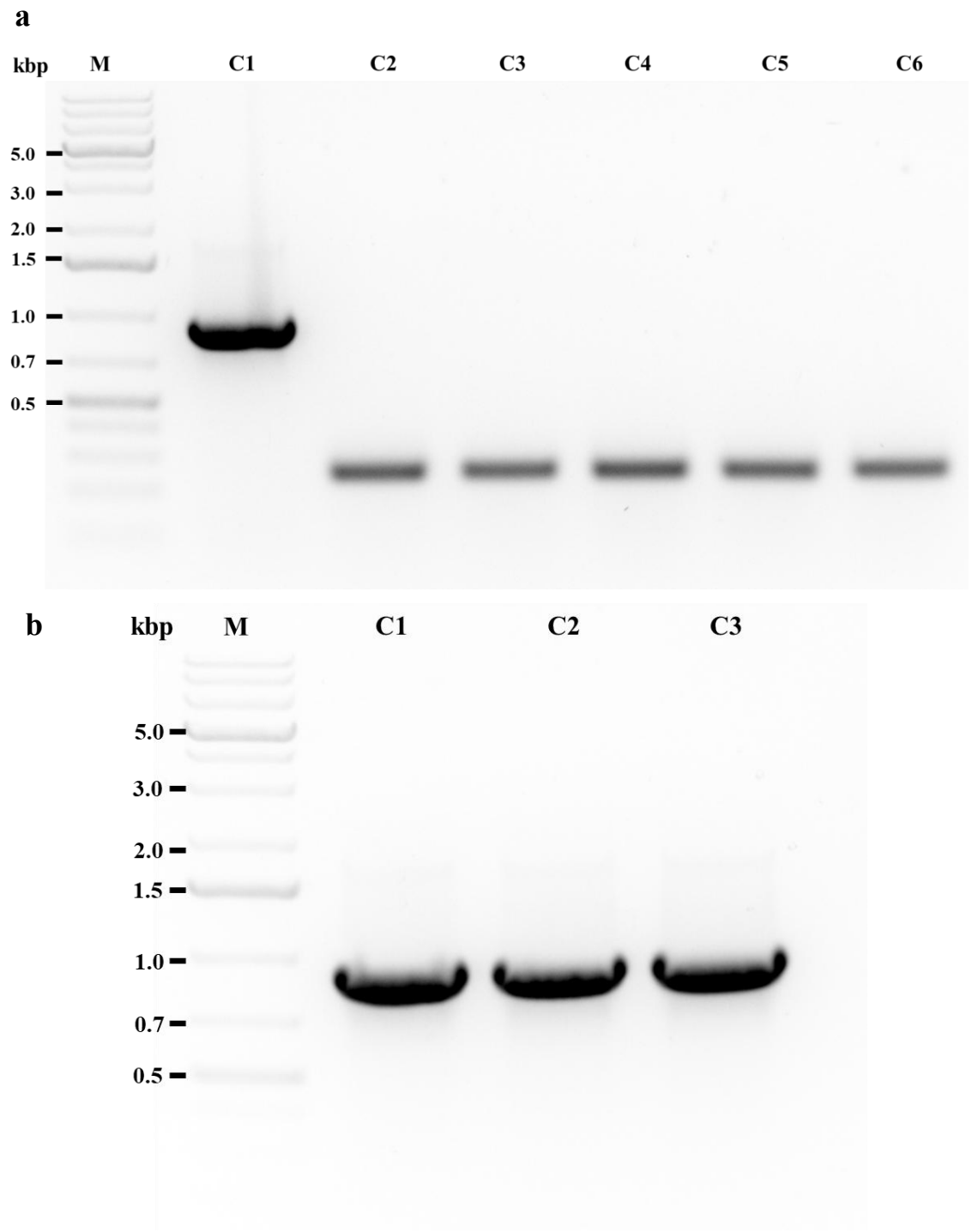

Figure 5. Colony PCR confirming successful transformation of **(a)** *E. coli* TOP10 and **(b)** *E. coli* BL21(DE3) with the pET28a-*PhaB*$_{(Jap)}$ construct using T7 primers. Lanes C1–C6 denote individual colonies.

3.2. Activity profiles of the investigated PhaB using different cofactors

The activity of the PhaB$_{(Jap)}$ was not described in the literature, so its activity was tested with NADH or NADPH as cofactor to be compared with the activities of PhaB$_{(Ther)}$ and PhaB$_{(Chim)}$. To achieve this, PhaB$_{(Jap)}$ was overexpressed using the BL21(DE3) transformed

with the assembled pET28a-T7_*PhaB*$_{(Jap)}$ to obtain the protein lysate. The PhaB$_{(Jap)}$ protein lysate obtained was compared with the PhaB$_{(Ther)}$ and PhaB$_{(Chim)}$ protein lysates in an SDS-PAGE gel (*Figure 6a*) to indicate their size and to contrast the protein abundance for normalization of the activity. It can be seen that PhaB$_{(Ther)}$ was very well expressed and PhaB$_{(Jap)}$ as well, but in the case of PhaB$_{(Chim)}$ there seems to be a low concentration in the lysate.

The protein lysates were used to perform NADH/NADPH assays showing us the difference in activities and preferences of the PhaBs (*Figure 6b*). Our experiment confirmed the high affinity of the PhaB$_{(Ther)}$ for NAHPH, showing the highest activity from all conditions,

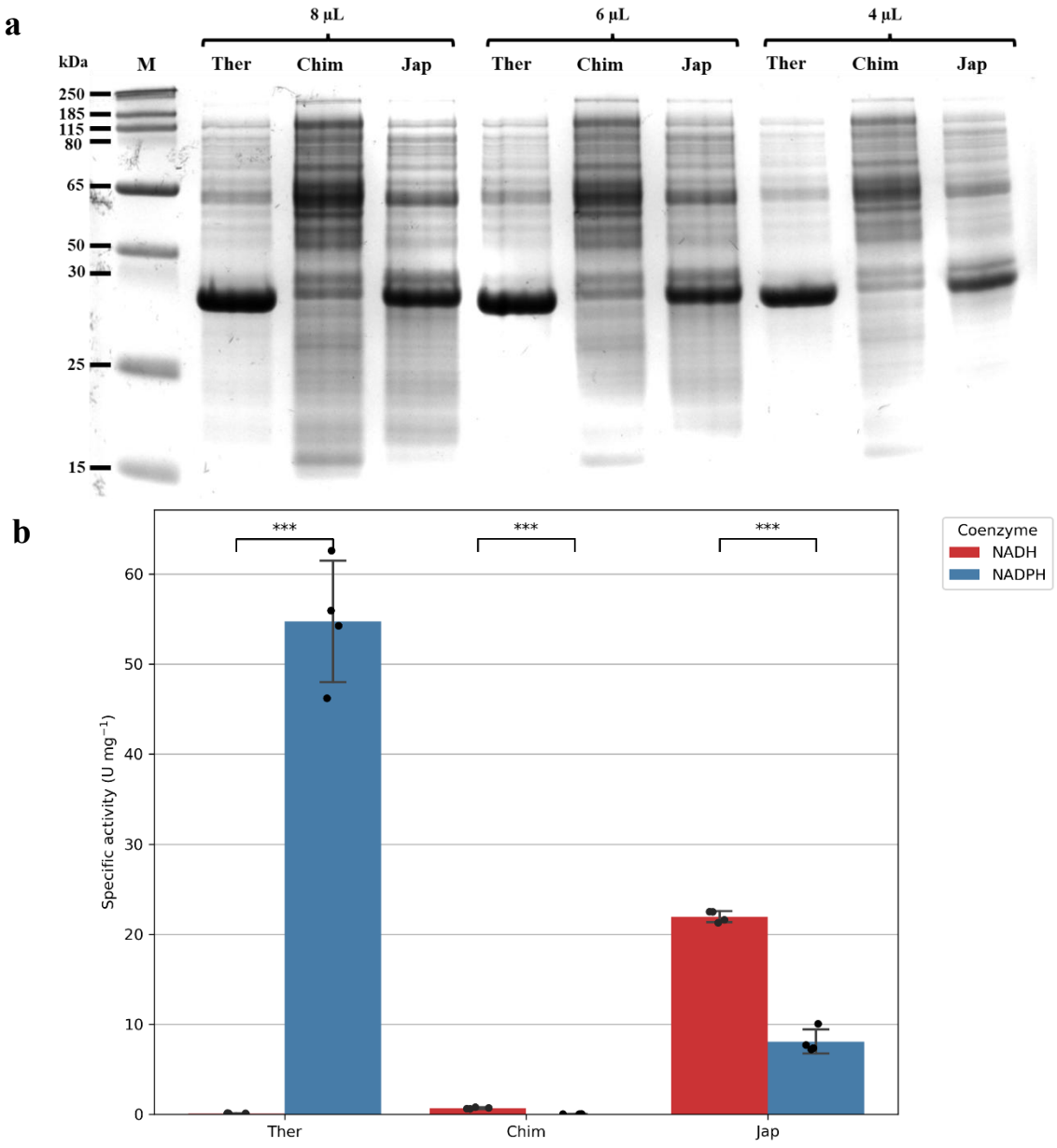

Figure 6. Characterization of lysates expressing PhaB$_{(Ther)}$, PhaB$_{(Chim)}$, and PhaB$_{(Jap)}$; **(a)** SDS-PAGE of increasing lysate loads. **(b)** Comparison of specific activities with different coenzymes (*** = p value < 0.001; ** = p value < 0.01; * = p value < 0.05; ns = non-significant).

with an average of 54.75 U mg^{-1}, but it is almost not active with NADH (0.09 U mg^{-1}). $PhaB_{(Jap)}$ had a high affinity for NADH indicated by the high activity with NADH of 21.96 U mg^{-1}, compared with the avenge activity of 8.07 U mg^{-1} with NADPH. The activity of the $PhaB_{(Chim)}$ was low compared to the other enzymes but still has a better activity with NADH (0.67 U mg^{-1}), compared to a negliable activity with NADPH (0.01 U mg^{-1}).

3.3. Confirmation the pArk-*PhaABC* vectors

The synthetic *PhaABC* (with the genes from C. thermodepolymerans) construct that was ordered was used for the creation of the first pArk-*PhaABC*. However, the first transformation with the ligation mix failed in Top10 *E. coli*, and hence it was decided to try to use DH5α *E. coli* strain that should better support the transformation of a plasmid with significant size (11,079 bp). With DH5α, more colonies were obtained, and after extracting the plasmid and cutting with restriction enzymes, it was identified on the gel (*Figure 7*) that colony 1 and colony 5 should have possessed the correct construct by comparing the cutting pattern with the pattern predicted with Snapgene simulation for the cutting of the desired pArk-*PhaABC*. The sequence of the constructed pArk-*PhaABC* was confirmed by the Plasmidsaurus results and was used for the transformation in S17-1 *E. coli*. With the same method of digestion, the colonies of S17-1 were shown to possess the right plasmid (*Figure 8*).

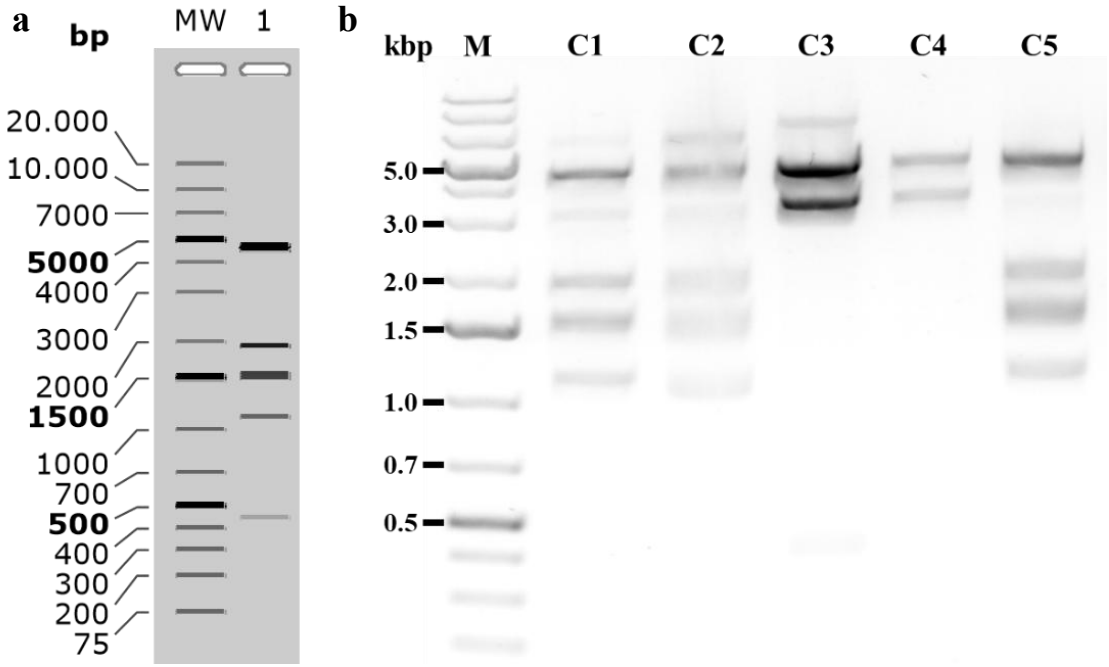

Figure 7. Restriction digest analysis of pArk-*PhaABC* confirming correct assembly; **(a)** In silico digest predicted in SnapGene for KpnI and XhoI; **(b)** Diagnostic KpnI/XhoI digest of plasmids isolated from *E. coli* DH5α colonies.

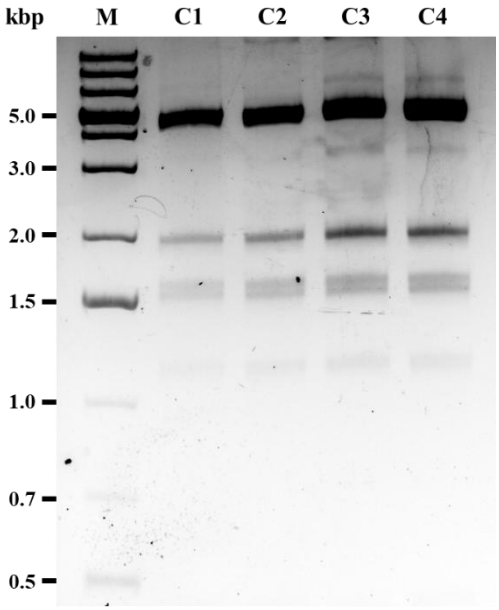

Figure 8. Screening of *E. coli* S17-1 colonies for the pArk-*PhaABC* plasmid by KpnI/XhoI digest.

The assembled pArk-*PhaABC* that contains the $PhaB_{(Ther)}$ gene can be used versatilely to exchange the *PhaB* gene with other variants. The first procedure attempted was replacing $PhaB_{(Ther)}$ with the chimeric variation $PhaB_{(Chim)}$ that had been chosen (Chimera II-vin). Because different restriction enzymes that could cut and distinguish between *PhaB*s were not available, a primer specific for the nucleotide change in the Chimera II was used in combination with a primer for a region in the $PhaA_{(Ther)}$ sequence, resulting in a PCR fragment of 1,012 bp. The pArk-*PhaABC* and the $PhaB_{(Chim)}$ were assembled after a PCR purification of the reaction, without separating the backbone (pArk-*PhaAC*) from the cut fragment

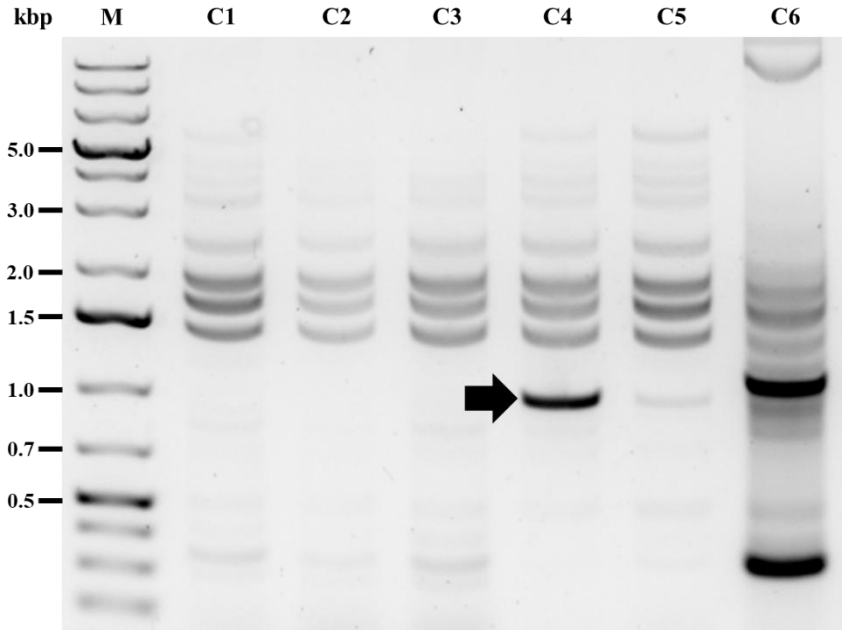

Figure 9. Colony PCR of *E. coli* DH5α transformants verifying the pArk-$PhaAB_{(Chim)}C$ construct; The arrow marks the expected *PhaAB* amplification product.

(*PhaB*$_{(Ther)}$). After the transformation into DH5α, colonies were picked and checked using the above described primers for the verification of the plasmid on the agarose gel (*Figure 9*). These PCR results showed that the primers used in this combination were not specific, and a lot of non-specific bands were observed that may have contaminated the reaction. Despite that, colony 4 showed promising development and it was decided to send it to be sequenced. The results confirmed that this colony contained the desired pArk-*PhaAB*$_{(Chim)}$*C* construct. After purification of the plasmid, this was used to transform the S17-1 cells to be used for conjugation.

For the replacement of *PhaB*$_{(Ther)}$ with *PhaB*$_{(Jap)}$, a different approach was used for the exchange procedure. The first step was the PCR amplification of the ordered *PhaB*$_{(Jap)}$ construct and the purification of a high-concentration pArk-*PhaABC* sample. Both were cut with restriction enzymes, and after complete digestion all the reaction volume was loaded and migrated on an agarose gel (*Figure 10a*) to separate the pArk-*PhaAC* backbone (10,152 bp) and the *PhaB*$_{(Jap)}$ fragment (930 bp). The band for the indicated signal was cut and purified, and the generated linearized DNA fragment was used for the assembly of the plasmid and transformation into DH5α competent cells. Grown colonies were checked using primers for the PhaA region and the end region of the PhaB region, resulting in a fragment of 1,695 bp. Both colonies investigated on the gel presented the signal (*Figure 10b*). Colony 1 was chosen, and sequencing confirmed the presence of the *PhaB*$_{(Jap)}$ in the pArk-*PhaAB*$_{(Jap)}$*C*. This construct was also transformed into S17-1 cells to be used for conjugations.

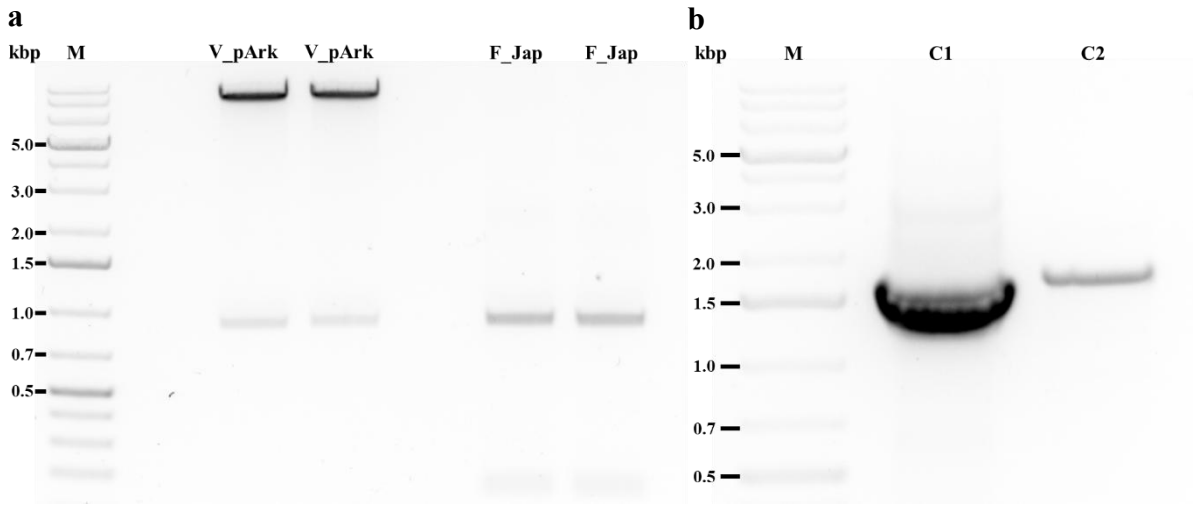

Figure 10. Construction of pArk-*PhaAB*$_{(Jap)}$*C* by inserting *PhaB*$_{(Jap)}$ into pArk-*PhaAC*; **(a)** pArk-*PhaAC* vector (V_pArk) and *PhaB*$_{(Jap)}$ fragment (F_Jap) digested with MfeI and PacI; **(b)** Colony PCR confirming pArk-*PhaAB*$_{(Jap)}$*C* in *E. coli* DH5α.

3.4. Successful integration of the *PhaABC* genes into the genome of *M. marburgensis* and isolation of the mutants

M. marburgensis Δhpt can be distinguished from the wild-type or other mutants using primers that were on the outside of the *hpt* up (O_up) and down (O_down) regions, which generates by PCR a fragment of ~2.2 kbp (*Figure 11*). These primers could also be indicating the presence of insertions, generating bigger fragment in this case, as also used for confirming mutants by Klein et al. (2025). In our case, the insertion of the neomycin resistance gene, *hpt* gene and the *PhaABC* operon will generate a distance between O_up and O_down primers too large to obtain a complete fragment using the same PCR procedure. In this way, the absence of the signal would indicate the probability of an insertion in our case. Other primer combinations were checked that would facilitate obtaining a PCR signal for the mutants. It was found that the use of a primer for the *hpt* gene from the plasmid (I hpt) and the O_down primer gave the best results, confirming the double homologous recombination event by the presence of a ~1.7 kbp fragment (*Figure 11*). This was done to ensure that the genes for the new metabolic pathway are also kept. In PCR testing, primers for the *PhaB* sequence that will give a ~0.9 kbp signal were used, or the primer combination for a region on *PhaA* to the end of the *PhaB* was used, generating a fragment of ~1.7 kbp (*Figure 11*).

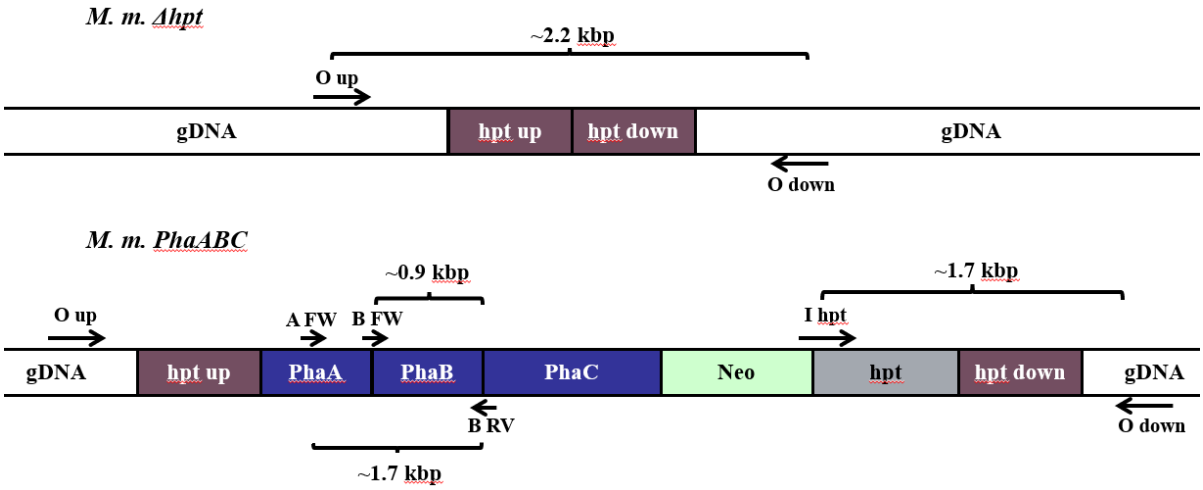

Figure 11. Schematic representation of fragments amplified by PCR to confirm integration of the *PhaABC* operon into *M. marburgensis* genome.

The PCR results showed us that signal for the *Δhpt* it is present in the first 2 transfers, but the reduced signal in the second transfer is a sign that the mutants are more abundant and this can be just sighs if DNA remains from the other transfers. The first positive results for the transformations were obtained with the pArk-*PhaAB*$_{(Chim)}$*C* and are represented in the *Figure 12a*. On the PCR gel, it can be observed that the signal for *Δhpt* was completely lost, and the

signals that indicate the transformation were still present. The signal for the recombination was not high in the recovery sample, which could be because of the low DNA concentration of the mutant in that culture. The mutants managed to grow and overcome the *Δhpt* only in the selective medium. Transfer 2 was used to generate single colonies of *M. marburgenis* that were picked and checked the purity of the *M. marburgensis PhaA*$_{(Ther)}$ *PhaB*$_{(Chim)}$ *PhaC*$_{(Ther)}$ mutant cultures (*Figure 12b*). The final step before preservation of the mutant was to sequence the genome of a culture from a positive colony, and this gave confidence that the genetic modification took place in the intended way, and that the genes are the same.

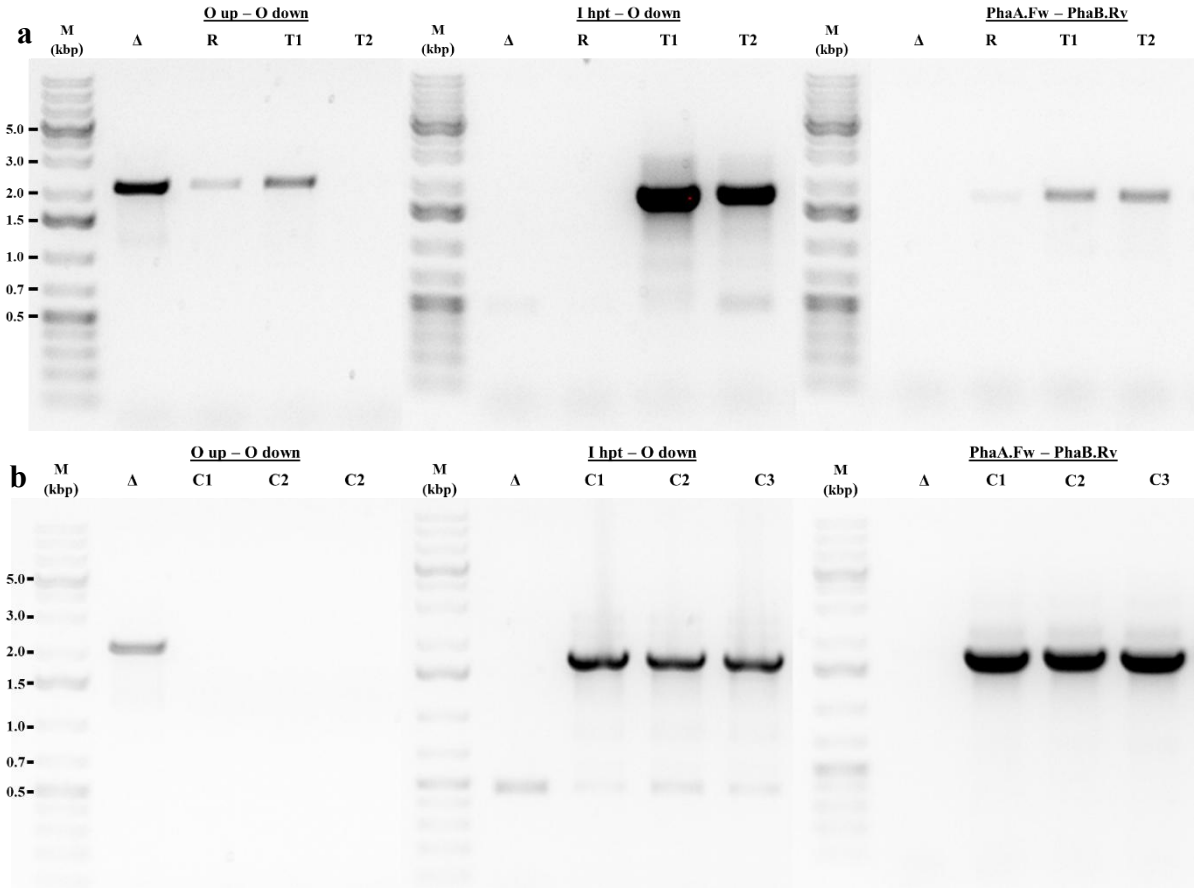

Figure 12. Agarose gels of the PCR analysis of *M. marburgensis* Chim mutants; **(a)** Conjugation results; **(b)** Single colonies culture integration purity analysis (Δ = *M. marburgensis Δhpt* control culture; R = recovery culture; T = selective enrichment; C = single colony culture).

The second positive results were from 2 different transformation transfers with pArk-*PhaAB*$_{(Jap)}$*C*. The agarose gel (*Figure 13a*) indicates that the first transfer still has high signal for *Δhpt* in both, but in the second transfer the first transformation had a more reduced signal. In this way, it was decided to use the second transfer from the first transformation to generate single colonies, and so the *Δhpt* signal might be completely lost. From the single-colony cultures, C1 and C2 completely lost the *Δhpt* signal (*Figure 13b*), indicating that pure mutant strains are present. By also looking at the signal for the *PhaB* gene, C1 showed a stronger

signal, so it was decided to preserve and use that culture. From that culture, a DNA sample was sent for sequencing to ensure that the *PhaB* gene is the same as the *C. japonicum* gene that was used for the transformation.

The last mutants confirmed were from the transformation with the pArk-*PhaAB*$_{(Ther)}$*C*. On the agarose gel, it was shown that the *Δhpt* signal was almost lost in the second transfer (*Figure 13c*), and that single colony selection could be continued. From the single-colony cultures, really good signals were obtained (*Figure 13d*), confirming that these are mutants. The later sequencing of the *PhaB* gene confirmed that it is present and is the desired one.

In the end of the conjugation experiment, *M. marburgensis PhaA*$_{(Ther)}$ *PhaB*$_{(Ther)}$ *PhaC*$_{(Ther)}$, *M. marburgensis PhaA*$_{(Ther)}$ *PhaB*$_{(Chim)}$ *PhaC*$_{(Ther)}$ and *M. marburgensis PhaA*$_{(Ther)}$ *PhaB*$_{(Jap)}$ *PhaC*$_{(Ther)}$ mutant strains were obtained, which, for readability, will hereafter be referred to as *M. marburgensis* Ther, *M. marburgensis* Chim and *M. marburgensis* Jap respectively.

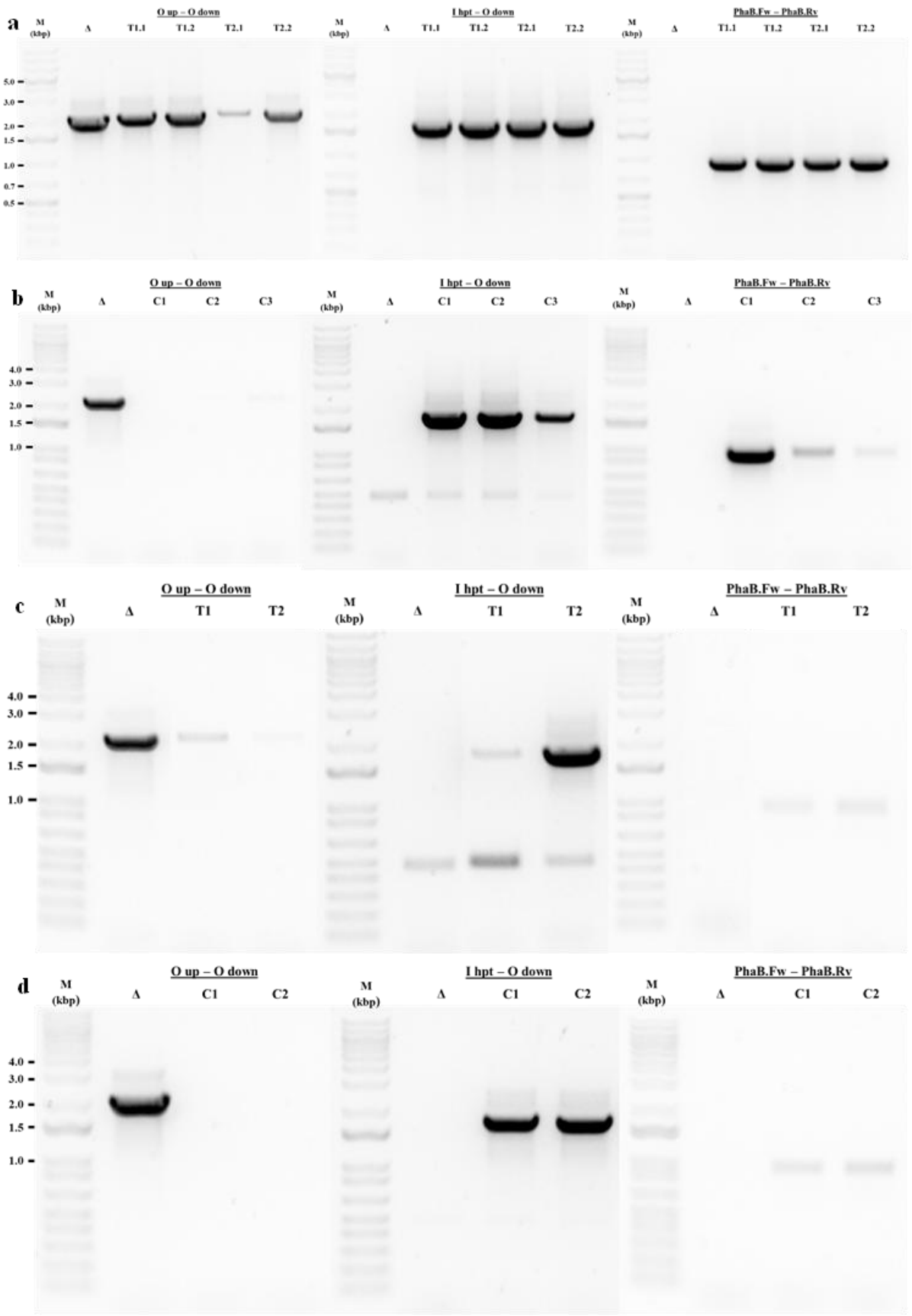

Figure 13. Agarose gels of the PCR analysis for *M. marburgensis* mutants; **(a)** Conjugation results for and **(b)** single colonies culture integration purity analysis for *M. marburgensis* Ther; **(c)** Conjugation results for and **(d)** single colonies culture integration purity analysis for *M. marburgensis* Jap (Δ = *M. marburgensis Δhpt* control culture; R = recovery culture; T = selective enrichment; C = single colony culture).

3.5. Growth comparison of the mutants

To investigate if the obtained mutants would be different in growth compared to the control strain (*M. marburgensis Δhpt*), it was decided to set up an experiment in which each mutant will be grown and a negative control included for 10 days. In this experiment the cultures were provided with sufficient H_2/CO_2 feeding in the first 3 days to maintain a high exponential growth and letting them stay longer in the stationary phase for further observation of their ability to accumulate PHB. The temperature was set to 55 ºC to ensure the thermostability of the proteins that come from organisms that grow at a maximum of 55 ºC. The resulting growth curves of the 4 strains can be seen in *Figure 14*, which showed that the mutants seem to grow better in the conditions of the experiment but with a really high standard deviation of the growth of mutants. In order to visualise the behaviour of each replicate, the individual growth curves for each strain were plotted to represent the high variability that was present in this cultivation setup as well (*Figure 15*). It was observed that some cultures reached the plateau phase early from the same strain, otherwise having similar growth behaviour. This seems to be a common behaviour of methanogens, that show high variability in the OD reached in the same condition.

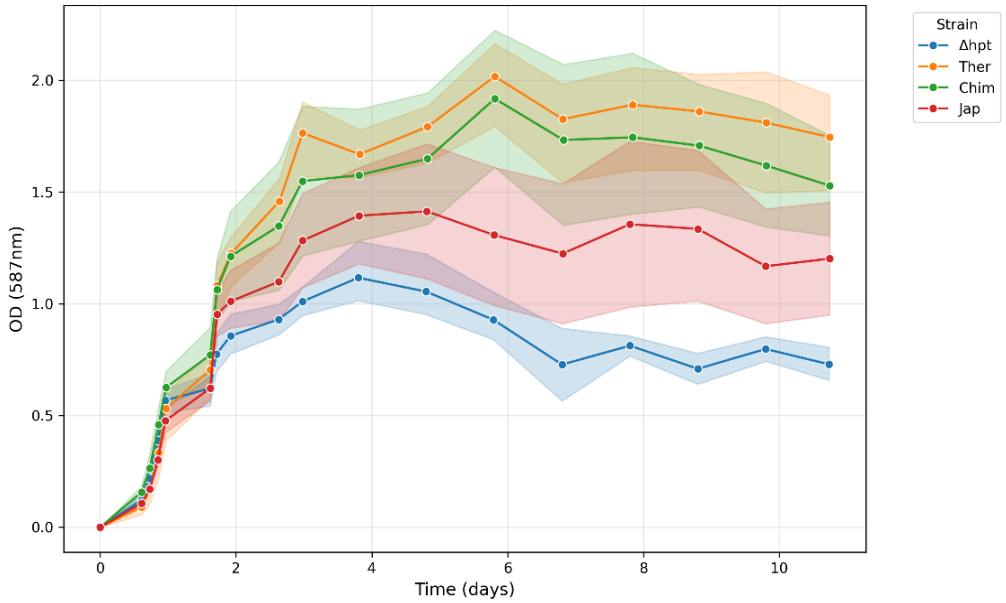

Figure 14. Growth of *M. marburgensis* variants (Ther, Chim, Jap) compared to the *Δhpt* control.

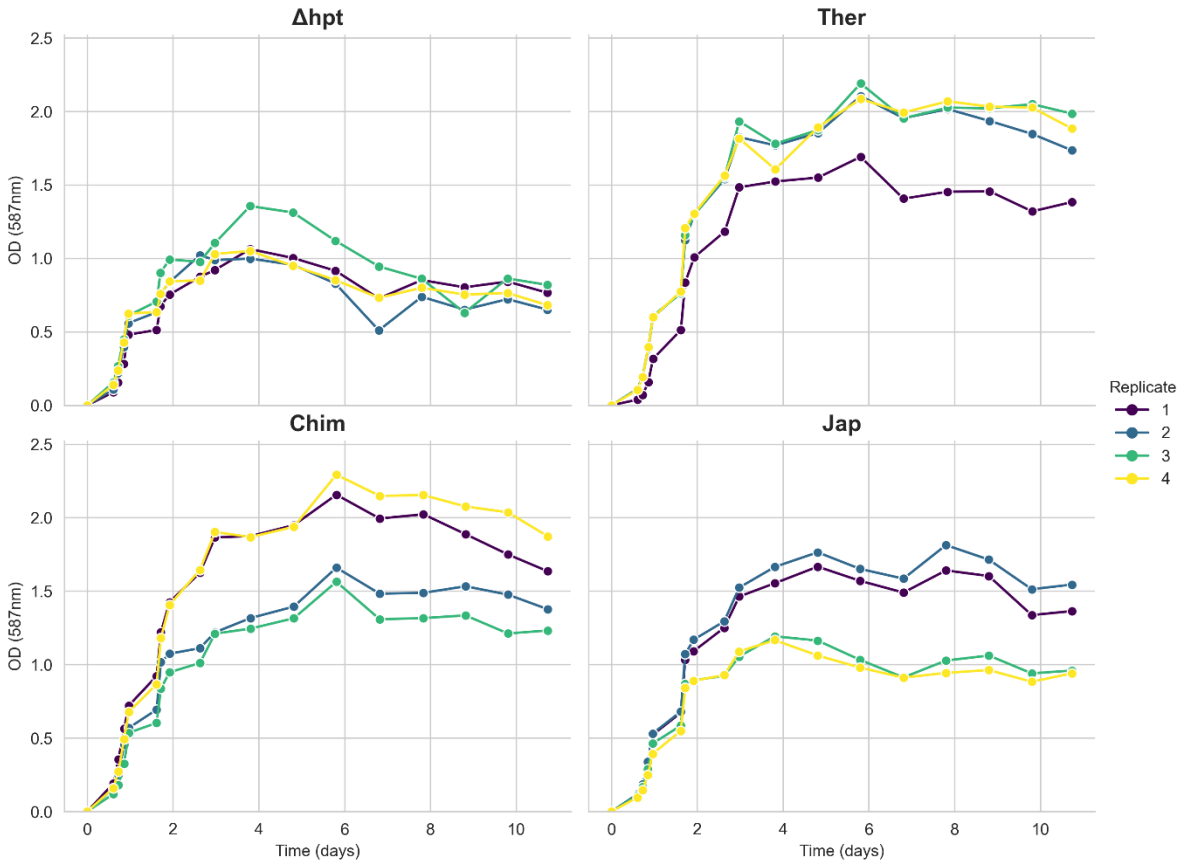

Figure 15. Growth curve comparison for *M. marburgensis* strains (Δhpt, Ther, Chim, Jap), showing individual growth curves (n = 4) for each strain.

For a better representation of the different stages of the cultivation, the specific growth rate in the exponential growth phase, the decay rate, and the final OD of the cultures were used to make comparisons. The specific growth rate was calculated for the first day of cultivation, during which the cultures grew rapidly. In this aspect, no significant differences for the mutants compared to the control were observed. The Dunnett test indicated no significant statistical difference (p-values: 0.061 Ther-control; 0.157 Chim-control; 0.851 Jap-control), suggesting that the introduced modification did not significantly affect their growth capabilities (*Figure 16a*).

An interesting aspect is that the mutants seem to resist better to the limiting conditions set in this experiment. The mutants are growing longer and reach higher OD compared with the control. After reducing the amount of feeding per day to 1 time, the mutants were resisting better under the stress, and they didn't lower there OD so quickly. The decay rate was determined by the slope of the line starting from the fourth day of incubation, when feeding was provided only once per day, ending with the last measurement before harvesting. The decay rate indicated that the mutants survived better during this experiment with a significant difference in the case of *M. marburgensis* Ther and *M. marburgensis* Chim (p-values: 0.008

Ther-control; 0.048 Chim-control; 0.252 Jap-control), that have the p-value of the Dunnett test under 0.05, but not an significant p-value for *M. marburgensis* Jap (*Figure 16b*).

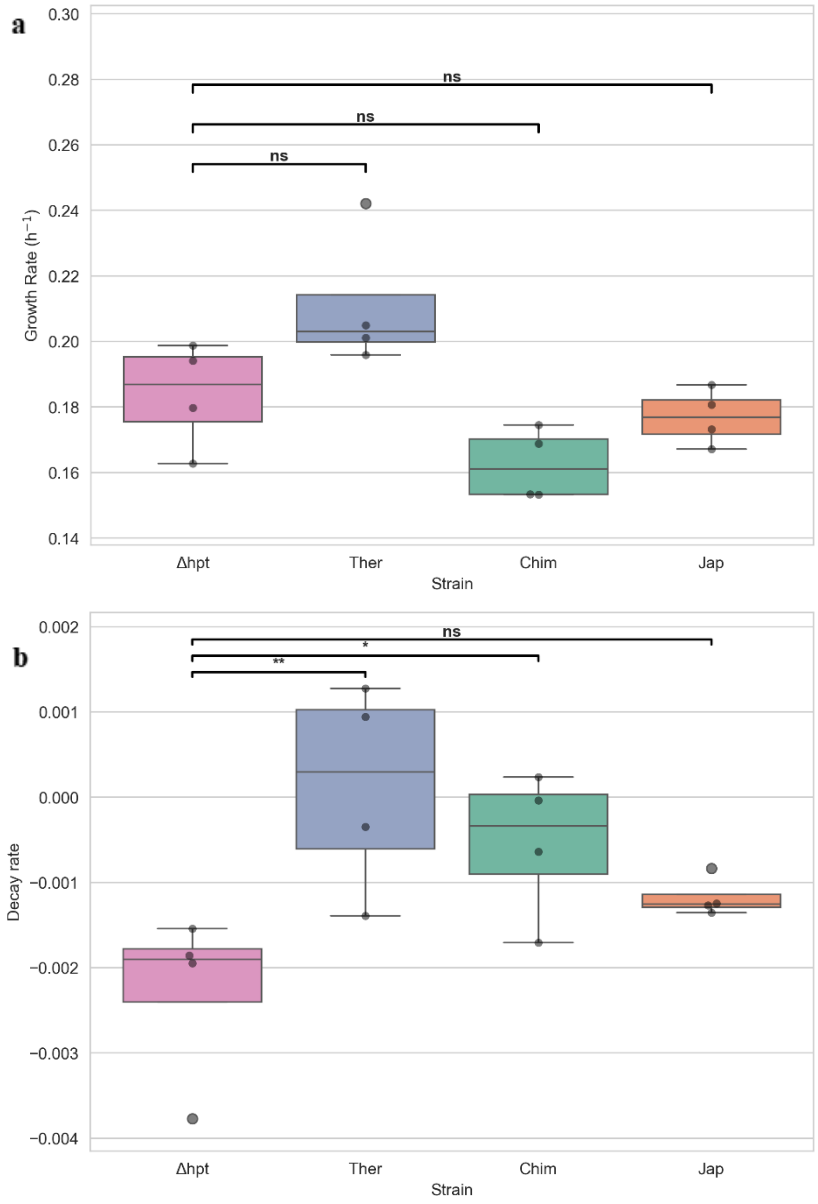

Figure 16. Comparison of mutant strains to the control for **(a)** growth rate during the high-feeding phase and **(b)** decay rate under once-daily feeding; significance assessed by Dunnett's test (*** = p value < 0.001; ** = p value < 0.01; * = p value < 0.05; ns = non-significant).

The biggest difference is represented by the final OD, in which all the mutants performed way better than the control, where all replicates have an OD under 0.9, that are lower than the OD of every mutant replication (*Figure 17*). The best performing strain when it comes of final OD being *M. marburgensis* Ther, with the biggest difference to the control in the Dunnett test (p-values: 0.000 Ther-control; 0.002 Chim-control; 0.048 Jap-control).

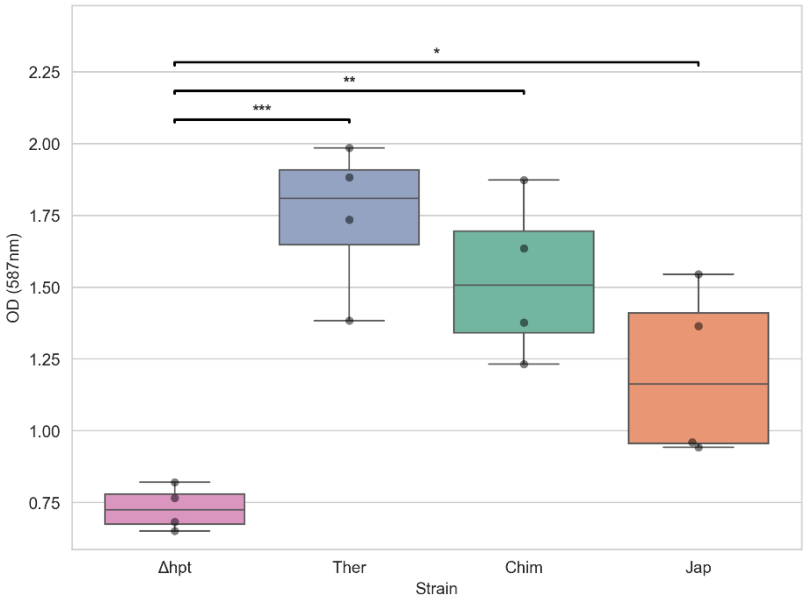

Figure 18. Comparison of the final OD_{587} achieved by mutant strains versus the control assessed by the Dunnett's test (*** = p value < 0.001; ** = p value < 0.01; * = p value < 0.05; ns = non-significant).

Another important aspect of the hydrogenotrophic methanogens growth is their gas consumption rate. The gas consumption was monitored by measuring the pressure in the bottles before taking the sample of the OD measurements, and after that refuelling the bottles to 3 bar overpressures with H_2/CO_2. The measurements were plotted to show how the gas consumption evolved during the experiment (*Figure 18*). Frome here a similar pattern of the OD evolution can be distinguished, in which the control stops to consume gas earlier than the mutants. The behaviours of individual replicate can be seen in *Figure 19*, and it is remarkable how in the same replicate, same mutants may reach liquid limitation quicker and stop

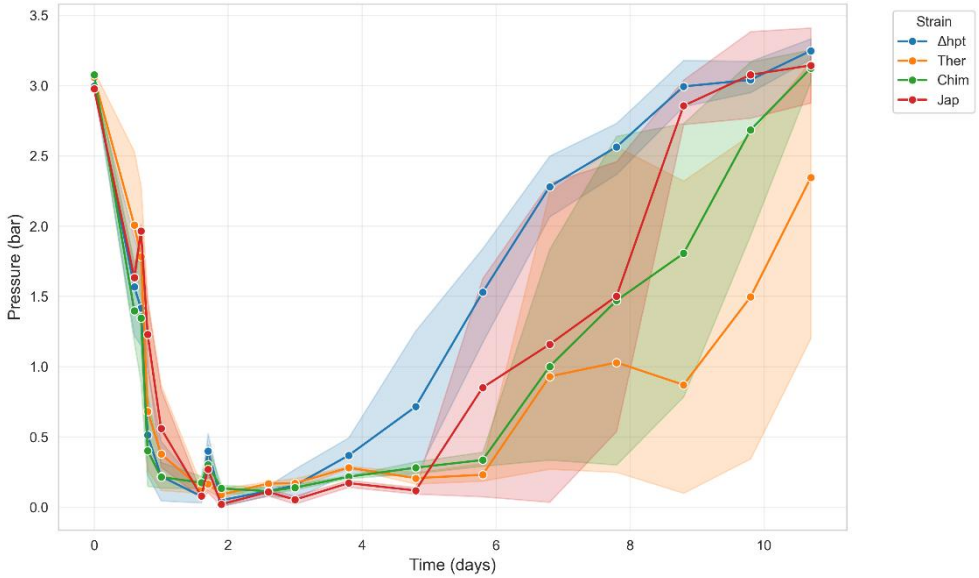

Figure 17. Gas consumption over a 10-day incubation for *M. marburgensis* mutants and the control strain.

consuming gas but still have better resistance to starvation and OD reached than the control. Looking at the *M. marburgensis* replicate, one culture stands out by still having a high consumption rate before the end of the experiment.

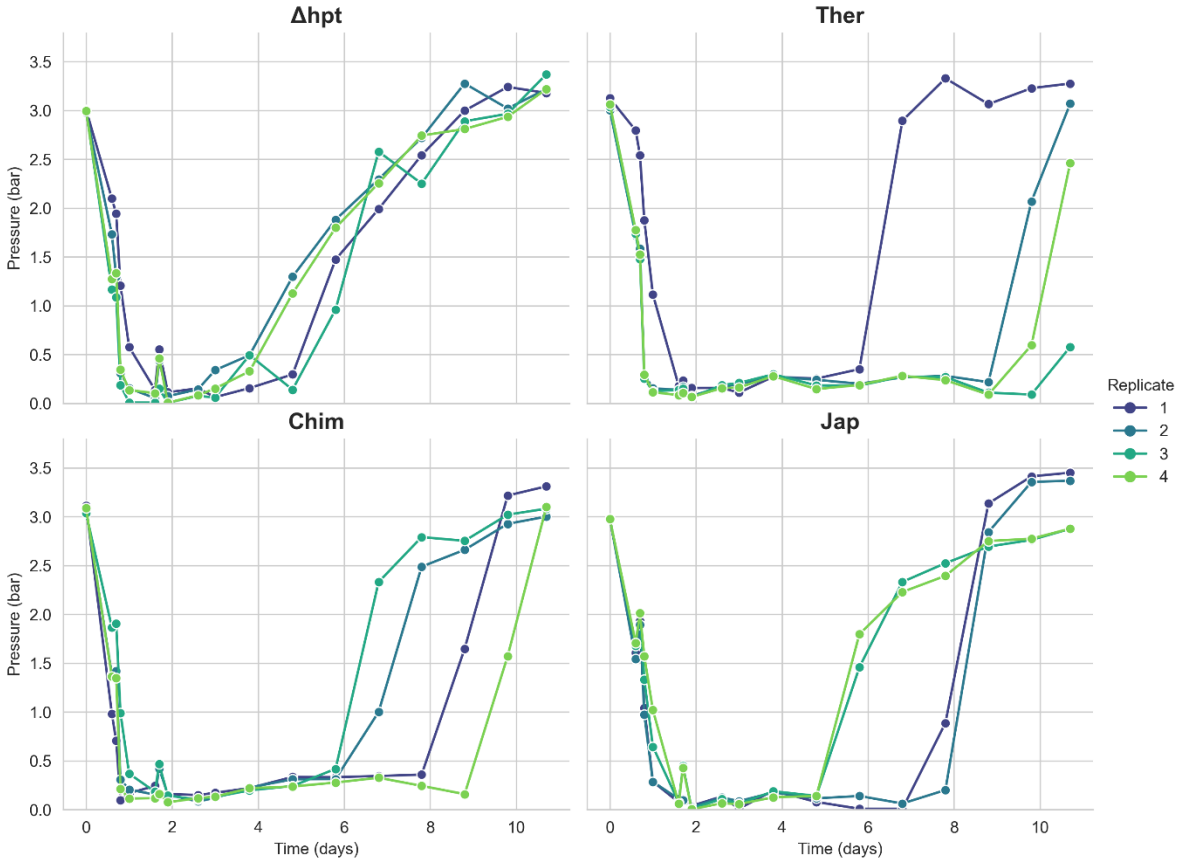

Figure 19. Individual replicate gas consumption data for each culture (n = 4).

3.6. Confirmation of PHB accumulation using BODIPY staining

The BODIPY staining is it an easy and quick technique to check for the potential PHB accumulation that is frequently used. In this case, samples were taken from the growth experiment to see signs of accumulation. In the screening test to adjust the BODIPY. In our screening test to adjust the BODIPY staining protocol for our culture. However, a signal has not been detected until only after a longer period of accumulation. In this way, only the accumulation of PHA from the 10th day of cultivation onwards, had been visualized. Representative images of the cultures form the microscope can be seen in the *Figure 20*, showing how the PHB accumulation in our cultures are visible.

The microscopy results shows that *M. marburgensis* Jap should be the best strain in accumulating PHB, with strong signal present in most of the cell, indicating that the activity of the PhaB inserted gives good results because of the NADH dependency. A strong signal

was also observed for *M. marburgensis* Ther, but only in a small number of cells. In the case of the *M. marburgensis* Chim strain, only a faint signal was observed in the cells, which cannot confirm whether it is the result of PHB granules starting to accumulate. This proves that the low activity of the $PhaB_{(Chim)}$ seems to be unsuitable for the accumulation of PHB.

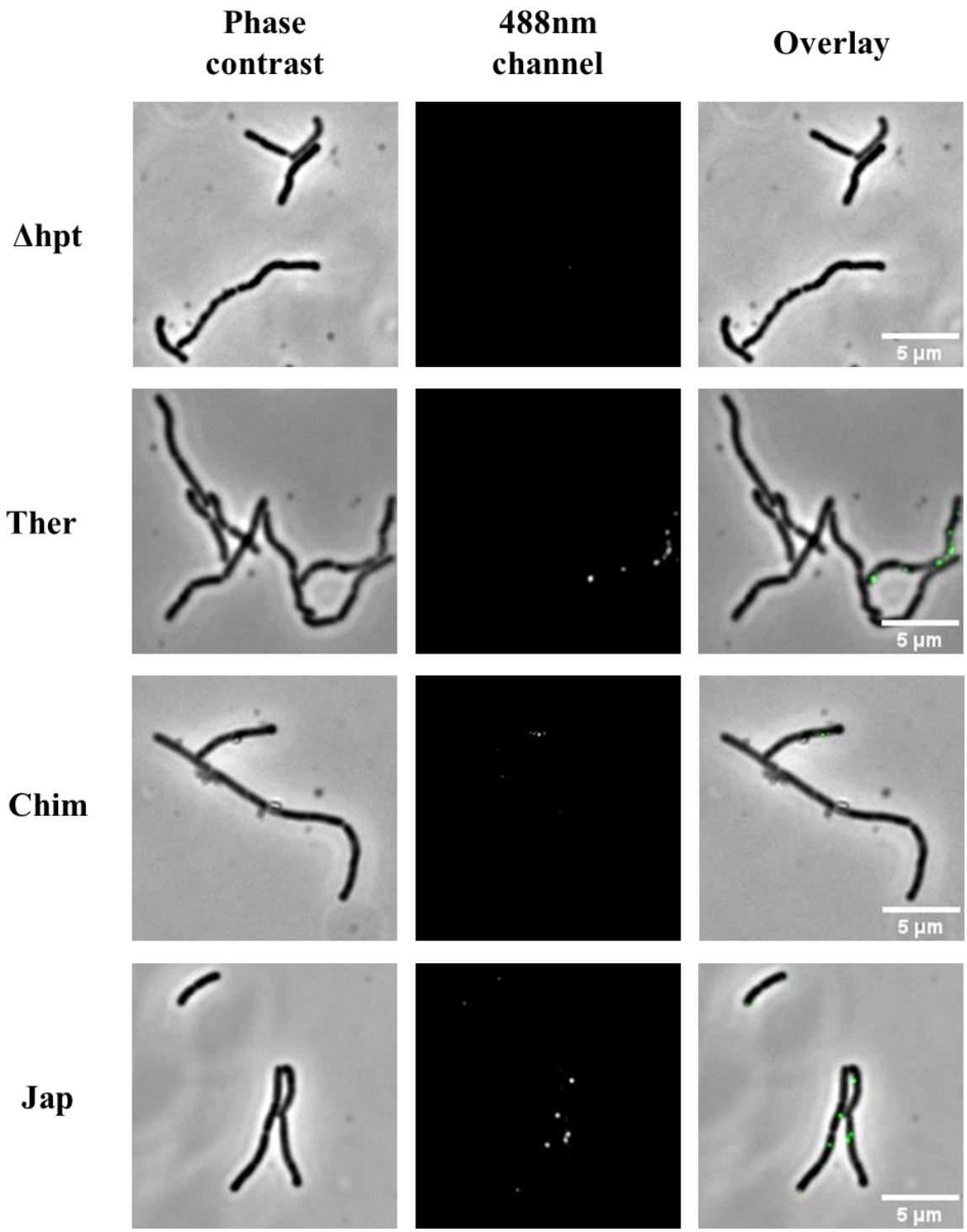

Figure 20. Microscopic images of *M. marburgensis Δhpt* and engineered mutants (*M. marburgensis* Ther, Chim, and Jap); PHB granules are visualized with BODIPY staining (488nm channel) and overlay of phase contrast, with the 488 channels.

The results described above are coherent and visible within images from all 4 replicates of the strains analysed. The representative images from every replicate are listed in the Annex 1, *Figure S2*.

3.7. PCR analysis of the extended grown cultures

To ensure that the mutants kept the modifications of the duration of the 10 days growth experiment, a PCR was performed from samples of the cultures. This should indicate whether the pattern is the same as the one investigated when the mutants were selected. In *Figure 21* is represented the agarose gel results from every replicate. The *Δhpt* culture appears to be strongly affected by the long incubation, because only one culture had enough DNA material to generate a specific *Δhpt* signal. The *Δhpt* signal is not present in the mutants and a strong signal for the *hpt* insertion is indicated the mutants, except for one replicate of the *M. marburgensis* Ther. This could be caused by the dying culture or by a pipetting error. Similarly, the signal for the presence of PhaA-PhaB fragment was visible in most of the samples, indicating that the genetic modification of the genome of *M. marburgensis Δhpt* was successful.

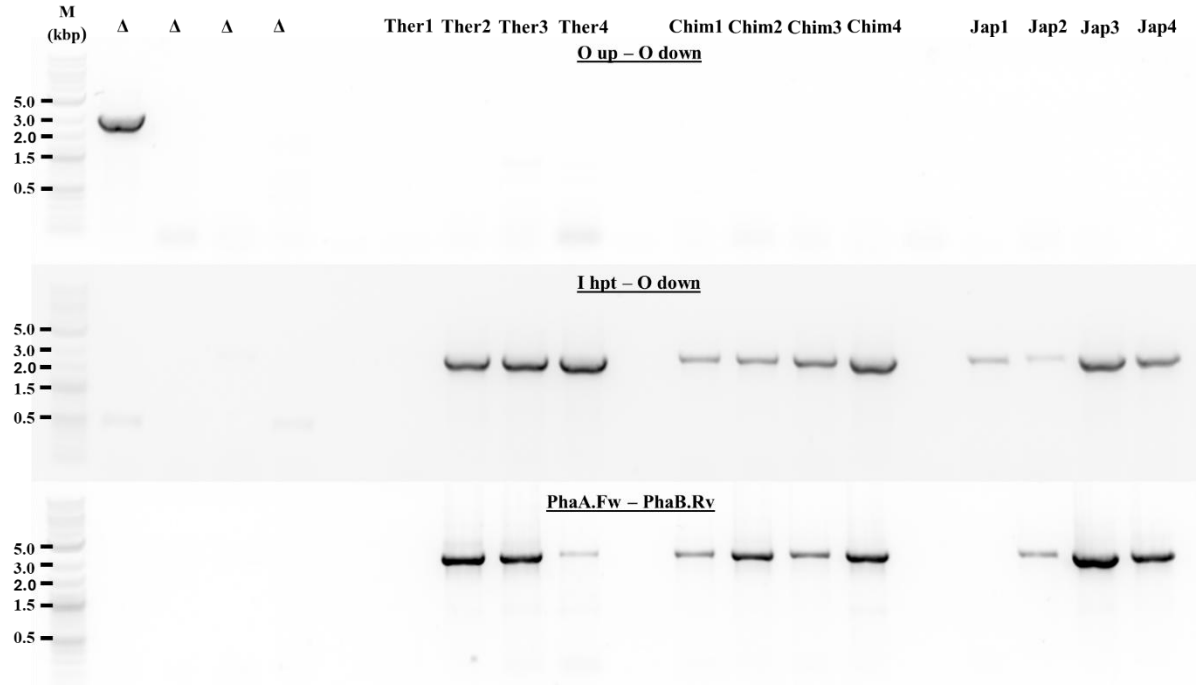

Figure 21. PCR analysis of *M. marburgensis Δhpt* and engineered mutants (*M. marburgensis* Ther, Chim, and Jap) after 10 days of growth.

3.8. Protein expression

The protein content of the samples taken from the growth experiments was examined to explore if there are any significant differences in the protein expression. The SDS-PAGE

gel after migration is shown in *Figure 22*. There are not specific bands in the gels that could show us the presence of our genes. Because the used promoter is not very strong, it prevents the overexpression and the ability to distinguish the PhaA, PhaB and PhaC proteins in our gels. The quality of the samples was proved to be poor, showing that, because many of the cultures were not in growing condition, a good representation of the proteins couldn't be seen. Additionally, the use of a precast Tris-glycerine gel had an atypical reaction with the loading dye and the Coomassie, resulting in the loss of visibility of the proteins in the lower part of the gel due to the colouring of the gel.

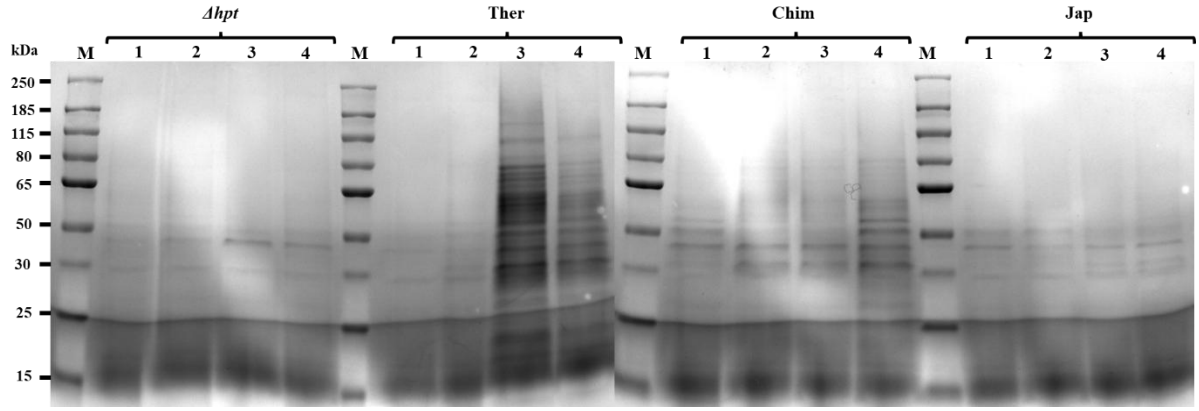

Figure 22. SDS-PAGE of protein lysates from *M. marburgensis Δhpt* and mutant strains (*M. marburgensis* Ther, Chim, and Jap) after 10 days of growth.

Discussion

NADH/NADPH-dependency of the investigated PhaB

The selection of *PhaABC* genes to transform *M. marburgensis* was an important part of this study. The PhaA, PhaB, and PhaC from *C. thermodepolymerans* were chosen because this organism is an established thermophilic PHB producer, which suggested thermostability of the proteins (Zhou et al., 2023; Jang et al., 2026). $PhaB_{(Ther)}$ was defined by Zhou et al. (2023) as NADPH-dependent, which was also demonstrated in the enzymatic assays of Liu (2025). The activity of $PhaB_{(Ther)}$ shown in *Figure 6b* supports the same dependence with the buffer described in materials and methods. It can be concluded that $PhaB_{(Ther)}$ activity with NADPH of 54.75 U mg^{-1} at pH 7.2 is very high compared with the 1.69 U mg^{-1} reported by Liu (2026) using a buffer at pH 8.0. However, the NADH activity did not increase significantly (0.09 U mg^{-1} at pH 7.2 vs 0.03 U mg^{-1} at pH 8) (Liu, 2026). This is a good indication that $PhaB_{(Ther)}$ would also work properly in *M. marburgensis*, which prefers extracellular neutral pH (Rittmann et al., 2012).

Another large improvement in activity was determined for Chimera-II-vin with NADH (0.67 U mg^{-1}) in the pH 7.2 buffer, compared with the activity reported by Liu (2025) (0.05 U mg^{-1}). This suggests that this chimera may have NADH activity, especially since the NADPH activity was unchanged (0.01 U mg^{-1} at pH 7.2 and 0.01 U mg^{-1} at pH 8.0) (Liu, 2026). Even with these improvements, the relative activity is substantially lower compared to the other PhaB investigated and may not be sufficient to observe PHB accumulation. It was shown that the strategy for changing cofactor dependency described by Olavarría et al. (2022) worked, but with significant limitations for the chimeras generated from $PhaB_{(Ther)}$ by Liu (2026). This could be due to differences in PhaB structure between *C. necator* and *C. thermodepolymerans*, or other unknown structural features that affect the NADH/NADPH binding site, besides those shown in the *Figure 23* (Ling et al., 2018; Olavarría et al., 2022). Additionally, the chimera results may have been affected by the low proportion of $PhaB_{(Chim)}$ in the BL21(DE3) lysate relative to the high yields of $PhaB_{(Ther)}$ and $PhaB_{(Jap)}$, as shown in *Figure 6a*. Liu (2026) tried different strategies to improve expression but obtained only slight improvements, possibly due to vector-specific expression issues or deficient folding efficiency caused by the changed amino acids.

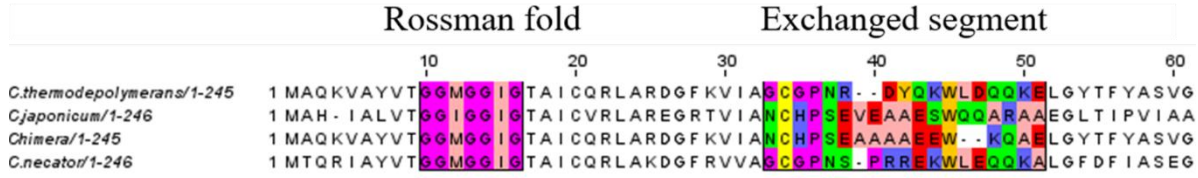

Figure 23. Multiple sequence alignment of the PhaB$_{(Ther)}$, PhaB$_{(Chim)}$ and PhaB$_{(Jap)}$ enzymes with the PhaB from *C. necator* performed using MAFFT (Katoh et al., 2002); The Rossmann fold and the exchanged moieties are highlighted; Residues are color-coded according to their physicochemical properties (Zappo scheme).

The third enzyme investigated, PhaB$_{(Jap)}$, was experimentally characterized for the first time in this study. *Figure 6b* shows that PhaB$_{(Jap)}$ has a strong affinity for NADH, consistent with its predicted similarity to PhaB from *A. vinosum* (81.7%), which is also NADH-dependent (Liebergesell & Steinbüchel, 1992; Saini et al., 2020). From these results, PhaB$_{(Jap)}$ appears to be a good prototype to test whether anaerobic PHB accumulation in *M. marburgensis* requires NADH coupling (Olavarría et al., 2022). Additionally, because PhaB$_{(Jap)}$ comes from *C. japonicum*, which grows at 55 ºC and pH 7.2 (Saini et al., 2020), conditions similar to those for *M. marburgensis* (65 ºC, pH 7; Rittmann et al., 2012), this should facilitate enzyme activity. However, the NADH-dependent activity of PhaB$_{(Jap)}$ is around half of the NADPH-dependent activity of PhaB$_{(Ther)}$ (*Figure 6b*), suggesting that monomer production and accumulation may be slower with PhaB$_{(Jap)}$.

From all the enzyme assays, it should be stated that these results represent a screening characterization of the preferred coenzyme for PhaB$_{(Ther)}$, PhaB$_{(Chim)}$, and PhaB$_{(Jap)}$. The PhaB proteins were not separated from the other proteins expressed by BL21(DE3) *E. coli*, which introduces potential sources of error into the assays. Therefore, the activities stated in this thesis are relevant only under these specific conditions.

Genetic modification of *M. marburgensis*

The interdomain conjugation protocol developed by Klein et al. (2025) was successfully applied, demonstrating the reliability of this method for creating genetic modifications in *M. marburgensis*. One point to note is that during the modification of *M. marburgensis Δhpt* with pArk-*PhaABC*, growth in the first selective enrichment was not observed within 60 h, as stated by Klein et al. (2025). All positive selective enrichments showed visible growth only 4–5 days after the recovered *M. marburgensis* cell suspension was transferred. This may suggest that the mutants grew more slowly under the selection conditions (62 ºC) and that successful transformants can also be obtained after longer incubation times for selection.

The same protocol for genetic modification of *M. marburgensis* was also used by Unger et al. (2025) to develop increase valine production from *M. marburgensis*. And in another study combination of genetic engineering and random mutagenesis was used for leucine overproduction by *M. marburgensis* (C. Fink et al., 2025). These results highlight the significant progress made in using *M. marburgensis* as a genetically tractable thermophilic methanogen and in implementing this knowledge to create genetically engineered *M. marburgensis* for biotechnology.

Effect of *PhaABC* integration on the growth of *M. marburgensis*

The effect of expression of PhaA, PhaB, and PhaC, together with Hpt and NeoR on the growth phenotype of *M. marburgensis* cultures, has been assessed. Due to its low NADH-activity, $PhaB_{(Chim)}$ would not overly stress cellular metabolism or cause PHB accumulation that could harm the cell. This allows us to assess whether other enzymes may have an effect. This growth experiments showed that *M. marburgensis* Chim and *M. marburgensis* Ther grew comparable to the wild-type. These two cultures have similar growth curves and maximum OD (*Figures 14 and 17*). *M. marburgensis* Jap performed better than the negative control but grew visibly less than the other two mutants. We also observed that *M. marburgensis* Ther and *M. marburgensis* Chim had little to no PHB signal (*Figure 20*), suggesting that slow or negligible PHB accumulation may have been beneficial for growth of the mutants. It was expected that high PHB accumulation would divert some carbon flow from biomass formation, but we cannot completely explain the positive effect on growth of the introduced genes without a systems biotechnology experiments and concomitant physiological modeling (Casini et al., 2023).

Regarding the introduced genes, three potential mechanisms may account for the observed growth effect. First, the introduction of the *hpt* gene results in expression of hypoxanthine phosphoribosyltransferase, which is the exclusive purine recycling system in methanogens (Klein et al., 2025). The reintroduction of this gene into the *Δhpt* strain may result in more energy-efficient growth (Worrell & Nagle, 1990). Second, besides conferring resistance to neomycin, the introduced resistance gene could have allowed the use of neomycin added to the medium as a supplementary nutrient source, possibly leading to a prolonged growth (Zhang & Dick, 2014; Stenholm et al., 2022). The third possibility is that PhaA and PhaC could have unknown roles in other metabolic pathways of *M. marburgensis* that facilitate

cellular integrity and increase tolerance in the stationary phase, particularly when *PhaB* activity is low in Chim or Ther (because of insufficient NADPH).

PHB accumulation in *M. marburgensis*

At the time of writing, the accumulation of PHB by *M. marburgensis* $PhaA_{(Ther)}$ $PhaB_{(Ther)}$ $PhaC_{(Ther)}$, *M. marburgensis* $PhaA_{(Ther)}$ $PhaB_{(Chim)}$ $PhaC_{(Ther)}$, and *M. marburgensis* $PhaA_{(Ther)}$ $PhaB_{(Jap)}$ $PhaC_{(Ther)}$ strains was demonstrated only by BODIPY staining and imaging, which is an indirect indication of PHB accumulation (*Figure 20*). BODIPY staining is a highly sensitive, lipophilic fluorescent technique, but it is not specific to PHB granules and does not bind covalently (Müllerová et al., 2022; Pei et al., 2023). Due to this, the cell wall, membrane, or other neutral lipids could have interfered and trapped the hydrophobic stain, resulting in false-positive signals (Müllerová et al., 2022; Pei et al., 2023). Hence, the putative PHB accumulations in the three mutants should be confirmed with an analytical method sensitive to the building blocks of the putative PHB, such as liquid chromatography combined with mass spectrometry (LC-MS). LC-MS is a well-established method to determine monomers and may thus be used to quantify the amount of PHB (g g^{-1} CDW) (Ge et al., 2016; Conners & Bose, 2025). Because of this, we preserved the biomass for LC-MS measurements; however, within the scope of this thesis, the BODIPY microscopy results are the only, yet preliminary, evidence that we may have PHB accumulation in the *M. marburgensis* Ther*, M. marburgensis* Chim, and *M. marburgensis* Jap strains.

M. marburgensis Jap was the most productive mutant observed, with multiple putative granules in almost every cell and strong signals in all four culture replicates (Annex 1, *Figure S2*). This shows how important it is to align the existing physiological characteristics to genetic engineering goals. In this case, $PhaB_{(Jap)}$ that uses NADH as a coenzyme and exhibiting strong NADH activity, was the best among the three PHBs. In comparison, $PhaB_{(Ther)}$ had a stronger specific activity in vitro but did not result in high accumulation of PHB in the *M. marburgensis* Ther mutant because of the assumed intracellular limitation of NADPH. There are a few *M. marburgensis* Ther cells that show multiple signals in the BODIPY staining, but it is unknown under which conditions they were produced, or whether they might even be false positives. This also raises the question of whether $PhaB_{(Jap)}$ enzyme would perform better in *M. marburgensis* with PhaA and PhaC from the same organism (*C. japonicum*), compared to the alternatives from *C. thermodepolymerans* used in this study. However, at the moment it is not known whether this represents a bottleneck and it may be a

subject of investigation for optimization. In addition, this study expanded the knowledge about the activity of PhaB from *C. japonicum*, which can aid further work investigating the activity of PhaA and PhaC and describing the PHB metabolic pathway in that thermophilic organism (Saini et al., 2020).

In *M. marburgensis* Chim, no signs of PHB accumulation could been detected with BODIPY staining in any culture (Annex 1, *Figure S2*). The PCR analysis that had been performed after the PHB accumulation experiments indicates that the genes are still in the genome, but the lack of accumulation could be due to the low activity of $PhaB_{(Chim)}$, even though it is NADH-dependent. Further LC-MS measurements on harvested *M. marburgensis* Chim cells could indicate whether the monomer is produced in very low amounts, insufficient for PhaC to generate granules large enough to be seen under the microscope by staining. This would show that NADH activity was present but not the main issue, and that changing the coenzyme specificity of $PhaB_{(Ther)}$ from NADPH to NADH came with a significant drawback compared with changing it in PhaB of *C. necator* (Olavarría et al., 2022).

The NADH pool of *M. marburgensis*

In previous attempts to use methanogens for PHB production, the NADH pool was a significant limiting factor. Thevasundaram et al. (2022) used multiple approaches (medium optimization and engineering new NADH scavenging pathways) to improve the NADH pool of *M. maripaludis* in order to detect monomer formation, yet it still remained a bottleneck. In contrast, with *M. marburgensis* Jap we obtained visible PHB accumulation without intensive pathway optimization or additional modifications to improve the NADH pool. This might be a result of the NADH:quinone oxidoreductase found in *M. marburgensis*, a cytosolic, FMN-dependent enzyme (MmNQO) that oxidizes NADH to NAD^+ by reducing quinones, though its precise physiological role in *M. marburgensis* is not yet defined (Ullmann et al., 2014). This suggests that *M. marburgensis* has a larger NADH pool than *M. maripaludis*, because NADH:quinone oxidoreductase has been shown to have high activity in *E. coli* (Ullmann et al., 2014).

However, it is not known whether NADH is a limiting factor for PHB production by *M. marburgensis* Jap. Therefore, tests to further increase NADH availability might indicate whether PHB accumulation is affected by differt intracellular concentrations of NADH In this context, supplementing the medium with amino acids, precursor metabolites (such as adenine and nicotinic acid), and reducing the growth temperature may increase NADH availability

(Foster & Moat, 1980; Knepper et al., 2008). Another strategy would be genetic modification by knocking out NADH:quinone oxidoreductase to make PhaB the main NADH consumer, or identifying which system is responsible for the direct reduction of NAD^+ in *M. marburgensis* in order to tune the process (Ullmann et al., 2014; Mühling et al., 2024).

Further optimization of PHB accumulation

In this thesis, the first steps on the avenue to thermophilic CO_2 into biodegradable plastic conversion by *M. marburgensis* have been completed, but still many questions remain regarding metabolic flux balance and optimization of PHB accumulation. Using MM medium in combination with Novasign TE and a lower temperature, good results were achieved for PHB production by *M. marburgensis* Jap. This medium combination was also used for scale-up of leucine production, but it has not been optimized further (C. Fink et al., 2025). After finally confirming PHB accumulation by LC-MS measurements, which is still outstanding, the first next step might be to grow the best mutant (*M. marburgensis* Jap) in different media under H_2/CO_2 unlimited closed batch conditions using GPC for initial screening optimization (Hofmann et al., 2025). This would contribute to building up the knowledge needed to improve PHB accumulation.

A crucial aspect would be to evaluate the acetyl-CoA routes in *M. marburgensis* and to find ways to improve their pool and direct it into PHB production. This may be realized by performing flux balance analysis and building a mathematical model. For this purpose, the Genome-Scale Metabolic Models (GEMs) built by Casini et al. (2023) can be employed and adapted to include the engineered PHB pathway. With these methods combined, and with the implementation of machine learning tools, the real bottlenecks could be predicted in the process of maximizing CO_2-to-PHB conversion (Nielsen & Petranovic, 2025).

At the same time, with the constant development of genetic tools for methanogens, design and addition of further genetic modifications could improve PHB accumulation. The P_{hmtB} promoter used for all inserted genes is considered to have weak expression. As an alternative, P_{glnA} is another constitutive promoter that was demonstrated to initiate high gene expression in *M. marburgensis* (Klein et al., 2025). However, for biotechnological applications, the introduction of a strong inducible promoter is more desirable. In this context, the tetracycline-based inducible promoter (TetR), which was also used in *M. marburgensis*, could induce high expression when tetracycline is added to the medium and also when the

temperature is above 60 ºC (Unger et al., 2025). This strategy could be feasible if the activity of the introduced PhaABC enzymes remains sufficient at temperatures above 60 ºC.

Another aspect to consider for PHB accumulation is whether phasins would be important in the PHB accumulation in *M. marburgensis*. Phasins are a class of PHB granule-associated proteins that help with granule structure, and PhaP1 and PhaP2 improve PHB production in *C. necator* under non-stress chemoautotrophic and heterotrophic conditions (Mezzina & Pettinari, 2016; Tang et al., 2022). The introduction of phasins together with the PhaABC pathway was shown to help maintain cell integrity in the transformation of cyanobacteria to produce PHB (P. Fink et al., 2025). If PHB granules affect the cell structure of *M. marburgensis* Jap, this should be investigated using transmission electron microscopy (P. Fink et al., 2025). Phasin PhaP1 from Arctic *Pseudomonas sp.* B14-6 improves PHB accumulation and increases tolerance to elevated temperature (H. Lee et al., 2021). It should be noted that *C. thermodepolymerans* also has genes for thermostable PhaP that could improve PHB granule structure in *M. marburgensis* (Musilova et al., 2023; Zhou et al., 2023).

Process development for PHB production and scalability

An important aspect to discuss is the potential development of biotechnological processes for engineered, PHB-producing *M. marburgensis*. For this purpose, an in-depth techno-economic analysis and life cycle assessment specific to this application should be investigated (Wojnarowska et al., 2025). A techno-economic analysis was recently conducted by Fink et al. (2025) for the production of leucine from *M. marburgensis* in pilot scale, which could serve as a starting point and be adapted further for PHB production. The sensitivity analysis for the techno-economic model from Fink et al. (2025) shows that the price of inputs and downstream processing efficiency have the most significant effects on the cost of chemical production from *M. marburgensis*. Their analysis indicates a leucine production cost of 9.35 € kg^{-1}, which is close to their internal threshold for economic feasibility of 8.40 € kg^{-1}. Adapting this model would involve scaling cultivation to larger volumes and establishing appropriate bioreactor designs and cultivation types (Amabile et al., 2024). During adaptation to the new environment, special attention should be directed toward PHB content measurements to ensure they remain within an economically viable range (Amabile et al., 2024).

Another critical factor when scaling up cultivation is gas-liquid mass transfer, as both H_2 and CO_2 play essential roles in methanogen metabolism. Because of that, the bioreactor

should include intensive stirring mechanisms and the capacity to withstand high pressures (Enriquez & Ahring, 2023). Also, CFD (computational fluid dynamics) aided cultivation of *M. marburgensis* would reduce the risks of gas limitations (Haslinger, Reischl et al., submitted to Communications Biology).

Downstream processing significantly influences the overall production cost and environmental sustainability of PHB, particularly for PHB Thiele and Riedel (2025). Because PHB accumulates intracellularly, it requires energy-intensive extraction and purification steps that can account for up to 70% of the total production costs and environmental burden Thiele and Riedel (2025). Consequently, recovery and purification strategies must be integrated into the early stages of biotechnological process design. Thiele and Riedel (2025) highlight various optimization strategies, such as replacing traditional chlorinated solvents with greener alternatives like dimethyl carbonate or implementing an acetone-water extraction protocol that avoids the high energy demand of biomass drying. Furthermore, non-solvent methods including mechanical disruption via high-pressure homogenization or chemical digestion using alkaline or acid treatments are identified as more economically favorable options compared to traditional solvent-based processes (Thiele & Riedel, 2025). Innovative strategies based on cell biology can also be applied, such as engineering cells to grow larger by slowing down cell division (Y. Wang et al., 2019). Using this method, cells can be centrifuged much more easily and would also have more space within the cells to accumulate PHB (Y. Wang et al., 2019). Selecting a strategy that balances purity requirements with energy efficiency is essential for ensuring the economic feasibility of PHB production.

As a final point, the broader scalability narrative of this platform could also be supported by its potential integration with existing anaerobic infrastructures, such as power-to-methane or waste gas–capturing plants such as Electrochaea GmbH or Krajete GmbH (Rittmann et al., 2018; Contreras et al., 2022; Chegini, 2025). However, in the near future, this would not position methanogen-based PHB production as a direct competitor to established sugar-fed processes, but rather as a complementary carbon capture and use strategy that would allow the technology to evolve (Reddy et al., 2019; Y. Wang et al., 2026). Additionally, collected PHB plastics could be degraded by microorganisms (Muiruri et al., 2022). This would release CO_2, which should be captured and re-utilized for methanogenic PHB production (Muiruri et al., 2022; J. Wang et al., 2024). Hence, the end goal would be to create a closed loop for CO_2 use in the bioplastic industry.

6. Conclusions

This work establishes *M. marburgensis* as a credible, genetically tractable platform for biobased PHB production directly from CO_2 and H_2 under thermophilic conditions. By identifying and functionally validating the thermostable, predominantly NADH-dependent acetoacetyl-CoA reductase from *C. japonicum*, we confirmed our hypothesis of the first research question. Assembling an effective *PhaABC* module, we demonstrated that *M. marburgenis* can be repurposed for putative polymer biosynthesis without abolishing its native metabolism, in this way answering our second research question. Among three genome-integrated mutants, the *M. marburgensis* $PhaA_{(Ther)}$ $PhaB_{(Jap)}$ $PhaC_{(Ther)}$ strains achieved robust intracellular PHB accumulation, confirming both pathway compatibility and engineering reliability in this host with the NADH-dependent acetoacetyl-CoA reductase as the best option, closing our last research question.

Our results highlight a key cofactor alignment between thermophilic methanogenesis and PHB biosynthesis: the NADH preference of the characterized PhaB reduces redox mismatch and likely improves flux efficiency at elevated temperatures. This mechanistic fit, combined with thermostable pathway components, support sustained polymer formation at 55 ºC and offer an advantage over mesophilic chassis operating on H_2/CO_2. The engineered strains also exhibited higher optical density and improved tolerance to liquid limitations, indicating that PHB pathway installation may confer growth or stress-resilience benefits under our tested conditions.

From the BODIPY staining perspective, the best-performing strain is *M. marburgensis* Jap, which showed strong signal for PHB accumulation in all our images and in most of the cells. This finding should also be confirmed soon by LC-MS measurements and polymer characterization should demonstrate that the material properties are within desired specifications.

Future work should focus on: (i) reinforcing the acetyl-CoA precursor or redix pool supply via NADH:quinone oxidoreductase; (ii) tuning expression balance among *PhaABC* or possibly adding granule-associated proteins to control granule numbers and size; (iii) scaling up the process and optimisation of intracellular PHA accumulation.

In summary, we delivered a thermophilic, CO_2-based PHB production platform grounded in an NADH-aligned, thermostable PhaB and stable genomic integration in *M. marburgensis*. All of this provide a strong foundation for sustainable gas-to-plastic

bioprocesses. With targeted pathways and process optimization, this platform can advance toward industrially relevant rates, amounts, and polymer properties while leveraging the inherent efficiencies of thermophilic gas fermentation.

References

Abdel Azim A., Pruckner C., Kolar P., Taubner R.-S., Fino D., Saracco G., Sousa F. L., Rittmann S. K.-M. R. (2017). The physiology of trace elements in biological methane production. *Bioresource technology*, 241:775–786. https://doi.org/10.1016/j.biortech.2017.05.211

Akinyemi, T. S., Shao, N., Lyu, Z., Drake, I. J., Liu, Y., & Whitman, W. B. (2021). Tuning gene expression by phosphate in the methanogenic archaeon *Methanococcus maripaludis*. *ACS Synthetic Biology*, *10*(11), 3028-3039. https://doi.org/10.1021/acssynbio.1c00322

Akkoyunlu, B., Daly, S., Syron, E., & Casey, E. (2024). Fermentation strategies for PHB production in a novel membrane bioreactor: Investigating batch and fed-batch operations. *Biochemical Engineering Journal*, *204*, 109239. https://doi.org/10.1016/j.bej.2024.109239

Amabile, C., Abate, T., Chianese, S., Munoz, R., & Musmarra, D. (2024). Economic Evaluation of a Large-Scale PHBV Production Facility: Impact of Polymer Content on the Final Selling Price. *Chemical Engineering Transactions*, *110*, 259-264. https://doi.org/10.3303/CET24110044

Aparici-Carratalá, D., Esclapez, J., Bautista, V., Bonete, M. J., & Camacho, M. (2023). Archaea: current and potential biotechnological applications. *Research in Microbiology*, *174*(7), 104080. https://doi.org/10.1016/j.resmic.2023.104080

Atarés, L., Chiralt, A., González-Martínez, C., & Vargas, M. (2024). Production of polyhydroxyalkanoates for biodegradable food packaging applications using *Haloferax mediterranei* and agrifood wastes. *Foods*, *13*(6), 950. https://doi.org/10.3390/foods13060950

Baur, T., Allaart, M. T., Zipperle, A., Contreras, G., Fink, C., Angenent, L. T., & Molitor, B. (2025). Metabolic engineering of *Methanothermobacter thermautotrophicus* ΔH for recombinant acetoin production. *bioRxiv*, 2025-12. https://doi.org/10.64898/2025.12.10.693358

Chegini, S. (2025). Unlocking the Power of Methanogens: Revolutionary Applications in Sustainable Energy and Biotechnology. In *Methanogens - Unique Prokaryotes. IntechOpen*. https://doi.org/10.5772/intechopen.1009384

Conners, E. M., & Bose, A. (2025). State-of-the-art methods for quantifying microbial polyhydroxyalkanoates. *Applied and Environmental Microbiology*, *91*(9), e00274-25. https://doi.org/10.1128/aem.00274-25

Contreras, G., Thomsen, J., Pfitzer, M., Hafenbradl, D., Kostner, D., Holtmann, D., ... & Molitor, B. (2022). New perspectives for biotechnological applications of methanogens. *Current Research in Biotechnology*, *4*, 468-474. https://doi.org/10.1016/j.crbiot.2022.10.001

De Lise, F., Iacono, R., Moracci, M., Strazzulli, A., & Cobucci-Ponzano, B. (2023). Archaea as a model system for molecular biology and biotechnology. *Biomolecules*, *13*(1), 114.

Du, Q., Wei, Y., Zhang, L., Ren, D., Gao, J., Dong, X., ... & Li, J. (2024). An improved CRISPR and CRISPR interference (CRISPRi) toolkit for engineering the model methanogenic archaeon *Methanococcus maripaludis*. *Microbial Cell Factories*, *23*(1), 239. https://doi.org/10.1186/s12934-024-02492-0

Enriquez, F. A., & Ahring, B. K. (2023). Strategies to overcome mass transfer limitations of hydrogen during anaerobic gaseous fermentations: a comprehensive review. *Bioresource Technology*, *377*, 128948. https://doi.org/10.1016/j.biortech.2023.128948

Enzmann, F., Mayer, F., Rother, M., & Holtmann, D. (2018). Methanogens: biochemical background and biotechnological applications. *Amb Express*, *8*(1), 1. https://doi.org/10.1186/s13568-017-0531-x

Ergal, İ., Fuchs, W., Hasibar, B., Thallinger, B., Bochmann, G., & Rittmann, S. K.-M. R. (2018). The physiology and biotechnology of dark fermentative biohydrogen production. *Biotechnology advances*, *36*(8), 2165-2186. https://doi.org/10.1016/j.biotechadv.2018.10.005

European Bioplastics. (2026, March 6). *Bioplastics Market Development Update 2025*. https://www.european-bioplastics.org/bioplastics-market-development-update-2025/

Fink, C., Steger, F., Schmidt, S., Hilts, E., Unger, F., Ruddyard, A., ... & Rittmann, S. K.-M. R. (2025). Pilot-scale production of leucine from CO_2. *bioRxiv*, 2025-11. https://doi.org/10.1101/2025.11.05.686735

Fink, C., Beblawy, S., Enkerlin, A. M., Mühling, L., Angenent, L. T., & Molitor, B. (2021). A shuttle-vector system allows heterologous gene expression in the thermophilic methanogen *Methanothermobacter thermautotrophicus* ΔH. *MBio*, *12*(6), e02766-21. https://doi.org/10.1128/mBio.02766-21

Fink, C., Angenent, L. T., & Molitor, B. (2022). An interdomain conjugation protocol for plasmid-DNA transfer into *Methanothermobacter thermautotrophicus* ΔH. In *Archaea: methods and protocols* (pp. 119-133). New York, NY: Springer US. https://doi.org/10.1007/978-1-0716-2445-6_7

Fink, P., Menzel, C., Kwon, J. H., & Forchhammer, K. (2025). A novel recombinant PHB production platform in filamentous cyanobacteria avoiding nitrogen starvation while under different carbon stress situations. *Journal of Applied Phycology*, 24(2), 157-162. https://doi.org/10.1186/s12934-025-02650-y

Foster, J. W., & Moat, A. G. (1980). Nicotinamide adenine dinucleotide biosynthesis and pyridine nucleotide cycle metabolism in microbial systems. *Microbiological reviews*, *44*(1), 83-105. https://doi.org/10.1128/mr.44.1.83-105.1980

Fu, S., Angelidaki, I., & Zhang, Y. (2021). In situ biogas upgrading by CO2-to-CH4 bioconversion. *Trends in Biotechnology*, *39*(4), 336-347. https://doi.org/10.1016/j.tibtech.2020.08.006

Garcia-Gonzalez, L., Mozumder, M. S. I., Dubreuil, M., Volcke, E. I., & De Wever, H. (2015). Sustainable autotrophic production of polyhydroxybutyrate (PHB) from CO_2 using a two-stage cultivation system. *Catalysis Today*, *257*, 237-245. https://doi.org/10.1016/j.cattod.2014.05.025

Ge, L., Tan, G. Y. A., Wang, L., Chen, C. L., Li, L., Tan, S. N., & Wang, J. Y. (2016). Determination of monomeric composition in polyhydroxyalkanoates by liquid chromatography coupled with on-line mass spectrometry and off-line nuclear magnetic resonance. *Talanta*, *146*, 107-113. https://doi.org/10.1016/j.talanta.2015.08.029

Haase, S. M., Huchzermeyer, B., & Rath, T. (2012). PHB accumulation in *Nostoc muscorum* under different carbon stress situations. *Journal of Applied Phycology*, 24(2), 157-162. https://doi.org/10.1007/s10811-011-9663-6

Hannon, M., Gimpel, J., Tran, M., Rasala, B., & Mayfield, S. (2010). Biofuels from algae: challenges and potential. *Biofuels*, *1*(5), 763-784. https://doi.org/10.4155/bfs.10.44

Haque, R. U., Paradisi, F., & Allers, T. (2020). *Haloferax volcanii* for biotechnology applications: challenges, current state and perspectives. *Applied microbiology and biotechnology*, *104*(4), 1371-1382. https://doi.org/10.1007/s00253-019-10314-2

Hofmann, W., Orthofer, M., Salas Wallach, N., Ruddyard, A., Ungerank, M., Paulik, C., & Rittmann, S. K.-M. R. (2025). Method for automated high performance closed batch cultivation of gas-utilizing methanogens. *AMB Express*, 15(1), 67. https://doi.org/10.1186/s13568-025-01872-y

Jang, J. W., Hwang, I. Y., Lee, O. K., & Lee, E. Y. (2025). Production of polyhydroxybutyrate with high cell density cultivation using thermophile *Caldimonas thermodepolymerans*. *Bioresource Technology*, 419, 132073. https://doi.org/10.1016/j.biortech.2025.132073

Katoh, K., Misawa, K., Kuma, K. I., & Miyata, T. (2002). MAFFT: a novel method for rapid multiple sequence alignment based on fast Fourier transform. *Nucleic acids research*, *30*(14), 3059-3066. https://doi.org/10.1093/nar/gkf436

Knepper, A., Schleicher, M., Klauke, M., & Weuster-Botz, D. (2008). Enhancement of the NAD(P)(H) pool in *Saccharomyces cerevisiae*. *Engineering in Life Sciences*, *8*(4), 381-389. https://doi.org/10.1002/elsc.200800031

Koller M, Puppi D, Chiellini F, Braunegg G (2016) Comparing Chemical and Enzymatic Hydrolysis of Whey Lactose to Generate Feedstocks for *Haloarchaeal* Poly(3-hydroxybutyrate-*co*-3-hydroxyvalerate) Biosynthesis. *International Journal of Pharmaceutical Sciences Research* 3: 112. http://dx.doi.org/10.15344/2394-1502/2016/112

Lee, H. S., Lee, H. J., Kim, S. H., Cho, J. Y., Suh, M. J., Ham, S., ... & Yang, Y. H. (2021). Novel phasins from the Arctic *Pseudomonas* sp. B14-6 enhance the production of polyhydroxybutyrate and increase inhibitor tolerance. *International journal of biological macromolecules*, *190*, 722-729. https://doi.org/10.1016/j.ijbiomac.2021.08.236

Lee, J., Park, H. J., Moon, M., Lee, J. S., & Min, K. (2021). Recent progress and challenges in microbial polyhydroxybutyrate (PHB) production from CO_2 as a sustainable feedstock: A state-of-the-art review. *Bioresource technology*, *339*, 125616. https://doi.org/10.1016/j.biortech.2021.125616

Liebergesell, M., & Steinbüchel, A. (1992). Cloning and nucleotide sequences of genes relevant for biosynthesis of poly (3-hydroxybutyric acid) in *Chromatium vinosum* strain D. *European journal of biochemistry*, *209*(1), 135-150. https://doi.org/10.1111/j.1432-1033.1992.tb17270.x

Ling, C., Qiao, G. Q., Shuai, B. W., Olavarría, K., Yin, J., Xiang, R. J., ... & Chen, G. Q. (2018). Engineering NADH/NAD+ ratio in *Halomonas bluephagenesis* for enhanced production of polyhydroxyalkanoates (PHA). *Metabolic Engineering*, *49*, 275-286. https://doi.org/10.1016/j.ymben.2018.09.007

Liu, W. (2026). Genetic Engineering of *Caldimonas thermodepolymerans* PhaB Chimeras with Altered Cofactor Preference. Bachelor Thesis, University of Vienna.

MacLeod, M., Arp, H. P. H., Tekman, M. B., & Jahnke, A. (2021). The global threat from plastic pollution. *Science*, *373*(6550), 61-65. https://doi.org/10.1126/science.abg5433

Mauerhofer, L. M., Zwirtmayr, S., Pappenreiter, P., Bernacchi, S., Seifert, A. H., Reischl, B., ... & Rittmann, S. K.-M. R. (2021). Hyperthermophilic methanogenic archaea act as high-pressure CH4 cell factories. *Communications biology*, *4*(1), 289. https://doi.org/10.1038/s42003-021-01828-5

Mauerhofer, L. M., Reischl, B., Schmider, T., Schupp, B., Nagy, K., Pappenreiter, P., ... & Rittmann, S. K.-M. R. (2018). Physiology and methane productivity of *Methanobacterium thermaggregans*. *Applied microbiology and biotechnology*, *102*(17), 7643-7656. https://doi.org/10.1007/s00253-018-9183-2

Markl, E., Grünbichler, H., & Lackner, M. (2018). PHB-bio based and biodegradable replacement for PP: a review. *Nov. Tech. Nutr. Food Sci*, *2*(5), 206-209. http://dx.doi.org/10.31031/ntnf.2018.02.000546

Mezzina, M. P., & Pettinari, M. J. (2016). Phasins, multifaceted polyhydroxyalkanoate granule-associated proteins. Applied and environmental microbiology, 82(17), 5060-5067. https://doi.org/10.1128/AEM.01161-16

Mitrano, D. M., & Wohlleben, W. (2020). Microplastic regulation should be more precise to incentivize both innovation and environmental safety. *Nature communications*, *11*(1), 5324. https://doi.org/10.1038/s41467-020-19069-1

Miyahara, Y., Yamamoto, M., Thorbecke, R., Mizuno, S., & Tsuge, T. (2020). Autotrophic biosynthesis of polyhydroxyalkanoate by *Ralstonia eutropha* from non-combustible gas mixture with low hydrogen content. *Biotechnology letters*, *42*(9), 1655-1662. https://doi.org/10.1007/s10529-020-02876-3

Mozumder, M. S. I., Garcia-Gonzalez, L., De Wever, H., & Volcke, E. I. (2015). Poly (3-hydroxybutyrate) (PHB) production from CO_2: Model development and process optimization. *Biochemical Engineering Journal*, 98, 107-116. https://doi.org/10.1016/j.bej.2015.02.031

Muiruri, J. K., Yeo, J. C. C., Zhu, Q., Ye, E., Loh, X. J., & Li, Z. (2022). Poly (hydroxyalkanoates): production, applications and end-of-life strategies–life cycle assessment nexus. *ACS Sustainable Chemistry & Engineering*, *10*(11), 3387-3406. https://doi.org/10.1021/acssuschemeng.1c08631

Mukhopadhyay, B. (2024). A reminder—peptidoglycan cell walls indeed occur in the archaeal domain, specifically in the members of *Methanobacteria* and *Methanopyri* classes. *Frontiers in microbiology*, *15*, 1329047. https://doi.org/10.3389/fmicb.2024.1329047

Musilova, J., Kourilova, X., Hermankova, K., Bezdicek, M., Ieremenko, A., Dvorak, P., ... & Sedlar, K. (2023). Genomic and phenotypic comparison of polyhydroxyalkanoates producing strains of genus *Caldimonas/Schlegelella*. *Computational and Structural Biotechnology Journal*, *21*, 5372-5381. https://doi.org/10.1016/j.csbj.2023.10.051

Mühling, L., Baur, T., & Molitor, B. (2024). *Methanothermobacter thermautotrophicus* and alternative methanogens: Archaea-based production. In *Advances in Biochemical Engineering/Biotechnology.* Springer. https://doi.org/10.1007/10_2024_270

Müllerová, L., Marková, K., Obruča, S., & Mravec, F. (2022). Use of flavin-related cellular autofluorescence to monitor processes in microbial biotechnology. *Microorganisms*, *10*(6), 1179. https://doi.org/10.3390/microorganisms10061179

Myers, T., & Dykstra, C. M. (2024). Teaching old dogs new tricks: genetic engineering methanogens. *Applied and Environmental Microbiology*, *90*(7), e02247-23. https://doi.org/10.1128/aem.02247-23

Nagrale, D. T., & Gawande, S. P. (2018). Archaea: ecology, application, and conservation. In *Microbial resource conservation: Conventional to modern approaches* (pp. 431-451). Cham: Springer International Publishing. https://doi.org/10.1007/978-3-319-96971-8_16

Narancic, T., Cerrone, F., Beagan, N., & O'Connor, K. E. (2020). Recent Advances in Bioplastics: Application and Biodegradation. *Polymers*, 12(4), 920. https://doi.org/10.3390/polym12040920

Orthofer, M., Hofmann, W., Rittmann, S. K.-M. R., & Paulik, C. (2025). A high-pressure bioreactor system for the cultivation of *Methanothermobacter marburgensis* on advanced growth medium for sustainable energy applications. *Scientific Reports*, *15*(1), 35519. https://doi.org/10.1038/s41598-025-19544-z

Olavarría, K., Pijman, Y. O., Cabrera, R., van Loosdrecht, M. C., & Wahl, S. A. (2022). Engineering an acetoacetyl-CoA reductase from *Cupriavidus necator* toward NADH preference under physiological conditions. *Scientific Reports*, 12(1), 3757. https://doi.org/10.1038/s41598-022-07663-w

Pais, J., Serafim, L. S., Freitas, F., & Reis, M. A. (2016). Conversion of cheese whey into poly (3-hydroxybutyrate-co-3-hydroxyvalerate) by *Haloferax mediterranei*. *New biotechnology*, *33*(1), 224-230. https://doi.org/10.1016/j.nbt.2015.06.001

Pei, R., Vicente-Venegas, G., Tomaszewska-Porada, A., Van Loosdrecht, M. C., Kleerebezem, R., & Werker, A. (2023). Visualization of polyhydroxyalkanoate accumulated in waste activated sludge. *Environmental Science & Technology*, 57(30), 11108-11121. https://doi.org/10.1021/acs.est.3c02381

Pfeifer, K., Ergal, İ., Koller, M., Basen, M., Schuster, B., & Rittmann, S. K.-M. R. (2021). Archaea biotechnology. *Biotechnology Advances*, *47*, 107668. https://doi.org/10.1016/j.biotechadv.2020.107668

Plastics Europe. (2026, March 6). *Plastics the Fast Facts 2025*. https://plasticseurope.org/knowledge-hub/plastics-the-fast-facts-2025/

Reddy, M. V., Mawatari, Y., Onodera, R., Nakamura, Y., Yajima, Y., & Chang, Y. C. (2019). Bacterial conversion of waste into polyhydroxybutyrate (PHB): A new approach of bio-circular economy for treating waste and energy generation. *Bioresource Technology Reports*, *7*, 100246. https://doi.org/10.1016/j.biteb.2019.100246

Reischl, B., Schupp, B., Fink, C., & Rittmann, S. K.-M. R. (2026). Quantitative analysis of amino acid excretion and consumption by *Methanothermobacter marburgensis* in fed-batch cultivation mode. *Amino acids*, 58(1), 9. https://doi.org/10.1007/s00726-026-03498-1

Reischl, B., Schupp, B., Palabikyan, H., Steger-Mähnert, B., Fink, C., & Rittmann, S. K.-M. R. (2025). Quantitative analysis of amino acid excretion by *Methanothermobacter marburgensis* under N2-fixing conditions. *Scientific Reports*, *15*(1), 3755. https://doi.org/10.1038/s41598-025-87686-1

Rittmann, S. K.-M. R., Seifert, A. H., & Bernacchi, S. (2018). Kinetics, multivariate statistical modelling, and physiology of CO_2-based biological methane production. *Applied Energy*, *216*, 751-760. https://doi.org/10.1016/j.apenergy.2018.01.075

Rittmann, S. K.-M. R. (2015). A critical assessment of microbiological biogas to biomethane upgrading systems. *Biogas science and technology*, 117-135. https://doi.org/10.1007/978-3-319-21993-6_5

Rittmann, S. K.-M. R., Seifert, A., & Herwig, C. (2012). Quantitative analysis of media dilution rate effects on *Methanothermobacter marburgensis* grown in continuous culture on H2 and CO2. *Biomass and Bioenergy*, *36*, 293-301.

Rueda, E., Senatore, V., Zarra, T., Naddeo, V., García, J., & Garfí, M. (2023). Life cycle assessment and economic analysis of bioplastics production from cyanobacteria. *Sustainable Materials and Technologies*, *35*, e00579. https://doi.org/10.1016/j.susmat.2023.e00579

Sabel-Becker, B., Jost, N. P., Kaster, A. K., & Holtmann, D. (2025). A co-feeding strategy of formate and H_2 for methanogens–Enhancing growth parameters and methane production. *Journal of CO2 Utilization*, *93*, 103049. https://doi.org/10.1016/j.jcou.2025.103049

Saini, M. K., ChihChe, W., Soulier, N., Sebastian, A., Albert, I., Thiel, V., ... & Tank, M. (2020). *Caldichromatium japonicum* gen. nov., sp. nov., a novel thermophilic phototrophic purple sulphur bacterium of the *Chromatiaceae* isolated from Nakabusa hot springs, Japan. *International journal of systematic and evolutionary microbiology*, *70*(11), 5701-5710. https://doi.org/10.1099/ijsem.0.004465

Seifert, A. H., Rittmann, S. K.-M. R., & Herwig, C. (2014). Analysis of process related factors to increase volumetric productivity and quality of biomethane with *Methanothermobacter marburgensis*. *Applied Energy*, *132*, 155-162. http://dx.doi.org/10.1016/j.apenergy.2014.07.002

Serna-García, R., Morlino, M. S., Bucci, L., Savio, F., Favaro, L., Morosinotto, T., ... & Treu, L. (2024). Biological carbon capture from biogas streams: insights into *Cupriavidus*

necator autotrophic growth and transcriptional profile. *Bioresource Technology*, *399*, 130556. https://doi.org/10.1016/j.biortech.2024.130556

Sieborg, M. U., Oliveira, J. M. S., Ottosen, L. D. M., & Kofoed, M. V. W. (2024). Flue-to-fuel: Bio-integrated carbon capture and utilization of dilute carbon dioxide gas streams to renewable methane. *Energy Conversion and Management*, *302*, 118090. https://doi.org/10.1016/j.enconman.2024.118090

Stenholm, Å., Hedeland, M., & Pettersson, C. E. (2022). Investigation of neomycin biodegradation conditions using ericoid mycorrhizal and white rot fungal species. *BMC biotechnology*, *22*(1), 29. https://doi.org/10.1186/s12896-022-00759-1

Stoett, P., Scrich, V. M., Elliff, C. I., Andrade, M. M., Grilli, N. D. M., & Turra, A. (2024). Global plastic pollution, sustainable development, and plastic justice. *World Development*, 184, 106756. https://doi.org/10.1016/j.worlddev.2024.106756

Subramanian, B., Basak, S., Thirumurugan, R., & Saleena, L. M. (2024). Metabolic flux analysis and metabolic engineering for polyhydroxybutyrate (PHB) production. *Polymer Bulletin*, *81*(12), 10589-10608. https://doi.org/10.1007/s00289-024-05215-y

Takagi, M., Nishioka, M., Kakihara, H., Kitabayashi, M., Inoue, H., Kawakami, B., ... & Imanaka, T. (1997). Characterization of DNA polymerase from *Pyrococcus* sp. strain KOD1 and its application to PCR. *Applied and environmental microbiology*, *63*(11), 4504-4510.

Tang, R., Peng, X., Weng, C., & Han, Y. (2022). The overexpression of phasin and regulator genes promoting the synthesis of polyhydroxybutyrate in Cupriavidus necator H16 under nonstress conditions. *Applied and Environmental Microbiology*, 88(2), e01458-21. https://doi.org/10.1128/AEM.01458-21

Taubner, R. S., Baumann, L. M., Steiner, M., Pfeifer, K., Reischl, B., Korynt, K., ... & Rittmann, S. K. M. (2023). Lipidomics and comparative metabolite excretion analysis of methanogenic archaea reveal organism-specific adaptations to varying temperatures and substrate concentrations. *MSystems*, *8*(2), e01159-22. https://doi.org/10.1128/msystems.01159-22

Thevasundaram, K., Gallagher, J. J., Cherng, F., & Chang, M. C. (2022). Engineering nonphotosynthetic carbon fixation for production of bioplastics by methanogenic archaea. *Proceedings of the National Academy of Sciences*, *119*(23), e2118638119. https://doi.org/10.1073/pnas.2118638119

Thiele, I., & Riedel, S. L. (2025). How does downstream processing influence the sustainability and techno-economics of polyhydroxyalkanoates production?. *Journal of Cleaner Production*, *521*, 146257. https://doi.org/10.1016/j.jclepro.2025.146257

Ullmann, E., Tan, T. C., Gundinger, T., Herwig, C., Divne, C., & Spadiut, O. (2014). A novel cytosolic NADH: quinone oxidoreductase from *Methanothermobacter marburgensis*. *Bioscience Reports*, 34(6), e00167. https://doi.org/10.1042/BSR20140143

Unger, F., Marichez, S., Klein, M., Fennessy, R. T., Smith, J., Stehrer-Polašek, T., ... & Fink, C. (2025). Valine overproduction with metabolically engineered *Methanothermobacter marburgensis*. *bioRxiv*, 2025-12. https://doi.org/10.64898/2025.12.09.693116

Vlaeminck, E., Uitterhaegen, E., Quataert, K., Delmulle, T., De Winter, K., & Soetaert, W. K. (2022) Industrial side streams as sustainable substrates for microbial production of poly (3-hydroxybutyrate) (PHB). *World Journal of Microbiology and Biotechnology*, *38*(12), 238. https://doi.org/10.1007/s11274-022-03416-z

Wang, K., & Zhang, R. (2020). Production of polyhydroxyalkanoates (PHA) by Haloferax mediterranei from food waste derived nutrients for biodegradable plastic applications. *Journal of Microbiology and Biotechnology*, *31*(2), 338. https://doi.org/10.4014/jmb.2008.08057

Wang, J., Huang, J., & Liu, S. (2024). The production, recovery, and valorization of polyhydroxybutyrate (PHB) based on circular bioeconomy. *Biotechnology advances*, *72*, 108340. https://doi.org/10.1016/j.biotechadv.2024.108340

Wang, Y., Liang, J., Hu, G., Zhen, Y., Zhang, X., Cai, D., ... & Kong, D. (2026). Microbial production of polyhydroxyalkanoates and lactate-based biopolymers from C1 resources: current advances and trends. *Green Chemistry*, *28*, 4338-4368. https://doi.org/10.1039/D5GC03933A

Wang, Y., Ling, C., Chen, Y., Jiang, X., & Chen, G. Q. (2019). Microbial engineering for easy downstream processing. Biotechnology Advances, 37(6), 107365. https://doi.org/10.1016/j.biotechadv.2019.03.004

Wojnarowska, M., Rychwalski, M., & Witko, T. (2025). Environmental life cycle assessment of Poly (3-hydroxybutyrate)(PHB): a comparative study with petrochemical and bio-based polymers. *Resources*, 14(10), 162. https://doi.org/10.3390/resources14100162

Worrell, V. E., & Nagle Jr, D. P. (1990). Genetic and physiological characterization of the purine salvage pathway in the archaebacterium *Methanobacterium thermoautotrophicum* Marburg. *Journal of bacteriology*, *172*(6), 3328-3334. https://doi.org/10.1128/jb.172.6.3328-3334.1990

Worrell, V. E., Nagle Jr, D. P., McCarthy, D., & Eisenbraun, A. (1988). Genetic transformation system in the archaebacterium *Methanobacterium thermoautotrophicum* Marburg. *Journal of bacteriology*, *170*(2), 653-656. https://doi.org/10.1128/jb.170.2.653-656.1988

Zhang, C., Ottenheim, C., Weingarten, M., & Ji, L. (2022). Microbial utilization of next-generation feedstocks for the biomanufacturing of value-added chemicals and food ingredients. *Frontiers in Bioengineering and Biotechnology*, *10*, 874612.

Zhang, L., Jiang, Z., Tsui, T. H., Loh, K. C., Dai, Y., & Tong, Y. W. (2022). A review on enhancing Cupriavidus necator fermentation for poly (3-hydroxybutyrate) (PHB) production from low-cost carbon sources. *Frontiers in Bioengineering and Biotechnology*, *10*, 946085. https://doi.org/10.3389/fbioe.2022.946085

Zhang, Q., & Dick, W. A. (2014). Growth of soil bacteria, on penicillin and neomycin, not previously exposed to these antibiotics. *Science of the total environment*, *493*, 445-453. https://doi.org/10.1016/j.scitotenv.2014.05.114

Zhang, Z., Shao, M., Zhang, G., Sun, S., Yi, X., Zhang, Z., ... & Chen, G. Q. (2024). Engineering *Halomonas bluephagenesis* for synthesis of polyhydroxybutyrate (PHB) in the presence of high nitrogen containing medium. *Metabolic Engineering*, 86, 242-249. https://doi.org/10.1016/j.ymben.2024.10.012

Zhou, W., Colpa, D. I., Permentier, H., Offringa, R. A., Rohrbach, L., Euverink, G. J. W., & Krooneman, J. (2023). Insight into polyhydroxyalkanoate (PHA) production from xylose and extracellular PHA degradation by a thermophilic *Schlegelella thermodepolymerans*. *Resources, Conservation and Recycling*, *194*, 107006. https://doi.org/10.1016/j.resconrec.2023.107006

Annexes

Annex 1 – Supplementary tables and figures

Table S1. TE (10x) for *M. marburgensis* conjugation medium (Klein et al., 2025).

Chemical		Concentration (g L^{-1})	References
$MgSO_4$ $7H_2O$		30.00	Balch, W.E., Fox, G.E., & Wolfe, R.S reevaluation of *Microbiol*. Rev. Modified by: Sarbu, C. (2013). Un Fimbrien vo *thermoautotrop* Universität Reg
$MnSO_4$ H_2O		5.00	
NaCl		10.00	
$FeSO_4$ $7H_2O$		1.00	
$CoCl_2$ $6H_2O$		1.80	
$CaCl_2$ $2H_2O$		1.00	
$ZnSO_4$ $7H_2O$		1.80	
$CuSO_4$ $5H_2O$		0.10	
KAl $(SO_4)_2$ $12H_2O$		0.18	
H_3BO_3		0.10	
Na_2MoO_4 $2H_2O$		0.10	
$(NH_4)2Ni(SO_4)_2$ $6H_2O$		2.80	
Na_2WO_4 $2H_2O$		0.10	
Na_2SeO_4		0.10	
pH		Adjusted to 1 with HCl	

Table S2. Novasign TE (1x) for *M. marburgensis* medium (C. Fink et al., 2025).

Chemical	Concentration (g L^{-1})	pH adjustment indication
Nitrilotriacetic acid	90.00	First dissolve + adjust to pH 6.5 with KOH
$MgCl_2$ $6H_2O$	2.00	NA
$FeCl_2$ $4H_2O$	10.00	NA
$CoCl_2$ $6H_2O$	0.01	NA
$NiCl_2$ $6H_2O$	2.40	NA
Na_2MoO_4 $2H_2O$	0.01	In the end set to pH 7.0 with 1 mol L^{-1} NaOH

Table S3. Primers used in this study.

Name	Purpose	Sequence (5' --> 3')
Fragment.FW_dpol	Fragment generation for assembly	GATATACCATGGCGCAGAAAGTG
Fragment.REV_dpol	Fragment generation for assembly	GAGCATATGTTAGCCCATATGCAGGC
Fragment.FW_Jap	Fragment generation for assembly	TAAGAAGGAGATATACCATGGCGCATATTGCG
Fragment.REV_Jap	Fragment generation for assembly	CTCGAGCATATGTTAATGCATAAACAGGCCG
Vector.FW_dpol	Fragment generation for assembly	ATGGGCTAACATATGCTCGAGGATCC

Vector.REV_dpol	Fragment generation for assembly	CTGCGCCATGGTATATCTCCTTCTTAAAGTTAAAC
Vector.FW_Jap	Fragment generation for assembly	CTGTTTATGCATTAACATATGCTCGAGGATCC
Vector.REV_Jap	Fragment generation for assembly	TATGCGCCATGGTATATCTCCTTCTTAAAGTTAAAC
T7_prom_FW	Colony PCR analysis *E. coli*	TAATACGACTCACTATAGGG
T7_term_REV	Colony PCR analysis *E. coli*	CTAGTTATTGCTCAGCGGT
PhaA_mid_FW	Colony PCR analysis *M. marburgensis*	CGCCGAGAACGTCGCAA
PhaB_ins_FW	Colony PCR analysis *M. marburgensis*	CAGATCGTCAAGATTAATTAACGGTTGTAGC
PhaB_ins_RV	Colony PCR analysis *M. marburgensis*	CTGAAGCGTTCAATTGCTTACTCC
ChimI_specific_primer_RV	Colony PCR analysis *M. marburgensis*	GGAGGGATGGCAGTTGGC
Inside_hpt_RV	Colony PCR analysis *M. marburgensis*	GGGATGTCCTCAACGGTGACC
O_UP	Colony PCR analysis *M. marburgensis*	CCTCAACCTTTTCAAGGAGGCTC
O_DOWN	Colony PCR analysis *M. marburgensis*	CCACCGATCCCAGGTAAGATCG

Table S4. DNA sequence of the genes and constructs used in this study.

Name	**Sequence (5' --> 3')**
acetoacetyl-CoA reductase [*Caldimonas thermodepoly*] - original	ATGGCACAGAAAGTTGCGTACGTCACCGGCGGCATGGGCGG TATCGGCACCGCGATCTGCCAGCGCCTGGCACGCGATGGGTT CAAGGTCATCGCCGGCTGCGGGCCGAACCGCGACTACCAGA AGTGGCTCGACCAGCAGAAGGAGCTGGGCTACACCTTCTAC GCCTCGGTGGGCAACGTGGCCGACTGGGATTCGACGGTGGC CGCCTTCGCCAAGGCCAAGGCCGAGCACGGGCCGATCGACG TGCTGGTCAACAACGCCGGCATCACCCGCGACCGCATGTTCC TGAAGATGACGCCGGAGGACTGGCACGCGGTGATCAACACC AACCTCAACAGCATGTTCAACGTCACCAAGCAGGTGGTGCC GGACATGGTGGAGCGGGGCTGGGGCCGCATCATCCAGATCTC CTCGGTCAACGGCGAGAAGGGCCAGGCCGGGCAGACCAACT

	ACTCGGCGGCCAAGGCCGGCATGCACGGCTTCACGATGGCG CTGGCGCAGGAGCTGGCCTCCAAGGGCGTGACGGTCAACAC CGTGAGCCCCGGCTACATCGGCACCGACATGGTCCGCGCGAT CAAGCCCGAGATCCTGGAGAAGATCATCGCCACGATCCCGGT GCGGCGCCTGGGCACGCCGGAGGAAATCGCCTCCATCGTGTC CTGGGTGGCGTCGGAGGAATCGGGCTTCGCGACCGGTGCCG ATTTCTCGATCAACGGCGGCCTGCACATGGGCTGA
acetoacetyl-CoA reductase [Chimera-II-vin] - original	ATGGCACAGAAAGTTGCGTACGTCACCGGCGGCATGGGCGG TATCGGCACCGCGATCTGCCAGCGCCTGGCACGCGATGGGTT CAAGGTCATCGCCAACTGCCATCCGTCCGAGGCGGCCGCCGC CGAAGAGTGGAAGCAGGCCGAGCTGGGCTACACCTTCTACG CCTCGGTGGGCAACGTGGCCGACTGGGATTCGACGGTGGCC GCCTTCGCCAAGGCCAAGGCCGAGCACGGGCCGATCGACGT GCTGGTCAACAACGCCGGCATCACCCGCGACCGCATGTTCCT GAAGATGACGCCGGAGGACTGGCACGCGGTGATCAACACCA ACCTCAACAGCATGTTCAACGTCACCAAGCAGGTGGTGCCG GACATGGTGGAGCGGGGCTGGGGCCGCATCATCCAGATCTCC TCGGTCAACGGCGAGAAGGGCCAGGCCGGGCAGACCAACTA CTCGGCGGCCAAGGCCGGCATGCACGGCTTCACGATGGCGCT GGCGCAGGAGCTGGCCTCCAAGGGCGTGACGGTCAACACCG TGAGCCCCGGCTACATCGGCACCGACATGGTCCGCGCGATCA AGCCCGAGATCCTGGAGAAGATCATCGCCACGATCCCGGTGC GGCGCCTGGGCACGCCGGAGGAAATCGCCTCCATCGTGTCCT GGGTGGCGTCGGAGGAATCGGGCTTCGCGACCGGTGCCGAT TTCTCGATCAACGGCGGCCTGCACATGGGCTGA
acetoacetyl-CoA reductase [*Caldichromatium japonicum*] - original	ATGGCCCATATCGCACTTGTCACCGGCGGCATCGGTGGTATCG GTACCGCGATCTGCGTCCGTCTTGCTCGGGAAGGTCGTACCG TGATCGCCAACTGTCATCCCAGTGAGGTCGAGGCCGCTGAGT CCTGGCAGCAGGCCCGTGCCGCCGAGGGATTGACGATACCA GTGATCGCCGCTGATGTGGCCTCGTTTGCGGATTGTGCCCGG ATGGTGCGCGAGATCGAGGCGCAATTCGGCCCTGTCGACATT TTGGTCAATTGTGCTGGGATTACCCGCGATAAGACATTCAAG AAGATGGAGCCGTCCCACTGGGAGGCGGTGATCAACGTCAA TCTCAACAGCGTCTTCAATGTCACCCGTCAGGTGTGGGAGGG CATGTTAGAGCGTGGATTCGGGCGGATCATCAATATCTCATCG GTTAATGGTCAGCGCGGTCAGTTCGGCCAGGCCAACTATGCA GCAGCCAAGGCCGGTATGCACGGCTTTACCATGTCACTGGCG CAAGAGGGTGCGGCCAAGGGGGTTACGGTGAACACGGTTTC GCCAGGCTATATCGAGACCGCCATGACCCTGGCGATGGATGA GGGCGTGCGCAACAGCATCATCAACGGTATCCCGATGCGGCG CATGGGTCGACCCGAAGAGGTCGCCGCTGCCGTGGCCTTCCT GGCGAGTGACGAGAGCGCCTATATCACCGGCGCTAACCTCCA GATCAATGGCGGTTTGTTCATGCATTAA
acetoacetyl-CoA reductase [*Caldimonas thermodepoly*] - codon optimised for *E. coli* expression	ATGGCGCAGAAAGTGGCGTATGTGACCGGCGGCATGGGCGG CATTGGCACCGCGATTTGCCAGCGCCTGGCGCGCGATGGCTT TAAAGTGATTGCGGGCTGCGGCCCGAACCGCGATTATCAGAA ATGGCTGGATCAGCAGAAAGAACTGGGCTATACCTTTTATGC GAGCGTGGGCAACGTGGCGGATTGGGATAGCACCGTGGCGG CGTTTGCGAAAGCGAAAGCGGAACATGGCCCGATTGATGTGC TGGTGAACAACGCGGGCATTACCCGCGATCGCATGTTTCTGA

	AAATGACCCCGGAAGATTGGCATGCGGTGATTAACACCAACC TGAACAGCATGTTTAACGTGACCAAACAGGTGGTGCCGGATA TGGTGGAACGCGGCTGGGGCCGCATTATTCAGATTAGCAGCG TGAACGGCGAAAAAGGCCAGGCGGGCCAGACCAACTATAGC GCGGCGAAAGCGGGCATGCATGGCTTTACCATGGCGCTGGCG CAGGAACTGGCGAGCAAAGGCGTGACCGTGAACACCGTGAG CCCGGGCTATATTGGCACCGATATGGTGCGCGCGATTAAACCG GAAATTCTGGAAAAAATTATTGCGACCATTCCGGTGCGCCGC CTGGGCACCCCGGAAGAAATTGCGAGCATTGTGAGCTGGGT GGCGAGCGAAGAAAGCGGCTTTGCGACCGGCGCGGATTTTA GCATTAACGGCGGCCTGCATATGGGCTAA
acetoacetyl-CoA reductase [Chimera-II-vin] - codon optimised for *E. coli* expression	ATGGCGCAGAAAGTGGCGTATGTGACCGGCGGCATGGGCGG CATTGGCACCGCGATTTGCCAGCGCCTGGCGCGCGATGGCTT TAAAGTGATTGCGAACTGCCATCCGAGCGAAGCGGCGGCGG CGGAAGAATGGAAACAGGCGGAACTGGGCTATACCTTTTATG CGAGCGTGGGCAACGTGGCGGATTGGGATAGCACCGTGGCG GCGTTTGCGAAAGCGAAAGCGGAACATGGCCCGATTGATGT GCTGGTGAACAACGCGGGCATTACCCGCGATCGCATGTTTCT GAAAATGACCCCGGAAGATTGGCATGCGGTGATTAACACCAA CCTGAACAGCATGTTTAACGTGACCAAACAGGTGGTGCCGG ATATGGTGGAACGCGGCTGGGGCCGCATTATTCAGATTAGCA GCGTGAACGGCGAAAAAGGCCAGGCGGGCCAGACCAACTAT AGCGCGGCGAAAGCGGGCATGCATGGCTTTACCATGGCGCTG GCGCAGGAACTGGCGAGCAAAGGCGTGACCGTGAACACCGT GAGCCCGGGCTATATTGGCACCGATATGGTGCGCGCGATTAAA CCGGAAATTCTGGAAAAAATTATTGCGACCATTCCGGTGCGC CGCCTGGGCACCCCGGAAGAAATTGCGAGCATTGTGAGCTG GGTGGCGAGCGAAGAAAGCGGCTTTGCGACCGGCGCGGATT TTAGCATTAACGGCGGCCTGCATATGGGCTAA
acetoacetyl-CoA reductase [*Caldichromatium japonicum*] - codon optimised for *E. coli* expression	ATGGCGCATATTGCGCTGGTGACCGGCGGCATTGGCGGCATT GGCACCGCGATTTGCGTGCGCCTGGCGCGCGAAGGCCGCAC CGTGATTGCGAACTGCCATCCGAGCGAAGTGGAAGCGGCGG AAAGCTGGCAGCAGGCGCGCGCGGCGGAAGGCCTGACCATT CCGGTGATTGCGGCGGATGTGGCGAGCTTTGCGGATTGCGCG CGCATGGTGCGCGAAATTGAAGCGCAGTTTGGCCCGGTGGAT ATTCTGGTGAACTGCGCGGGCATTACCCGCGATAAAACCTTT AAAAAAATGGAACCGAGCCATTGGGAAGCGGTGATTAACGT GAACCTGAACAGCGTGTTTAACGTGACCCGCCAGGTGTGGG AAGGCATGCTGGAACGCGGCTTTGGCCGCATTATTAACATTA GCAGCGTGAACGGCCAGCGCGGCCAGTTTGGCCAGGCGAAC TATGCGGCGGCGAAAGCGGGCATGCATGGCTTTACCATGAGC CTGGCGCAGGAAGGCGCGGCGAAAGGCGTGACCGTGAACA CCGTGAGCCCGGGCTATATTGAAACCGCGATGACCCTGGCGA TGGATGAAGGCGTGCGCAACAGCATTATTAACGGCATTCCGA TGCGCCGCATGGGCCGCCCGGAAGAAGTGGCGGCGGCGGTG GCGTTTCTGGCGAGCGATGAAAGCGCGTATATTACCGGCGCG AACCTGCAGATTAACGGCGGCCTGTTTATGCATTAA
MonocisPhmtB_PhaA_PhaB_PhaC_Ther_KasI_	GGCGCCCCCATGAACCAACCGATGGCTCAGAAAAACCTTAA AATTAGCGATATATTTATATAGGATTATATGAATAGATAATATCA CATAAAATGAGGTGGTTAATTATGTCAGACATCGTCATCGTTT

XbaI_PacI_MfeI – *M. marburgensis* optimised	CCGCCGCAAGGACAGCAGTCGGCAAGTTCGGCGGCACACTG GCAAAGACACCCGCAGCCGAGCTGGGGGCCACCGTGATCAA GGAGGTGCTGAGGAGGGCCGGCCTTTCAGGCGAGCAGGTCA GCGAGGTGATCATGGGCCAGGTGCTGCAGGCCGGCTGCGGG CAGAACCCCGCAAGGCAGGCAGTCATCAAGGCCGGGCTCCC CGAAGGCGTGCCCGCAATGACCATCAACAAGGTGTGCGGCT CAGGCCTGAAGGCCGTGATGCTGGCAGCACAGGCCATCAGG GACGGCGACGCCGACATCGTCGTGGCCGGCGGGCAGGAGAA CATGAGCCTGGCACCCCACGTGCTGCTCGGCTCAAGGGAGG GCCAGAGGATGGGTGACTGGAAGATGGTCGACTCAATGATCA CCGACGGCCTGTGGGACGTCTACAACCAGTACCACATGGGCA TCACCGCCGAGAACGTCGCAAAGAAGTACGGCATCAGCAGG GAGGAGCAGGACGCACTGGCACTGGCCTCACAGCAGAAGGC CGCCGCCGCACAGGACGCCGGGAGGTTCAAGGACGAGATCG TGCCCGTGGTGATCCCCCAGAGGAAGGGCGACCCCGTGGTG TTCGACACCGACGAGTTCATCAACAGGAAGACCAGCGCCGA GGCACTGGCCGGGCTGAGGCCCGCCTTCGACAAGGCAGGCA CAGTGACCGCAGGCAATGCCTCAGGCATCAACGACGGCGCA GCCGCAGTGGTGGTGATGAGCGCAAAGAGGGCCGAGCAGCT GGGCCTCAAGCCCCTGGCAAGGATCGCCTCCTATGCCAGCGC CGGCCTGGATCCCGCCTACATGGGCATGGGCCCCGTGCCCGC AGCAAGGAAGGCACTGGACAGGGCCGGCTGGAAGCCCGCC GACCTCGACCTGCTCGAGATCAACGAGGCCTTCGCAGCACA GGCCTGCGCAGTGCACAAGGAAATGGGCTGGGACACCAGCA AGGTCAACGTCAACGGCGGCGCAATCGCAATCGGGCACCCC ATCGGCGCATCCGGCTGCAGGATCCTGGTCACACTGCTGCAC GAGATGCAGAGGAGGGACGCCAGGAAGGGCATCGCCTCACT GTGCATCGGCGGCGGCATGGGCGTGGCACTGACCGTCGAGA GGTGAGTTAGATGGCTCGCTGAGCTAATAGTTGCCGACAGAT CGTCAAGATTAATTAACGGTTGTAGCATTATCGGAGGTTCTCT ACCTAGTATCGATAGCCGTGCCCATGAACCAACCGATGGCTC AGAAAAACCTTAAAATTAGCGATATATTTATATAGGATTATATG AATAGATAATATCACATAAAATGAGGTGGTTAATTATGGCACA GAAAGTTGCATACGTCACCGGCGGCATGGGCGGTATCGGCAC CGCAATCTGCCAGAGGCTGGCAAGGGATGGGTTCAAGGTCAT CGCCGGCTGCGGGCCCAACAGGGACTACCAGAAGTGGCTCG ACCAGCAGAAGGAGCTGGGCTACACCTTCTACGCCTCAGTG GGCAACGTGGCCGACTGGGATTCAACAGTGGCCGCCTTCGC CAAGGCCAAGGCCGAGCACGGGCCCATCGACGTGCTGGTCA ACAACGCCGGCATCACCAGGGACAGGATGTTCCTGAAGATG ACACCCGAGGACTGGCACGCAGTGATCAACACCAACCTCAA CAGCATGTTCAACGTCACCAAGCAGGTGGTGCCCGACATGGT GGAGAGGGGCTGGGGCAGGATCATCCAGATCTCCTCAGTCA ACGGCGAGAAGGGCCAGGCCGGGCAGACCAACTACTCAGCA GCCAAGGCCGGCATGCACGGCTTCACAATGGCACTGGCACA GGAGCTGGCCTCCAAGGGCGTGACAGTCAACACCGTGAGCC CCGGCTACATCGGCACCGACATGGTCAGGGCAATCAAGCCCG AGATCCTGGAGAAGATCATCGCCACAATCCCCGTGAGGAGGC TGGGCACACCCGAGGAAATCGCCTCCATCGTGTCCTGGGTGG CATCAGAGGAATCAGGCTTCGCAACCGGTGCCGATTTCTCAA

	TCAACGGCGGCCTGCACATGGGCTGAGGGAAACAGTAAGGC CTAATTAGGTAAAGGGAGTAAGCAATTGAACGCTTCAGATGT AACCATATACTTACGCTGGATCTTCTCCCGCGAATTTTAACCC CCCATGAACCAACCGATGGCTCAGAAAAACCTTAAAATTAGC GATATATTTATATAGGATTATATGAATAGATAATATCACATAAAA TGAGGTGGTTAATTATGACACAGAGGTCAGCACCCAGGCCTG CCCAGGACAAGCAGCCCCCCGCAGGTCCCACAGTCCAGGCC CTCGGCGAACACGTCAGCCAGGCAGTCAACGCACTGATGAG GCTGAACCTGCCCCTCGAGAGGGTCTCACAGCTGCAGAACG AATACCTGCAGGAAGCCGCAAAGATCTGGAACGCCGCACTG GCACAGCCCGGCCAGGCACCCAGGATCGAGGACAGGAGGTT CAGCGGGCCCGGCTGGGCAGAAAACCCCGCCGCATCATACG TGGCAGCAATGTACCTGCTCAACGCCAGGACAATGCTGCAGC TGGCCGACGCCGTGCAGGGCGACGAGAAGACCAGGCAGAG GATCAGGTTCGCAGTGCAGCAGTGGATCGAGGCAAGCGCAC CCAGCAACTTCCTCGCCTTCAACCCCGAGGCACAGAGGAAG GCACTGGAGACCCAGGGCGAGAGCCTGACACAGGGCATGCT GAGGCTGCTGCACGACCTCAGGCAGGGGCACCTGTCACAGA CCGACGAGAGCGTCTTCGAGGTGGGCAGGAACGTGGCCACC ACCGAGGGCAGCGTGATCTACGAGAACCCCCTGTTCCAGCTG ATCGAGTACAAGCCCCTGACAGCCAAGGTGTACGAGAGGCC CCTGCTGATCGTGCCCCCCTGCATCAACAAGTACTACATCCTC GACCTGCAGCCCGACAACTCCTTCGTGAGGCATGCACTGGA GCAGGGGCTGAGGGTGTTCCTGGTCAGCTGGAGGAATGCCG ACGAGAGCCTCGCACAGGTCGGCTGGGACGAGTACATCGAG GACGGCGTGATCAGGGCCATCAGGGTCGTGCAGGAGGTGGC CAAAAGCCCCCAGCTGAACGCACTCGGCTTCTGCATCGGCG GCACCCTGCTGGCCACCGCACTGGCAGTGCTGGCCGCAAGG GGCGAGCAGCCCGCAGCCAGCCTGACACTGCTGACCTCATTC CTCGACTTCGGCCACACCGGGGTGATCGACGTGTTCGTCGAC GAGGCCGCAGTGCAGATGAGGGAGATGACCATCGGCCCCAA CAGCCCCACCGGCGGCGGGCTGATGAGGGGCAGGGAGCTGG CAGCAACCTTCTCATTCCTGAGGCCCAACGACCTGGTGTGGA ACTACGTGGTCGGCAACTACCTCAAGGGCGAGACACCACCC CCCTTCGACCTGCTGTACTGGAACTCCGACAGCACCAACCTG CCCGGGCCCATGTTCTGCTGGTACCTGAGGAACACCTACCTG GAGAACAACCTCAAGGAGCCCGGCAAGCTGACAGTGTGCGG CGCACCCGTGGACCTCGGCAGGATCCAGGCACCCGCATTCAT CTACGGCTCAAGGGAGGACCACATCGTGCCCTGGGAGTCAG CCTACGCCTCAACAAGGCTGCTCAAGGGCAAGCTGAGGTTC GTGCTGGGGGCCTCAGGCCACATCGCCGGCGTGATCAACCCC CCCGCCAGGAAGAAGAGGAGCTACTGGGTCAACGCCAGGCT GCCCGCCTCAGCAAGGGACTGGCTGGCCGGTGCAACCGAGC ACCCCGGCAGCTGGTGGCCCGAGTGGGCAGGCTGGATCAGG AGCCACGCCGGCAAGCAGGTCGCCGCACCCAGGACACCCGG CAACAGGACCTACAGGCCCATCGAGCCCGCACCCGGGAGGT ACGTCAAGGAAAGGGCCTGAGCCGATACTGATTAACGAAGG TGCATTGCACAAACTTTTTAAGTGTAATGCACCTAATTTTTTTT ATTTCAGGACATTTTCTAGA

PhmtB_acetoacetyl-CoA reductase_Chim_PacI_MfeI - for *M. marburgensis* codon optimised	GTTGCCGACAGATCGTCAAGATTAATTAACGGTTGTAGCATTA TCGGAGGTTCTCTACCTAGTATCGATAGCCGTGCCCATGAACC AACCGATGGCTCAGAAAAACCTTAAAATTAGCGATATATTTAT ATAGGATTATATGAATAGATAATATCACATAAAATGAGGTGGTT AATTATGGCACAGAAAGTTGCATACGTCACCGGCGGCATGGG CGGTATCGGCACCGCAATCTGCCAGAGGCTGGCAAGGGATG GGTTCAAGGTCATCGCCAACTGCCATCCCTCCGAGGCAGCCG CCGCCGAAGAGTGGAAGCAGGCCGAGCTGGGCTACACCTTC TACGCCTCAGTGGGCAACGTGGCCGACTGGGATTCAACAGT GGCCGCCTTCGCCAAGGCCAAGGCCGAGCACGGGCCCATCG ACGTGCTGGTCAACAACGCCGGCATCACCAGGGACAGGATG TTCCTGAAGATGACACCCGAGGACTGGCACGCAGTGATCAA CACCAACCTCAACAGCATGTTCAACGTCACCAAGCAGGTGG TGCCCGACATGGTGGAGAGGGGCTGGGGCAGGATCATCCAG ATCTCCTCAGTCAACGGCGAGAAGGGCCAGGCCGGGCAGAC CAACTACTCAGCAGCCAAGGCCGGCATGCACGGCTTCACAAT GGCACTGGCACAGGAGCTGGCCTCCAAGGGCGTGACAGTCA ACACCGTGAGCCCCGGCTACATCGGCACCGACATGGTCAGG GCAATCAAGCCCGAGATCCTGGAGAAGATCATCGCCACAATC CCCGTGAGGAGGCTGGGCACACCCGAGGAAATCGCCTCCAT CGTGTCCTGGGTGGCATCAGAGGAATCAGGCTTCGCAACCGG TGCCGATTTCTCAATCAACGGCGGCCTGCACATGGGCTGAGG GAAACAGTAAGGCCTAATTAGGTAAAGGGAGTAAGCAATTGA ACGCTTCAGATGTAACCATA
PhmtB_acetoacetyl-CoA reductase_Jap_PacI_MfeI - for *M. marburgensis* codon optimised	GTTGCCGACAGATCGTCAAGATTAATTAACGGTTGTAGCATTA TCGGAGGTTCTCTACCTAGTATCGATAGCCGTGCCCATGAACC AACCGATGGCTCAGAAAAACCTTAAAATTAGCGATATATTTAT ATAGGATTATATGAATAGATAATATCACATAAAATGAGGTGGTT AATTATGGCACACATAGCACTCGTTACAGGTGGTATAGGTGGT ATAGGTACAGCAATATGCGTTAGGCTCGCAAGGGAGGGTAGG ACAGTTATAGCAAACTGCCACCCCTCAGAGGTTGAGGCAGCA GAGTCATGGCAGCAGGCAAGGGCAGCAGAGGGTCTCACAAT ACCCGTTATAGCAGCAGATGTTGCATCATTCGCAGATTGCGCA AGGATGGTTAGGGAGATAGAGGCACAGTTCGGTCCCGTTGAT ATACTCGTTAACTGCGCAGGTATAACAAGGGATAAGACATTC AAGAAGATGGAGCCCTCACACTGGGAGGCAGTTATAAACGTT AACCTCAACTCAGTTTTCAACGTTACAAGGCAGGTTTGGGAG GGTATGCTCGAGAGGGGTTTCGGTAGGATAATAAACATATCAT CAGTTAACGGTCAGAGGGGTCAGTTCGGTCAGGCAAACTAC GCAGCAGCAAAGGCAGGTATGCACGGTTTCACAATGTCACTC GCACAGGAGGGTGCAGCAAAGGGTGTTACAGTTAACACAGT TTCACCCGGTTACATAGAGACAGCAATGACACTCGCAATGGA TGAGGGTGTTAGGAACTCAATAATAAACGGTATACCCATGAG GAGGATGGGTAGGCCCGAGGAGGTTGCAGCAGCAGTTGCAT TCCTCGCATCAGATGAGTCAGCATACATAACAGGTGCAAACC TCCAGATAAACGGTGGTCTCTTCATGCACTGAGGGAAACAGT AAGGCCTAATTAGGTAAAGGGAGTAAGCAATTGAA

Table S5. PCR program used for generation of fragments and vectors.

Steps		Temperature (°C)	Time
Initial denaturation		98	30 seconds
35×	**Denaturation**	98	10 seconds
	Annealing	51	25 seconds
	Extension	72	3 minutes – for vectors 30 seconds – for fragments
Final extension		72	2 minutes

Table S6. PCR program used for colony PCR for *E. coli* optimised genes premiers.

Steps		Temperature (°C)	Time
Initial denaturation		95	3 minutes
35×	**Denaturation**	95	15 seconds
	Annealing	50	25 seconds
	Extension	72	1 min 10 seconds
Final extension		72	3 minutes

Table S7. PCR program used for colony PCR for *M. marburgensis* optimised genes premiers.

Steps		Temperature (°C)	Time
Initial denaturation		95	3 minutes
35×	**Denaturation**	98	15 seconds
	Annealing	60	25 seconds
	Extension	72	1 min 10 seconds
Final extension		72	3 minutes

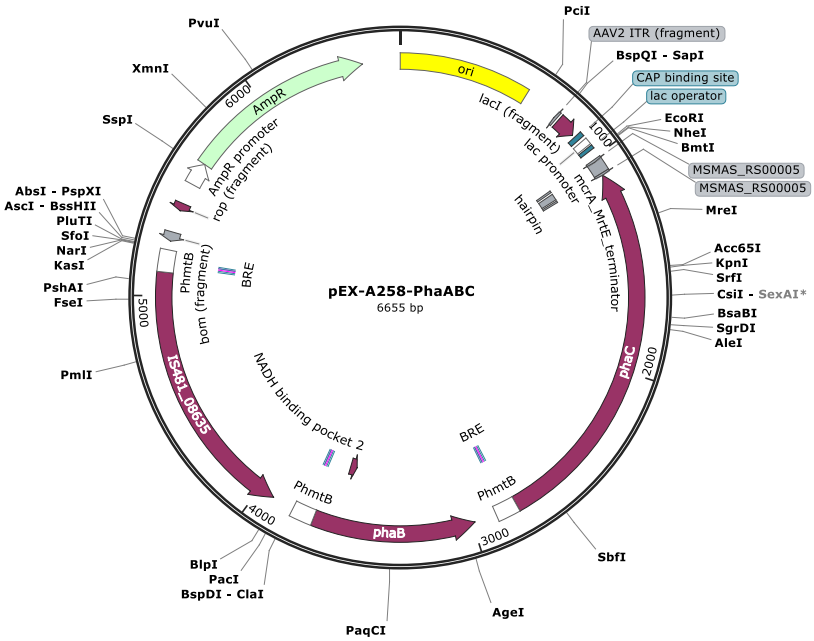

Figure S1. Plasmid map of the pEX-A258-*PhaABC* received for Eurofins Genomics with the Monocis*PhmtB_PhaA*(Ther)_*PhaB*(Ther)_*PhaC*(Ther)_KasI_XbaI_PacI_MfeI (*M. marburgensis* optimised) inserted.

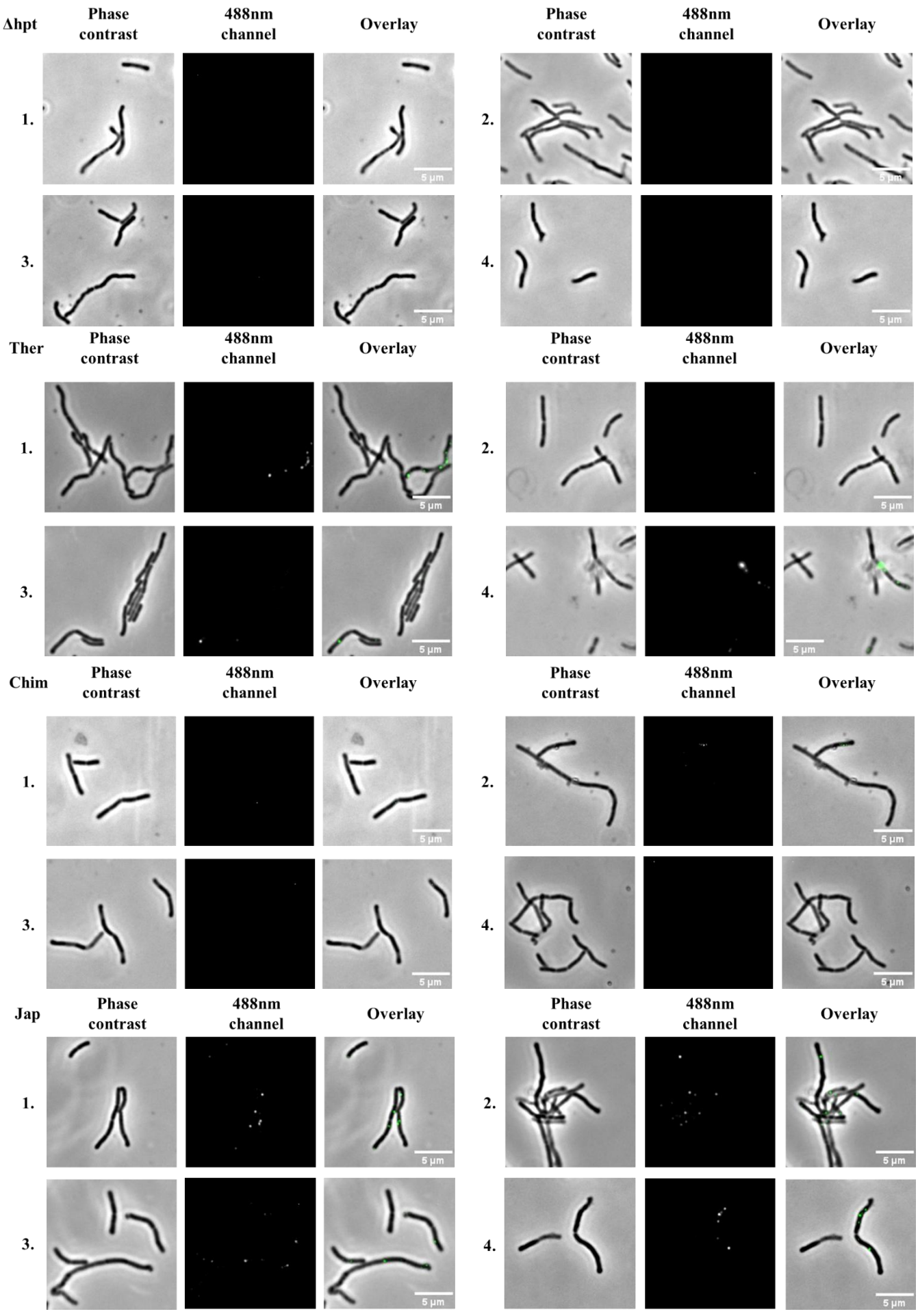

Figure S2. Microscopic images with *M. marburgensis Δhpt* and engineered mutants (*M. marburgensis* Ther, Chim, and Jap) from all 4 replicate cultures and their BODIPY staining imagines.

Annex 2 – Calculation sheets for PhaB specific activity

Calculation sheet for $PhaB_{(Ther)}$ specific activity.

		mmol L^{-1} s^{-1}	µmol L^{-1} s^{-1}	µmol L^{-1} min^{-1}	µmol min^{-1}	U mg^{-1}							
NADH	1	-3.34968E-06	-0.00335	-0.20098093	-8.0392E-05	0.20					V	400	µL
	2	-2.82708E-06	-0.002827	-0.16962471	-6.785E-05	0.17						0.4	mL
	3	-2.88141E-06	-0.002881	-0.17288472	-6.9154E-05	0.17						0.0004	L
	4	-1.85074E-06	-0.001851	-0.11104437	-4.4418E-05	0.11					c	1	µg ml^{-1}
NADPH	1	-0.000773427	-0.773427	-46.405604	-0.01856224	46.41						0.4	µg
	2	-0.001046624	-1.046624	-62.7974277	-0.02511897	62.80						0.0004	mg
	3	-0.000935691	-0.935691	-56.1414791	-0.02245659	56.14						2500	mg^{-1}
	4	-0.000907671	-0.907671	-54.4602664	-0.02178411	54.46							

blank								Corrected activity	
		mmol L^{-1} s^{-1}	mean	µmol L^{-1} s^{-1}	µmol L^{-1} min^{-1}	µmol min^{-1}	U mg^{-1}	U mg^{-1}	Mean
NADH	1	-1.64719E-06	-1.26E-06	-0.00125932	-0.07555892	-3.02E-05	0.08	**0.13**	0.09
	2	-1.58701E-06						**0.09**	
	3	-8.09389E-07						**0.10**	
	4	-9.93677E-07						**0.04**	
NADPH	1	-2.58881E-06	-3.36E-06	-0.00335671	-0.20140233	-8.06E-05	0.20	**46.20**	
	2	-3.96988E-06						**62.60**	
	3	-3.16447E-06						**55.94**	
	4	-3.70366E-06						**54.26**	

Calculation sheet for $PhaB_{(Chim)}$ specific activity.

		mmol L^{-1} s^{-1}	µmol L^{-1} s^{-1}	µmol L^{-1} mi	µmol min^{-1}	U mg^{-1}							
NADH	1	-0.0002043	-0.204254	-12.2553	-0.0049021	0.98					V	400	µL
	2	-0.0001869	-0.18686	-11.2116	-0.00448465	0.89						0.4	mL
	3	-0.0001656	-0.165575	-9.93452	-0.00397381	0.79						0.0004	L
	4	-0.0001703	-0.170252	-10.2151	-0.00408604	0.81					c	12.56544	µg ml^{-1}
NADPH	1	-8.683E-06	-0.008683	-0.521	-0.0002084	0.04						5.026177	µg
	2	-9.102E-06	-0.009102	-0.54613	-0.00021845	0.04						0.005026	mg
	3	-8.194E-06	-0.008194	-0.49165	-0.00019666	0.04						198.9584	mg^{-1}
	4	-7.477E-06	-0.007477	-0.4486	-0.00017944	0.04							

blank								Corrected activity	
		mmol L^{-1} s^{-1}	mean	µmol L^{-1} s^{-1}	µmol L^{-1} min^{-1}	µmol min^{-1}	U mg^{-1}	U mg^{-1}	Mean
NADH	1	-4.35E-05	-4.16E-05	-4.16E-02	-2.49385837	-0.000998	0.20	**0.78**	**0.67**
	2	-3.896E-05						**0.69**	
	3	-4.224E-05						**0.59**	
	4	-4.187E-05						**0.61**	
NADPH	1	-5.809E-06	-5.71E-06	-5.71E-03	-0.34288207	-0.000137	0.03	**0.01**	**0.01**
	2	-6.389E-06						**0.02**	
	3	-4.946E-06						**0.01**	
	4	-5.797E-06						**0.01**	

Calculation sheet for $PhaB_{(Jap)}$ specific activity.

		mmol L^{-1} s^{-1}	µmol L^{-1} s^{-1}	µmol L^{-1} min^{-1}	µmol min^{-1}	U mg^{-1}							
NADH	1	-0.00056117	-0.561169806	-33.6701883	-0.013468075	22.61					V	400	µL
	2	-0.000530738	-0.530738019	-31.8442811	-0.012737712	21.38						0.4	mL
	3	-0.000538777	-0.538776604	-32.3265962	-0.012930638	21.71						0.0004	L
	4	-0.000560787	-0.560787016	-33.6472209	-0.013458888	22.59					c	1.489271	µg ml^{-1}
NADPH	1	-0.000251631	-0.25163136	-15.0978816	-0.006039153	10.14						0.595708	µg
	2	-0.000181054	-0.181053673	-10.8632204	-0.004345288	7.29						0.000596	mg
	3	-0.00019326	-0.193259955	-11.5955973	-0.004638239	7.79						1678.674	mg^{-1}
	4	-0.000184838	-0.184837992	-11.0902795	-0.004436112	7.45							

blank								Corrected activity	
		mmol L^{-1} s^{-1}	mean	µmol L^{-1} s^{-1}	µmol L^{-1} min^{-1}	µmol min^{-1}	U mg^{-1}	U mg^{-1}	Mean
NADH	1	-2.60689E-06	-2.91641E-06	-0.00291641	-0.174984309	-7E-05	0.12	**22.49**	**21.96**
	2	-2.60251E-06						**21.26**	
	3	-3.49844E-06						**21.59**	
	4	-2.95778E-06						**22.48**	
NADPH	1	-2.31406E-06	-2.4416E-06	-0.0024416	-0.146495895	-5.9E-05	0.10	**10.04**	**8.07**
	2	-2.31689E-06						**7.20**	
	3	-2.56393E-06						**7.69**	
	4	-2.57151E-06						**7.35**	

Annex 3 – Jupyter notebook scrips

Data analysis PhaB Enzymatic activity

In [1]:
```
import pandas as pd
import numpy as np
import matplotlib.pyplot as plt
import seaborn as sns
import statsmodels.api as sm
from scipy.stats import ttest_ind
from scipy import stats
```

In [2]:
```
df = pd.read_csv('NADH_NADPH_Assay_Walter.csv', sep=';')
df.head()
```

Out[2]:

	PhaB	Substrate	Activity	Replicate
0	Ther	NADH	0.125422	1
1	Ther	NADH	0.094066	2
2	Ther	NADH	0.097326	3
3	Ther	NADH	0.035485	4
4	Chim	NADH	0.776845	1

In [3]:
```
#Shapiro-Wilk test for normal distribution
for (enzyme, substrate), group_data in df.groupby(['PhaB', 'Substrate']):
    activity_values = group_data['Activity']

    if len(activity_values) >= 3:
        _, p_val = stats.shapiro(activity_values)
        status = "Normal" if p_val > 0.05 else "NON-normal"
        print(f"PhaB: {enzyme:10} | Substrate: {substrate:6} | p-val: {p_val:.4f} |
    else:
        print(f"PhaB: {enzyme:10} | Substrate: {substrate:6} | Date insuficiente (n
```

```
PhaB: Chim       | Substrate: NADH   | p-val: 0.5919 | Distribution: Normal
PhaB: Chim       | Substrate: NADPH  | p-val: 0.9124 | Distribution: Normal
PhaB: Jap        | Substrate: NADH   | p-val: 0.1923 | Distribution: Normal
PhaB: Jap        | Substrate: NADPH  | p-val: 0.0491 | Distribution: NON-normal
PhaB: Ther       | Substrate: NADH   | p-val: 0.4717 | Distribution: Normal
PhaB: Ther       | Substrate: NADPH  | p-val: 0.8919 | Distribution: Normal
```

In [4]:
```
print(f"{'PhaB':<12} | {'F-stat':<8} | {'p-value':<10} | {'final'}")
print("-" * 50)

for enzyme, enzyme_data in df.groupby('PhaB'):

    nadh = enzyme_data[enzyme_data['Substrate'] == 'NADH']['Activity'].values
    nadph = enzyme_data[enzyme_data['Substrate'] == 'NADPH']['Activity'].values

    var_nadh = np.var(nadh, ddof=1)
```

```
    var_nadph = np.var(nadph, ddof=1)

    if var_nadh > var_nadph:
        f_stat = var_nadh / var_nadph
        dfn = len(nadh) - 1
        dfd = len(nadph) - 1
    else:
        f_stat = var_nadph / var_nadh
        dfn = len(nadph) - 1
        dfd = len(nadh) - 1

    p_val = 2 * (1 - stats.f.cdf(f_stat, dfn, dfd))

    final = "Equal Variance" if p_val > 0.05 else "Different varianace"

    print(f"{enzyme:<12} | {f_stat:<8.4f} | {p_val:<10.4f} | {final}")
```

```
PhaB         | F-stat   | p-value    | final
--------------------------------------------------
Chim         | 633.1780 | 0.0002     | Different varianace
Jap          | 4.5435   | 0.2456     | Equal Variance
Ther         | 31819.3838 | 0.0000     | Different varianace
```

In [5]:
```
# Welch's t-test
from collections import defaultdict
p_values = defaultdict(float)
for PhaB in df["PhaB"].unique():
    group1 = df[(df["PhaB"] == PhaB) & (df["Substrate"] == "NADH")]["Activity"]
    group2 = df[(df["PhaB"] == PhaB) & (df["Substrate"] == "NADPH")]["Activity"]
    if len(group1) > 0 and len(group2) > 0:
        _, p = ttest_ind(group1, group2, equal_var=False)
        p_values[PhaB] = p

print(p_values)
```

```
defaultdict(<class 'float'>, {'Ther': np.float64(0.0005094504073800365), 'Chim': np.
float64(0.0005582518243077071), 'Jap': np.float64(2.8569443146576e-05)})
```

In [6]:
```
# ---- Bar plot ----
plt.figure(figsize=(9,6))
ax = sns.barplot(x="PhaB", y="Activity", hue="Substrate", data=df,
                 errorbar="sd", capsize=0.2, err_kws={"linewidth": 1.5}, palette="S

# ---- Add data points ----
sns.stripplot(x="PhaB", y="Activity", hue="Substrate", data=df,
              dodge=True, palette="dark:black", size=5, jitter=True, ax=ax)

# Remove duplicate legends from stripplot
handles, labels = ax.get_legend_handles_labels()
ax.legend(handles[:2], labels[:2], title="Coenzyme", bbox_to_anchor=(1.05, 1), loc=

# ---- Compute p-values for each enzyme pair ----

for PhaB in df["PhaB"].unique():
    group1 = df[(df["PhaB"] == PhaB) & (df["Substrate"] == "NADH")]["Activity"]
    group2 = df[(df["PhaB"] == PhaB) & (df["Substrate"] == "NADPH")]["Activity"]
    if len(group1) > 0 and len(group2) > 0:
        _, p = ttest_ind(group1, group2, equal_var=False)
        p_values[PhaB] = p

# ---- Add significance bars at equal height ----
def add_stat_annotation(ax, x, p_val, y_fixed=None):
    y_min, y_max = ax.get_ylim()
    y_range = y_max - y_min
    if y_fixed is None:
        y_fixed = y_max * 0.95

    # Left and right positions for paired bars
    x1, x2 = x - 0.2, x + 0.2
    bar_height = y_fixed
    text_y = y_fixed + y_range * 0.02

    # Draw the line
    ax.plot([x1, x1, x2, x2], [bar_height, bar_height + y_range * 0.02,
                               bar_height + y_range * 0.02, bar_height], c='black',

    # Significance stars
    if p_val < 0.001:
        text = "***"
    elif p_val < 0.01:
        text = "**"
    elif p_val < 0.05:
        text = "*"
    else:
        text = "ns"

    ax.text((x1+x2)/2, text_y, text, ha='center', va='bottom', fontsize=11)

# Add annotations at the same height for all enzymes
y_fixed = df["Activity"].max() + 0.00001
for i, PhaB in enumerate(df["PhaB"].unique()):
    add_stat_annotation(ax, i, p_values[PhaB], y_fixed=y_fixed)

# ---- Final touches ----
ax.set_ylabel("Specific activity (U mg$^{-1}$)")
ax.set_xlabel("")
ax.set_title("")
ax.yaxis.grid(True)
ax.set_axisbelow(True)
plt.tight_layout()
#plt.savefig("specific_activity_3_PhaB.png", dpi=300, bbox_inches='tight')
plt.show()
```

Data analysis Growth curves

Packages used

In [1]:
```
import pandas as pd
import numpy as np
import seaborn as sns
import matplotlib.pyplot as plt
```

In [2]:
```
from scipy.stats import linregress
from scipy.stats import dunnett
from scipy import stats
import statsmodels.api as sm
from statsmodels.formula.api import ols
from statsmodels.stats.multicomp import pairwise_tukeyhsd
from sklearn.preprocessing import StandardScaler
from sklearn.decomposition import PCA
```

Data preparation

In [3]:
```
hpt = pd.read_csv('dhpt.csv', sep=';')
hpt
```

Out[3]:

	time	Δhpt.1	Δhpt.2	Δhpt.3	Δhpt.4	NC.hpt
0	0.00	0.0171	0.0171	0.0184	0.0159	0.0108
1	0.61	0.0994	0.1186	0.1673	0.1477	0.0042
2	0.72	0.1727	0.2345	0.2850	0.2525	0.0100
3	0.85	0.2997	0.4112	0.4676	0.4430	0.0098
4	0.96	0.4937	0.5715	0.6241	0.6349	0.0064
5	1.62	0.5247	0.6456	0.7198	0.6466	0.0059
6	1.71	0.6848	0.7698	0.9138	0.7660	0.0032
7	1.92	0.7640	0.8488	1.0038	0.8530	0.0043
8	2.63	0.8876	1.0348	0.9916	0.8622	0.0072
9	2.98	0.9342	1.0014	1.1190	1.0419	0.0070
10	3.80	1.0743	1.0095	1.3683	1.0602	0.0049
11	4.80	1.0119	0.9654	1.3227	0.9573	0.0031
12	5.79	0.9228	0.8356	1.1280	0.8588	0.0012
13	6.80	0.7364	0.5196	0.9556	0.7392	0.0030
14	7.80	0.8652	0.7512	0.8752	0.8118	0.0067
15	8.80	0.8286	0.6768	0.6572	0.7780	0.0194
16	9.80	0.8530	0.7334	0.8754	0.7742	0.0046
17	10.73	0.7750	0.6602	0.8298	0.6896	0.0028

In [4]:
```
# 1. Def gowth data
col_gowth = [c for c in hpt.columns if c not in ['time', 'NC.hpt']]

# 2. NC substraction
for col in col_gowth:
    hpt[col] = hpt[col] - hpt['NC.hpt']

# 3. Baseline correction
for col in col_gowth:
    v_t0 = hpt.loc[hpt['time'] == 0, col].values[0]
    hpt[col] = hpt[col] - v_t0

# +del NC col
hpt = hpt.drop(columns=['NC.hpt'])

hpt.head()
```

Out[4]:

	time	Δhpt.1	Δhpt.2	Δhpt.3	Δhpt.4
0	0.00	0.0000	0.0000	0.0000	0.0000
1	0.61	0.0889	0.1081	0.1555	0.1384
2	0.72	0.1564	0.2182	0.2674	0.2374
3	0.85	0.2836	0.3951	0.4502	0.4281
4	0.96	0.4810	0.5588	0.6101	0.6234

In [5]:
```
jap = pd.read_csv('jap.csv', sep=';')
jap
```

Out[5]:

	time	Jap.1	Jap.2	Jap.3	Jap.4	NC.jap
0	0.00	0.0316	0.0332	0.0290	0.0293	0.0193
1	0.61	0.1543	0.1654	0.1514	0.1396	0.0327
2	0.73	0.2258	0.2281	0.2046	0.1850	0.0280
3	0.85	0.3698	0.3822	0.3271	0.2862	0.0282
4	0.96	0.5646	0.5750	0.5028	0.4329	0.0304
5	1.62	0.7132	0.7230	0.6230	0.5878	0.0282
6	1.72	1.0786	1.1186	0.9104	0.8852	0.0331
7	1.92	1.1362	1.2160	0.9354	0.9322	0.0321
8	2.63	1.2794	1.3244	0.9492	0.9550	0.0164
9	2.98	1.4946	1.5573	1.0839	1.1187	0.0192
10	3.81	1.5807	1.6932	1.2168	1.1910	0.0146
11	4.81	1.6911	1.7904	1.1853	1.0839	0.0123
12	5.80	1.5928	1.6756	1.0524	1.0004	0.0109
13	6.81	1.5124	1.6084	0.9324	0.9312	0.0098
14	7.80	1.6788	1.8528	1.0630	0.9794	0.0257
15	8.80	1.6344	1.7476	1.0910	0.9924	0.0195
16	9.80	1.3760	1.5536	0.9768	0.9200	0.0269
17	10.74	1.4056	1.5876	0.9984	0.9800	0.0290

In [6]:
```
# 1. Def gowth data
col_gowth = [c for c in jap.columns if c not in ['time', 'NC.jap']]

# 2. NC substraction
for col in col_gowth:
    jap[col] = jap[col] - jap['NC.jap']
```

```
# 3. Baseline correction
for col in col_gowth:
    v_t0 = jap.loc[jap['time'] == 0, col].values[0]
    jap[col] = jap[col] - v_t0

# +del NC col
jap = jap.drop(columns=['NC.jap'])

jap.head()
```

Out[6]:

	time	Jap.1	Jap.2	Jap.3	Jap.4
0	0.00	0.0000	0.0000	0.0000	0.0000
1	0.61	0.1093	0.1188	0.1090	0.0969
2	0.73	0.1855	0.1862	0.1669	0.1470
3	0.85	0.3293	0.3401	0.2892	0.2480
4	0.96	0.5219	0.5307	0.4627	0.3925

In [7]:
```
chim = pd.read_csv('chim.csv', sep=';')
chim
```

Out[7]:

	time	Chim.1	Chim.2	Chim.3	Chim.4	NC
0	0.00	0.0015	0.0128	0.0100	0.0075	0.0149
1	0.61	0.2015	0.1803	0.1390	0.1771	0.0241
2	0.73	0.3670	0.2718	0.2008	0.2919	0.0254
3	0.86	0.5787	0.4836	0.3511	0.5134	0.0291
4	0.97	0.7348	0.5948	0.5586	0.6972	0.0274
5	1.62	0.9276	0.7096	0.6166	0.8776	0.0183
6	1.72	1.2344	1.0406	0.8586	1.2004	0.0268
7	1.92	1.4300	1.0910	0.9616	1.4172	0.0191
8	2.63	1.6384	1.1360	1.0326	1.6636	0.0263
9	2.98	1.8856	1.2508	1.2392	1.9284	0.0335
10	3.81	1.8812	1.3352	1.2604	1.8804	0.0204
11	4.82	1.9508	1.4076	1.3256	1.9456	0.0150
12	5.81	2.1492	1.6644	1.5656	2.2916	0.0067
13	6.82	1.9916	1.4916	1.3148	2.1516	0.0111
14	7.84	2.0248	1.5016	1.3268	2.1616	0.0155
15	8.82	1.8808	1.5372	1.3364	2.0748	0.0064
16	9.81	1.7464	1.4844	1.2172	2.0392	0.0103
17	10.74	1.6304	1.3836	1.2360	1.8744	0.0090

In [8]:

```
# 1. Def gowth data
col_gowth = [c for c in chim.columns if c not in ['time', 'NC']]

# 2. NC substraction
for col in col_gowth:
    chim[col] = chim[col] - chim['NC']

# 3. Baseline correction
for col in col_gowth:
    v_t0 = chim.loc[chim['time'] == 0, col].values[0]
    chim[col] = chim[col] - v_t0

# +del NC col
chim = chim.drop(columns=['NC'])

chim.head()
```

Out[8]:

	time	Chim.1	Chim.2	Chim.3	Chim.4
0	0.00	0.0000	0.0000	0.0000	0.0000
1	0.61	0.1908	0.1583	0.1198	0.1604
2	0.73	0.3550	0.2485	0.1803	0.2739
3	0.86	0.5630	0.4566	0.3269	0.4917
4	0.97	0.7208	0.5695	0.5361	0.6772

In [9]:
```
cal = pd.read_csv('cal.csv', sep=';')
cal
```

Out[9]:

	time	Cal.1	Cal.2	Cal.3	Cal.4	NC
0	0.00	0.0025	0.0059	0.0052	0.0066	0.0149
1	0.61	0.0525	0.1287	0.1246	0.1221	0.0260
2	0.73	0.0852	0.2161	0.2191	0.2119	0.0275
3	0.86	0.1776	0.4079	0.4163	0.4178	0.0309
4	0.97	0.3344	0.6198	0.6302	0.6222	0.0307
5	1.62	0.5198	0.7828	0.7720	0.7866	0.0201
6	1.72	0.8514	1.1438	1.1754	1.2256	0.0276
7	1.93	1.0178	1.3104	1.3088	1.3184	0.0231
8	2.64	1.1974	1.5588	1.5712	1.5836	0.0280
9	2.98	1.5032	1.8480	1.9548	1.8396	0.0321
10	3.82	1.5320	1.7812	1.7920	1.6184	0.0214
11	4.82	1.5524	1.8592	1.8792	1.8996	0.0150
12	5.81	1.6848	2.1020	2.1872	2.0828	0.0066
13	6.81	1.4052	1.9560	1.9548	1.9956	0.0114
14	7.84	1.4564	2.0220	2.0312	2.0756	0.0153
15	8.82	1.4528	1.9348	2.0204	2.0332	0.0093
16	9.81	1.3180	1.8484	2.0504	2.0288	0.0109
17	10.74	1.3812	1.7360	1.9852	1.8844	0.0103

In [10]:
```
# 1. Def gowth data
col_gowth = [c for c in cal.columns if c not in ['time', 'NC']]

# 2. NC substraction
for col in col_gowth:
    cal[col] = cal[col] - cal['NC']
```

```
# 3. Baseline correction
for col in col_gowth:
    v_t0 = cal.loc[cal['time'] == 0, col].values[0]
    cal[col] = cal[col] - v_t0

# +del NC col
cal = cal.drop(columns=['NC'])

cal.rename(columns={"Cal.1": "Ther.1", "Cal.2": "Ther.2", "Cal.3": "Ther.3", "Cal.4

cal.head()
```

Out[10]:

	time	Ther.1	Ther.2	Ther.3	Ther.4
0	0.00	0.0000	0.0000	0.0000	0.0000
1	0.61	0.0389	0.1117	0.1083	0.1044
2	0.73	0.0701	0.1976	0.2013	0.1927
3	0.86	0.1591	0.3860	0.3951	0.3952
4	0.97	0.3161	0.5981	0.6092	0.5998

In [11]:
```
# Put the dataframes into a list
dataframes = {'Δhpt': hpt, 'Ther': cal, 'Chim': chim, 'Jap': jap}
temp_list = []

for strain_name, df in dataframes.items():
    # Transf long
    m_df = df.melt(id_vars=['time'], var_name='temp_col', value_name='OD')

    # Add Strains
    m_df['Strain'] = strain_name

    # Replication number
    # expand=False => serie
    m_df['Replicate'] = m_df['temp_col'].str.split('.').str[-1]

    temp_list.append(m_df)

# Combine all
all_long = pd.concat(temp_list, ignore_index=True)

# Clean up of useless columns
all_long = all_long[['time', 'OD', 'Strain', 'Replicate']]

# Replicate as numeric
all_long['Replicate'] = pd.to_numeric(all_long['Replicate'])

all_long.head()
```

Out[11]:

	time	OD	Strain	Replicate
0	0.00	0.0000	Δhpt	1
1	0.61	0.0889	Δhpt	1
2	0.72	0.1564	Δhpt	1
3	0.85	0.2836	Δhpt	1
4	0.96	0.4810	Δhpt	1

Gowth curvs vizualization

In [12]:
```
plt.figure(figsize=(10, 6))

sns.lineplot(data=all_long, x='time', y='OD', hue='Strain', marker='o')

plt.title('', fontsize=15)
plt.xlabel('Time (days)', fontsize=12)
plt.ylabel('OD (587nm)', fontsize=12)
plt.grid(True, alpha=0.3)
plt.legend(title='Strain', bbox_to_anchor=(1.05, 1), loc='upper left')

plt.tight_layout()
#plt.savefig("OD_mean.png", dpi=300, bbox_inches='tight')
plt.show()
```

In [13]:
```
sns.set_style("whitegrid")

# Small Multiples
g = sns.relplot(
```

```
    data=all_long,
    x='time',
    y='OD',
    hue='Replicate',      # Fiecare replică are culoarea ei
    col='Strain',         # Creează un grafic separat pentru fiecare tulpină
    col_wrap=2,           # Așază-le pe 2 coloane (rezultă un tabel 2x2)
    kind='line',          # Tip linie
    marker='o',           # Adaugă puncte pe linie
    palette='viridis',    # O paletă de culori plăcută vizual
    height=4,             # Înălțimea fiecărui sub-grafic
    aspect=1.2            # Proporția lățime/înălțime
)

# 3. Editări fine pentru aspect profesional
g.set_titles("{col_name}", weight='bold', size=14) # Pune numele tulpinii ca titlu
g.set_axis_labels("Time (days)", "OD (587nm)") # Redenumește axele

# Opțional: Forțăm axa Y să înceapă de la 0 pentru toate graficele (pentru comparaț
g.set(ylim=(0, all_long['OD'].max() * 1.1))

# Ajustăm spațierea pentru a nu se suprapune etichetele
plt.subplots_adjust(top=0.9)
g.fig.suptitle('', fontsize=16)

#plt.savefig("OD_individual.png", dpi=300, bbox_inches='tight')
plt.show()
```

Calculation of growth parameters

In [14]:
```
all_long['time'] = all_long['time'] * 24

print(all_long[['time']].head())
```

```
    time
0   0.00
1  14.64
2  17.28
3  20.40
4  23.04
```

In [15]:
```
def get_slope(time_series, od_series):
    # Returnează panta regresiei liniare
    slope, _, _, _, _ = linregress(time_series, od_series)
    return slope

results = []

# Iterăm prin fiecare tulpină și replică (folosind df_long creat anterior)
for (strain, replicate), group in all_long.groupby(['Strain', 'Replicate']):

    # 1. Faza Exponențială (calculăm pe ln_OD pentru rata specifică mu)
    exp_phase = group[(group['time'] >= 12.0) & (group['time'] <= 24)]
    mu = get_slope(exp_phase['time'], np.log(exp_phase['OD'] + 0.001))

    # 2. Faza de Platou (calculăm pe OD brut pentru a vedea rata de scădere)
    plateau_phase = group[group['time'] >= 90.0]
    decay_rate = get_slope(plateau_phase['time'], plateau_phase['OD'])

    results.append({
        'Strain': strain,
        'Replicate': replicate,
        'Growth_Rate': mu,
        'Decay_Rate': decay_rate
    })
df_stats = pd.DataFrame(results)
df_stats
```

Out[15]:

	Strain	Replicate	Growth_Rate	Decay_Rate
0	Chim	1	0.153185	-0.001707
1	Chim	2	0.153318	0.000233
2	Chim	3	0.174495	-0.000641
3	Chim	4	0.168805	-0.000042
4	Jap	1	0.186681	-0.001359
5	Jap	2	0.180602	-0.000836
6	Jap	3	0.173117	-0.001270
7	Jap	4	0.167063	-0.001246
8	Ther	1	0.242015	-0.001393
9	Ther	2	0.195845	-0.000348
10	Ther	3	0.201113	0.000938
11	Ther	4	0.204870	0.001274
12	Δhpt	1	0.198689	-0.001545
13	Δhpt	2	0.194069	-0.001950
14	Δhpt	3	0.162691	-0.003776
15	Δhpt	4	0.179702	-0.001861

In [16]:

```
#Take in Max_OD, Globa_Growth
new_metrics = all_long.groupby(['Strain', 'Replicate'])['OD'].agg(
    Max_OD='max',
    Global_Growth='last'
).reset_index()

#Put in Max_OD, Globa_Growth
df_stats = pd.merge(df_stats, new_metrics, on=['Strain', 'Replicate'])

df_stats.head()
```

Out[16]:

	Strain	Replicate	Growth_Rate	Decay_Rate	Max_OD	Global_Growth
0	Chim	1	0.153185	-0.001707	2.1559	1.6348
1	Chim	2	0.153318	0.000233	1.6598	1.3767
2	Chim	3	0.174495	-0.000641	1.5638	1.2319
3	Chim	4	0.168805	-0.000042	2.2923	1.8728
4	Jap	1	0.186681	-0.001359	1.6665	1.3643

Statistical analysis

Growth rates

In [17]:
```
#Shapiro-Wilk test for normal distribution of gorws
for strain in df_stats['Strain'].unique():
    data = df_stats[df_stats['Strain'] == strain]['Growth_Rate']
    _, p_val = stats.shapiro(data)
    print(f'Normal distribution {strain}: p = {p_val:.4f}')
```

```
Normal distribution Chim: p = 0.1845
Normal distribution Jap: p = 0.9248
Normal distribution Ther: p = 0.0839
Normal distribution Δhpt: p = 0.6077
```

In [18]:
```
#Levene's test for equality of variances
groups = [df_stats[df_stats['Strain'] == s]['Growth_Rate'] for s in df_stats['Strai
_, p_levene = stats.levene(*groups)

print(f'Homoscedasticity (Levene): p = {p_levene:.4f}')
```

```
Homoscedasticity (Levene): p = 0.8164
```

In [19]:
```
# Growth phase
model = ols('Growth_Rate ~ C(Strain)', data=df_stats).fit()
print(sm.stats.anova_lm(model))

# Differece between
tukey = pairwise_tukeyhsd(endog=df_stats['Growth_Rate'], groups=df_stats['Strain'],
print(tukey)
```

```
               df    sum_sq   mean_sq         F    PR(>F)
C(Strain)    3.0  0.004965  0.001655  7.378694  0.004624
Residual    12.0  0.002692  0.000224       NaN       NaN
Multiple Comparison of Means - Tukey HSD, FWER=0.05
=====================================================
group1 group2 meandiff p-adj   lower  upper  reject
-----------------------------------------------------
  Chim    Jap   0.0144 0.5447  -0.017 0.0459  False
  Chim   Ther   0.0485 0.0031  0.0171   0.08   True
  Chim   Δhpt   0.0213  0.236 -0.0101 0.0528  False
   Jap   Ther   0.0341 0.0323  0.0027 0.0655   True
   Jap   Δhpt   0.0069 0.9123 -0.0245 0.0384  False
  Ther   Δhpt  -0.0272 0.0991 -0.0586 0.0043  False
-----------------------------------------------------
```

In [20]:
```
# Data for the Dunnett test
wt_data = df_stats[df_stats['Strain'] == 'Δhpt']['Growth_Rate']
m1_data = df_stats[df_stats['Strain'] == 'Ther']['Growth_Rate']
m2_data = df_stats[df_stats['Strain'] == 'Chim']['Growth_Rate']
m3_data = df_stats[df_stats['Strain'] == 'Jap']['Growth_Rate']

# Dunnett test
res = dunnett(m1_data, m2_data, m3_data, control=wt_data)
```

```
# p-value extraction
p_values = res.pvalue

# Function for plot show
def get_stars(p):
    if p < 0.001: return '***'
    if p < 0.01: return '**'
    if p < 0.05: return '*'
    return 'ns'

print(res)
```

```
Dunnett's test (95.0% Confidence Interval)
Comparison               Statistic  p-value  Lower CI  Upper CI
 (Sample 0 - Control)      2.566     0.061    -0.001     0.056
 (Sample 1 - Control)     -2.015     0.157    -0.050     0.007
 (Sample 2 - Control)     -0.654     0.851    -0.035     0.021
```

In [21]:
```
# Order of the strains
order_strains = ['Δhpt', 'Ther', 'Chim', 'Jap']
```

In [22]:
```
plt.figure(figsize=(8, 6))

ax = sns.boxplot(
    data=df_stats,
    x='Strain',
    y='Growth_Rate',
    order=order_strains,
    hue='Strain',
    palette="Set2",
    legend=False
)

sns.swarmplot(
    data=df_stats,
    x='Strain',
    y='Growth_Rate',
    color='black',
    alpha=0.5,
    order=order_strains
)

# 2. Significance Bars Logic (using your Dunnett results)
y_max = df_stats['Growth_Rate'].max()
gap = y_max * 0.05

# Assuming 'res.pvalue' contains [p_M1, p_M2, p_M3]
for i, p_val in enumerate(res.pvalue):
    x1, x2 = 0, i + 1
    y = y_max + (i + 1) * gap
    h = gap * 0.2

    plt.plot([x1, x1, x2, x2], [y-h, y, y, y-h], lw=1.5, color='black')
    plt.text((x1 + x2) * .5, y, get_stars(p_val), ha='center', va='bottom', fontwei
```

```
plt.title('')
plt.ylabel('Growth rate (h$^{-1}$)')
plt.xlabel('Strain')

# Adjust limit so bars aren't cut off
plt.ylim(df_stats['Growth_Rate'].min() * 0.9, y + gap * 2)

#plt.savefig("Growth_rates.png", dpi=300, bbox_inches='tight')
plt.show()
```

Decay rates

In [23]:
```
#Shapiro-Wilk test for normal distribution of gorws
for strain in df_stats['Strain'].unique():
    data = df_stats[df_stats['Strain'] == strain]['Decay_Rate']
    _, p_val = stats.shapiro(data)
    print(f'Normal distribution {strain}: p = {p_val:.4f}')
```

```
Normal distribution Chim: p = 0.5703
Normal distribution Jap: p = 0.1233
Normal distribution Ther: p = 0.5891
Normal distribution Δhpt: p = 0.0743
```

In [24]:
```
#Levene's test for equality of variances
groups = [df_stats[df_stats['Strain'] == s]['Decay_Rate'] for s in df_stats['Strain
_, p_levene = stats.levene(*groups)
```

```
print(f'Homoscedasticity (Levene): p = {p_levene:.4f}')
```

```
Homoscedasticity (Levene): p = 0.2632
```

In [25]:
```
# Platou
model = ols('Decay_Rate ~ C(Strain)', data=df_stats).fit()
print(sm.stats.anova_lm(model))

# Tukey test
tukey = pairwise_tukeyhsd(endog=df_stats['Decay_Rate'], groups=df_stats['Strain'],
print(tukey)
```

```
              df    sum_sq       mean_sq         F    PR(>F)
C(Strain)   3.0  0.000013  4.180787e-06  5.039658  0.017328
Residual   12.0  0.000010  8.295776e-07       NaN       NaN
Multiple Comparison of Means - Tukey HSD, FWER=0.05
====================================================
group1 group2 meandiff p-adj   lower   upper  reject
----------------------------------------------------
  Chim    Jap  -0.0006 0.7568 -0.0026  0.0013  False
  Chim   Ther   0.0007 0.7413 -0.0013  0.0026  False
  Chim   Δhpt  -0.0017 0.0782 -0.0037  0.0002  False
   Jap   Ther   0.0013  0.237 -0.0006  0.0032  False
   Jap   Δhpt  -0.0011 0.3579  -0.003  0.0008  False
  Ther   Δhpt  -0.0024 0.0133 -0.0043 -0.0005   True
----------------------------------------------------
```

In [26]:
```
# Data for the Dunnett test
wt_data = df_stats[df_stats['Strain'] == 'Δhpt']['Decay_Rate']
m1_data = df_stats[df_stats['Strain'] == 'Ther']['Decay_Rate']
m2_data = df_stats[df_stats['Strain'] == 'Chim']['Decay_Rate']
m3_data = df_stats[df_stats['Strain'] == 'Jap']['Decay_Rate']

# Dunnett test
res = dunnett(m1_data, m2_data, m3_data, control=wt_data)

# p-value extraction
p_values = res.pvalue

# Function for plot show
def get_stars(p):
    if p < 0.001: return '***'
    if p < 0.01: return '**'
    if p < 0.05: return '*'
    return 'ns'

print(res)
```

```
Dunnett's test (95.0% Confidence Interval)
Comparison               Statistic  p-value  Lower CI  Upper CI
 (Sample 0 - Control)        3.727    0.008     0.001     0.004
 (Sample 1 - Control)        2.707    0.048     0.000     0.003
 (Sample 2 - Control)        1.716    0.252    -0.001     0.003
```

In [27]:
```
plt.figure(figsize=(8, 6))

ax = sns.boxplot(
    data=df_stats,
    x='Strain',
    y='Decay_Rate',
    order=order_strains,
    hue='Strain',
    palette="Set2",
    legend=False
)

sns.swarmplot(
    data=df_stats,
    x='Strain',
    y='Decay_Rate',
    color='black',
    alpha=0.5,
    order=order_strains
)

# 2. Significance Bars Logic (using your Dunnett results)
y_max = df_stats['Decay_Rate'].max()
gap = y_max * 0.05

# Assuming 'res.pvalue' contains [p_M1, p_M2, p_M3]
for i, p_val in enumerate(res.pvalue):
    x1, x2 = 0, i + 1
    y = y_max + (i + 1) * gap * 3
    h = gap * 0.9

    plt.plot([x1, x1, x2, x2], [y-h, y, y, y-h], lw=1.5, color='black')
    plt.text((x1 + x2) * .5, y, get_stars(p_val), ha='center', va='bottom', fontwei

plt.title('')
plt.ylabel('Decay rate')
plt.xlabel('Strain')

# Adjust limit so bars aren't cut off
plt.ylim(df_stats['Decay_Rate'].min() * 1.1, y + gap * 5)

#plt.savefig("Decay_rate.png", dpi=300, bbox_inches='tight')
plt.show()
```

Max OD

In [28]:
```
#Shapiro-Wilk test for normal distribution
for strain in df_stats['Strain'].unique():
    data = df_stats[df_stats['Strain'] == strain]['Max_OD']
    _, p_val = stats.shapiro(data)
    print(f'Normal distribution {strain}: p = {p_val:.4f}')
```

```
Normal distribution Chim: p = 0.3166
Normal distribution Jap: p = 0.2025
Normal distribution Ther: p = 0.1177
Normal distribution Δhpt: p = 0.0266
```

In [29]:
```
#Levene's test for equality of variances
groups = [df_stats[df_stats['Strain'] == s]['Max_OD'] for s in df_stats['Strain'].u
_, p_levene = stats.levene(*groups)

print(f'Homoscedasticity (Levene): p = {p_levene:.4f}')
```

```
Homoscedasticity (Levene): p = 0.0781
```

In [30]:
```
# Max OD Model
model = ols('Max_OD ~ C(Strain)', data=df_stats).fit()
print(sm.stats.anova_lm(model))

# Differece between
tukey = pairwise_tukeyhsd(endog=df_stats['Max_OD'], groups=df_stats['Strain'], alph
print(tukey)
```

```
             df    sum_sq   mean_sq         F    PR(>F)
C(Strain)   3.0  2.078021  0.692674  8.878904  0.002254
Residual   12.0  0.936161  0.078013       NaN       NaN
Multiple Comparison of Means - Tukey HSD, FWER=0.05
====================================================
group1 group2 meandiff p-adj   lower   upper  reject
----------------------------------------------------
  Chim    Jap  -0.4583 0.1477 -1.0447  0.1281  False
  Chim   Ther   0.0995 0.9566 -0.4869  0.6859  False
  Chim   Δhpt  -0.7954 0.0079 -1.3817  -0.209   True
   Jap   Ther   0.5578 0.0641 -0.0286  1.1442  False
   Jap   Δhpt  -0.3371 0.3622 -0.9234  0.2493  False
  Ther   Δhpt  -0.8949 0.0033 -1.4812 -0.3085   True
----------------------------------------------------
```

In [31]:
```python
# Data for the Dunnett test
wt_data = df_stats[df_stats['Strain'] == 'Δhpt']['Max_OD']
m1_data = df_stats[df_stats['Strain'] == 'Ther']['Max_OD']
m2_data = df_stats[df_stats['Strain'] == 'Chim']['Max_OD']
m3_data = df_stats[df_stats['Strain'] == 'Jap']['Max_OD']

# Dunnett test
res = dunnett(m1_data, m2_data, m3_data, control=wt_data)

# p-value extraction
p_values = res.pvalue

# Function for plot show
def get_stars(p):
    if p < 0.001: return '***'
    if p < 0.01: return '**'
    if p < 0.05: return '*'
    return 'ns'

print(res)
```

```
Dunnett's test (95.0% Confidence Interval)
Comparison               Statistic  p-value  Lower CI  Upper CI
 (Sample 0 - Control)        4.531    0.002     0.365     1.425
 (Sample 1 - Control)        4.027    0.005     0.266     1.325
 (Sample 2 - Control)        1.707    0.256    -0.193     0.867
```

In [32]:
```python
plt.figure(figsize=(8, 6))

ax = sns.boxplot(
    data=df_stats,
    x='Strain',
    y='Max_OD',
    order=order_strains,
    hue='Strain',
    palette="Set2",
    legend=False
)

sns.swarmplot(
    data=df_stats,
    x='Strain',
    y='Max_OD',
    color='black',
    alpha=0.5,
    order=order_strains
)

# 2. Significance Bars Logic (using your Dunnett results)
y_max = df_stats['Max_OD'].max()
gap = y_max * 0.05

# Assuming 'res.pvalue' contains [p_M1, p_M2, p_M3]
for i, p_val in enumerate(res.pvalue):
    x1, x2 = 0, i + 1
    y = y_max + (i + 1) * gap * 3
    h = gap * 0.3

    plt.plot([x1, x1, x2, x2], [y-h, y, y, y-h], lw=1.5, color='black')
    plt.text((x1 + x2) * .5, y, get_stars(p_val), ha='center', va='bottom', fontwei

plt.title('Max OD: Mutants vs WT (Dunnett Test)')
plt.ylabel('OD')
plt.xlabel('Strain')

# Adjust limit so bars aren't cut off
plt.ylim(df_stats['Max_OD'].min() * 0.7, y + gap * 2)

plt.show()
```

Global Growth

In [33]:
```
#Shapiro-Wilk test for normal distribution
for strain in df_stats['Strain'].unique():
    data = df_stats[df_stats['Strain'] == strain]['Global_Growth']
    _, p_val = stats.shapiro(data)
    print(f'Normal distribution {strain}: p = {p_val:.4f}')
```

```
Normal distribution Chim: p = 0.8426
Normal distribution Jap: p = 0.2574
Normal distribution Ther: p = 0.5657
Normal distribution Δhpt: p = 0.6704
```

In [34]:
```
#Levene's test for equality of variances
groups = [df_stats[df_stats['Strain'] == s]['Global_Growth'] for s in df_stats['Str
_, p_levene = stats.levene(*groups)

print(f'Homoscedasticity (Levene): p = {p_levene:.4f}')
```

```
Homoscedasticity (Levene): p = 0.1347
```

In [35]:
```
# Global Growth
model = ols('Global_Growth ~ C(Strain)', data=df_stats).fit()
print(sm.stats.anova_lm(model))

# Differece between
```

```
tukey = pairwise_tukeyhsd(endog=df_stats['Global_Growth'], groups=df_stats['Strain'
print(tukey)
```

```
               df    sum_sq   mean_sq          F    PR(>F)
C(Strain)   3.0  2.346210  0.782070  12.742104  0.000486
Residual   12.0  0.736522  0.061377        NaN       NaN
Multiple Comparison of Means - Tukey HSD, FWER=0.05
=====================================================
group1 group2 meandiff p-adj   lower   upper  reject
-----------------------------------------------------
  Chim    Jap  -0.3266 0.2927 -0.8467  0.1935  False
  Chim   Ther   0.2172 0.6151 -0.3029  0.7373  False
  Chim   Δhpt  -0.7995 0.0031 -1.3196 -0.2794   True
   Jap   Ther   0.5438 0.0395  0.0237  1.0639   True
   Jap   Δhpt  -0.4729 0.0792  -0.993  0.0472  False
  Ther   Δhpt  -1.0167 0.0004 -1.5368 -0.4966   True
-----------------------------------------------------
```

In [36]:
```
# Data for the Dunnett test
wt_data = df_stats[df_stats['Strain'] == 'Δhpt']['Global_Growth']
m1_data = df_stats[df_stats['Strain'] == 'Ther']['Global_Growth']
m2_data = df_stats[df_stats['Strain'] == 'Chim']['Global_Growth']
m3_data = df_stats[df_stats['Strain'] == 'Jap']['Global_Growth']

# Dunnett test
res = dunnett(m1_data, m2_data, m3_data, control=wt_data)

# p-value extraction
p_values = res.pvalue

# Function for plot show
def get_stars(p):
    if p < 0.001: return '***'
    if p < 0.01: return '**'
    if p < 0.05: return '*'
    return 'ns'

print(res)
```

```
Dunnett's test (95.0% Confidence Interval)
Comparison               Statistic  p-value  Lower CI  Upper CI
 (Sample 0 - Control)        5.804    0.000     0.547     1.487
 (Sample 1 - Control)        4.564    0.002     0.329     1.270
 (Sample 2 - Control)        2.699    0.048     0.003     0.943
```

In [37]:
```
plt.figure(figsize=(8, 6))

ax = sns.boxplot(
    data=df_stats,
    x='Strain',
    y='Global_Growth',
    order=order_strains,
    hue='Strain',
    palette="Set2",
    legend=False
)
```

```
sns.swarmplot(
    data=df_stats,
    x='Strain',
    y='Global_Growth',
    color='black',
    alpha=0.5,
    order=order_strains
)

# 2. Significance Bars Logic (using your Dunnett results)
y_max = df_stats['Global_Growth'].max()
gap = y_max * 0.05

# Assuming 'res.pvalue' contains [p_M1, p_M2, p_M3]
for i, p_val in enumerate(res.pvalue):
    x1, x2 = 0, i + 1
    y = y_max + (i + 1) * gap
    h = gap * 0.1

    plt.plot([x1, x1, x2, x2], [y-h, y, y, y-h], lw=1.5, color='black')
    plt.text((x1 + x2) * .5, y, get_stars(p_val), ha='center', va='bottom', fontwei

plt.title('')
plt.ylabel('OD (587nm)')
plt.xlabel('Strain')

# Adjust limit so bars aren't cut off
plt.ylim(df_stats['Global_Growth'].min() * 0.9, y + gap * 2)

#plt.savefig("Max_OD.png", dpi=300, bbox_inches='tight')
plt.show()
```

PCA

In [38]:
```
features = ['Growth_Rate', 'Decay_Rate', 'Max_OD', 'Global_Growth']
x = df_stats[features].values

# Standadization: avrr 0 and SD 1
x_scaled = StandardScaler().fit_transform(x)

# PCA Run
pca = PCA(n_components=2)
principalComponents = pca.fit_transform(x_scaled)
```

In [39]:
```
df_pca_plot = pd.DataFrame(data = principalComponents, columns = ['PC1', 'PC2'])

#Put data togheter for ploting
df_pca_plot['Strain'] = df_stats['Strain'].values

#Results for PC1 and PC2
var_exp = pca.explained_variance_ratio_ * 100
print(f"PC1 explains {var_exp[0]:.2f}% of the differences.")
print(f"PC2 explains {var_exp[1]:.2f}% of the differences.")
```

```
PC1 explains 65.03% of the differences.
PC2 explains 24.81% of the differences.
```

In [40]:
```
plt.figure(figsize=(10, 7))
```

```
# Plotting points
sns.scatterplot(x='PC1', y='PC2', hue='Strain', data=df_pca_plot, s=100, palette='v

# Loadings and arrrows
loadings = pca.components_.T * np.sqrt(pca.explained_variance_)
features = ['Growth_Rate', 'Decay_Rate', 'Max_OD', 'Global_Growth']

for i, feature in enumerate(features):
    plt.arrow(0, 0, loadings[i, 0]*2, loadings[i, 1]*2, color='red', alpha=0.6, hea
    plt.text(loadings[i, 0]*2.2, loadings[i, 1]*2.2, feature, color='darkred', ha='

plt.xlabel(f'PC1 ({var_exp[0]:.1f}%)')
plt.ylabel(f'PC2 ({var_exp[1]:.1f}%)')
plt.title('PCA: Phenotypic Differentiation of Mutants')
plt.grid(alpha=0.3)
plt.axhline(0, color='black', lw=1, alpha=0.5)
plt.axvline(0, color='black', lw=1, alpha=0.5)
plt.show()
```

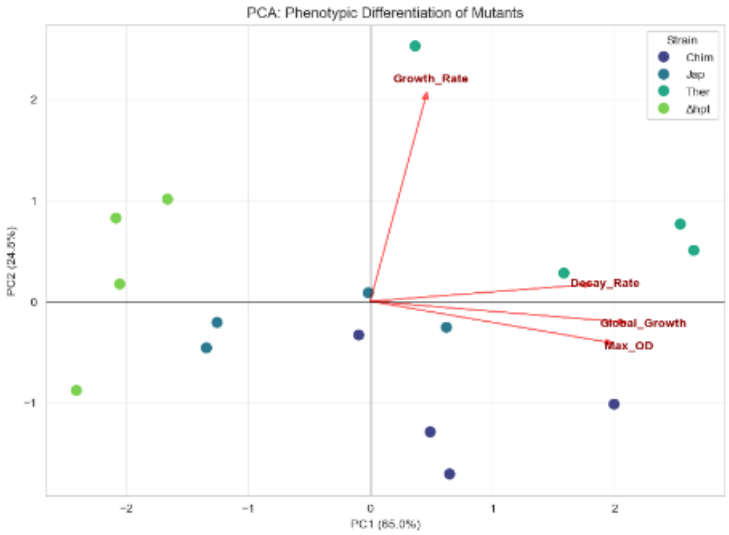

Data analysis Pressure consumption

In [1]:
```
import pandas as pd
import numpy as np
import seaborn as sns
import matplotlib.pyplot as plt
```

In [2]:
```
df = pd.read_csv('pressure.csv', sep=';')
df
```

Out[2]:

	time	Δhpt.1	Δhpt.2	Δhpt.3	Δhpt.4	Ther.1	Ther.2	Ther.3	Ther.4	Chim.1	Chim.2
0	0.0	3.008	2.979	3.0050	2.9950	3.125	3.004	3.037	3.063	3.113	3.072
1	0.6	2.097	1.731	1.1660	1.2720	2.795	1.719	1.737	1.774	0.979	1.380
2	0.7	1.943	1.296	1.0880	1.3350	2.540	1.585	1.478	1.523	0.704	1.419
3	0.8	1.205	0.311	0.1860	0.3440	1.877	0.299	0.252	0.294	0.096	0.307
4	1.0	0.578	0.154	0.0084	0.1360	1.115	0.153	0.123	0.114	0.168	0.205
5	1.6	0.139	0.053	0.0080	0.1040	0.178	0.138	0.137	0.084	0.242	0.153
6	1.7	0.552	0.437	0.1490	0.4600	0.234	0.171	0.151	0.106	0.160	0.420
7	1.9	0.113	0.073	0.0051	0.0058	0.157	0.076	0.060	0.065	0.161	0.153
8	2.6	0.153	0.143	0.0760	0.0820	0.158	0.168	0.187	0.155	0.148	0.083
9	3.0	0.063	0.340	0.0590	0.1520	0.110	0.199	0.209	0.162	0.172	0.120
10	3.8	0.156	0.493	0.4930	0.3280	0.272	0.274	0.297	0.278	0.220	0.226
11	4.8	0.296	1.297	0.1400	1.1250	0.253	0.241	0.183	0.146	0.334	0.310
12	5.8	1.473	1.881	0.9610	1.7980	0.350	0.200	0.182	0.188	0.332	0.313
13	6.8	1.990	2.295	2.5780	2.2560	2.895	0.266	0.275	0.282	0.344	1.000
14	7.8	2.542	2.720	2.2510	2.7430	3.329	0.281	0.269	0.237	0.358	2.488
15	8.8	2.998	3.276	2.8890	2.8100	3.065	0.217	0.109	0.089	1.648	2.661
16	9.8	3.241	3.020	2.9660	2.9350	3.228	2.068	0.090	0.596	3.217	2.927
17	10.7	3.179	3.220	3.3710	3.2190	3.276	3.069	0.578	2.460	3.311	3.001

In [3]:
```
# 1. Mealt table
df_long = df.melt(id_vars=['time'], var_name='column_name', value_name='Pressure')

# 2. Saparate 'column_name' în 'Strain' și 'Replicate'
#  ('.') as separator
df_long[['Strain', 'Replicate']] = df_long['column_name'].str.rsplit('.', n=1, expa
```

```
# 3. Deliting 'column_name'
df_long = df_long.drop(columns=['column_name'])
```

In [4]:
```
df_long
```

Out[4]:

	time	Pressure	Strain	Replicate
0	0.0	3.008	Δhpt	1
1	0.6	2.097	Δhpt	1
2	0.7	1.943	Δhpt	1
3	0.8	1.205	Δhpt	1
4	1.0	0.578	Δhpt	1
...	...	...	...	...
283	6.8	2.229	Jap	4
284	7.8	2.394	Jap	4
285	8.8	2.751	Jap	4
286	9.8	2.774	Jap	4
287	10.7	2.878	Jap	4

288 rows × 4 columns

In [5]:
```
order_strains = ['Δhpt', 'Ther', 'Chim', 'Jap']

plt.figure(figsize=(10, 6))

sns.lineplot(data=df_long, x='time', y='Pressure', hue='Strain', marker='o')

plt.title('', fontsize=15)
plt.xlabel('Time (days)', fontsize=12)
plt.ylabel('Pressure (bar)', fontsize=12)
plt.grid(True, alpha=0.3)
plt.legend(title='Strain', bbox_to_anchor=(1.05, 1), loc='upper left')

plt.tight_layout()
#plt.savefig("Pressure_mean.png", dpi=300, bbox_inches='tight')
plt.show()
```

In [6]:
```
sns.set_style("whitegrid")

# Small Multiples
g = sns.relplot(
    data=df_long,
    x='time',
    y='Pressure',
    hue='Replicate',      # Each replicate has a color
    col='Strain',         # Each strain a graph
    col_wrap=2,           # 2x2 grid for graphs
    kind='line',          # Tip linie
    marker='o',           # Add points
    palette='viridis',    # Color pallete
    height=4,             # Sub-graphs height
    aspect=1.2            # Width/high ratio
)

# Aspects editing
g.set_titles("{col_name}", weight='bold', size=14) # Stain name as title
g.set_axis_labels("Time (days)", "Pressure (bar)") # Axix name

# Start axies at 0
g.set(ylim=(0, df_long['Pressure'].max() * 1.1))

# Space adjustmens
plt.subplots_adjust(top=0.9)
g.fig.suptitle('', fontsize=16)
#plt.savefig("Pressure_individual.png", dpi=300, bbox_inches='tight')
plt.show()
```